POWER-TO-VOID TRANSFER FUNCTIONS

by

HELGE CHRISTENSEN

M.S., Royal Technical
University of Denmark
(1954)

SUBMITTED IN PARTIAL FULFILLMENT
OF THE REQUIREMENTS OF THE
DEGREE OF DOCTOR OF
PHILOSOPHY

at

MASSACHUSETTS INSTITUTE OF
TECHNOLOGY

September 1961

Signature of Author . . . . . /
Department of Nuclear Engineering, June 20, 1961

Certified by. . . . . /. . . . . .
Thesis Supervisor

Accepted by . . . . . .
Chairman, Departmental Committee
on Graduate Students

ABSTRACT

POWER-TO-VOID TRANSFER FUNCTIONS

by

Helge Christensen

Submitted to the Department of Nuclear Engineering, Massachusetts Institute of Technology, on June 20, 1961, in partial fulfillment of the requirements for the degree of Doctor of Philosophy.

Variations in the steam bubble distribution, the "void" distribution, in a boiling channel as a function of changes in heating power was studied.

A rectangular test tube, of cross section 1.11x4.44 cm and height 127 cm, was inserted in a forced circulation pressure loop. The tube was heated by passing an AC current through the tube walls. A power oscillator was built which could give a 10% peak-to-peak sinusoidal power modulation at any frequency in the interval 0.01 to 10 cycles per second.

Variations in steam volume fraction were observed by means of a gamma densitometer built for the purpose. Accurate void profiles could be taken by traversing the test channel vertically and horizontally.

With the void detector stationary at a given height, the amplitude and phase delay of the steam void variations were measured in the frequency range mentioned. The signal from the gamma detector was passed to a harmonic analyzer built for the experiment. This instrument could pick out the void variations coherent with the power variation, in the presence of much greater random signal variations caused by the boiling process.

The frequency response of steam voids was measured at 4 different pressures ranging from 27.2 to 68 Ata, at conditions comparable to those in pressurized boiling water reactors. Void phase and void amplitude have been plotted as functions of frequency, and the data have also been presented in tables.

The most important result of the experiments is to show that the void response falls off at a frequency that is much lower than that predicted by theoretically derived power-to-void transfer functions used previously in reactor calculations. Also the void amplitude in the lower part of the channel was larger than expected.

By taking into account the pressure changes in the channel caused by the power variations, an expression was derived for the power-to-void transfer function that could be fitted very well to the data. A constant, associated with the completeness of the mixing in the direction perpendicular to flow, had to be chosen in order to fit properly the break frequency in the amplitude curve. More experiments are needed to enable prediction of this constant in a given condition, in order to arrive at firm reactor design procedures.

This work was performed at Argonne National Laboratory, in Reactor Engineering Division's Heat Engineering Section, which is headed by Dr. Paul A. Lottes.

Thesis Supervisor: Dr. Elias P. Gyftopoulos
Title: Associate Professor in Nuclear Engineering.

ACKNOWLEDGEMENTS

Above all I would like to thank Professor Elias P. Gyftopoulos for his valuable support and guidance throughout the duration of this work, for his suggestions and criticisms, and for his willingness always to give freely of his time.

I am also very grateful to all members of the Heat Engineering Section of Argonne National Laboratory's Reactor Engineering Division, for their readiness to help and assist me at all times. My special thanks to Paul A. Lottes, John F. Marchaterre, and Michael Petrick for valuable discussions and helpful advice, to George T. Rezek who did the design work associated with the revision of the Small Scale Loop, to Barton M. Hoglund who wrote the computer program used, and to Joseph R. Kemp and Elmer R. Gunchin who helped in building the experimental equipment, and in taking and reducing the experimental data.

Final thanks to Jean Radcliff and to my wife Sylvi for their patience and skill in typing the manuscript.

TABLE OF CONTENTS

TABLE OF CONTENTS

TABLE OF CONTENTS

LIST OF ILLUSTRATIONS

LIST OF TABLES

PREFACE

The boiling water reactor is one of the types of reactors that shows the most promise for becoming a source of economic nuclear power. At the present, it seems clear that this goal can be achieved only by a concerted effort to improve the reactor design on all counts, particularly to try to reduce the capital cost per kilowatt of energy produced. It becomes vital, therefore, to understand completely all the different physical processes that take place in such reactors.

It is nearly a decade since the first boiling water reactor was built. Several such reactors have been operated, and much has been learned about their characteristics. Some uncertainties remain, however, and in particular, there are many problems related to the heat removal from the fuel, and the hydraulics of the reactor core for which only partial solutions have been found.

The present work concerns itself with one such problem: The prediction of the transient behavior of steam bubbles in the reactor core as the heat production in the fuel varies. This is expressed in a relation generally named the power-to-void transfer function.

This report is divided into four parts.

Part I consists of two chapters. The first gives a historical review of the field of boiling water reactor dynamics, with emphasis on points that have a bearing on the more narrow subject at hand. Chapter II sums up the present status, and points to several areas where further work is necessary.

The purpose of the present investigation is stated next, and the methods to be used are briefly mentioned.

Part II contains a description of the experimental equipment. Chapter III is designed to give the reader a general review of Part II, serving as an introduction to Chapters IV through IX, which treat separate parts of the system in greater detail. Although the pressure loop used was built previously, several revisions had to be made for the present experiment. The instrumentation used was designed and built as part of the present work. The system utilized to oscillate the test element heating power is believed to be unique.

Part III presents the theory of the experiment. Chapters X and XI give a general discussion of those aspects of nuclear boiling and two-phase flow phenomena believed to be of importance to the power-to-void transfer function. The derivation of this function at different conditions makes up the balance of Part III. Chapter XII presents the differential equations for the simplest case, and gives the solution in full to illustrate the general method used. In Chapter XII, the assumptions chosen allow the derivation of the transfer function from heat production in the wall to heat delivered to the coolant, separately from the problem of heat transport in the coolant channel.

This is no longer possible in Chapter XIII, where the heat transfer rate to the coolant is assumed to depend on the conditions in the coolant itself.

The transfer function thus becomes more complicated, but can be brought to a form similar to the results of Chapter XII. By comparing the two results, some interesting observations are made.

In Chapter XIV, the transfer functions applying to the conditions of the experiment have been derived, utilizing the results of the two previous chapters.

Part IV is a presentation of the experimental results. These are compared to the theory. Conclusions are drawn, and suggestions for future work in the field are listed.

Five appendixes at the end of the work treat some special problems which are related to the general material presented. Experimental data have also been tabulated here.

PART I

INTRODUCTION

CHAPTER I

HISTORICAL REVIEW

A. General Remarks

In boiling water reactors heat is removed from the core by the evaporation of water inside the core. Coolant water is passed through rectangular or annular channels, and nuclear boiling takes place along the channel walls.

The steam bubbles formed can be regarded as voids, where neither scattering nor absorption of neutrons take place. Therefore, the steam void population has an important effect upon the reactivity of the reactor system.

In the analysis of boiling water reactors, two problems arise which are unique to this type of reactor:

1. The distribution of steam bubbles within the reactor core must be found, and it is important to know how this distribution changes with conditions.
2. Methods must be found by which the reactivity effect of a certain steam void distribution can be calculated.

These points are of extreme importance to steady state as well as stability analysis of the reactor system.

The steam void distribution in the core is a strong function of many variables, such as: reactor power, reactor pressure, inlet temperature and flow rate of the coolant water. It was early realized that several possible mechanisms might exist that could give rise to instabilities in the steam void population, and therefore in the reactor power also. It was doubted whether boiling water reactors with natural circulation cooling would be safe.

The force driving the flow in a natural circulation system is supplied by the buoyancy of the steam bubbles in the heated section, and in the "riser section" above it. This steam volume, or void volume as it is generally referred to, can be ascribed a certain potential energy. It can be stated that oscillations can be sustained through one of two possible exchange mechanisms:

1. Oscillations between heat energy stored in the walls of the fuel element walls, and the "potential energy" of the voids as linked to reactivity.
2. Oscillations between the potential energy of the voids and the kinetic energy of the water around the hydraulic loop. Heat storage may, or may not, take part in this process.

In either case, oscillations will develop if the total phase shift around the complete signal flow path can reach a value of 180 degrees.

Careful design studies, and preliminary experimental work, mainly at Argonne National Laboratory, led to the conviction that boiling water reactors could be operated reliably and safely. This reactor concept was considered to show enough promise to warrant the building of a prototype.

B. Early Experimental Work

The history of the boiling water reactor up to 1958 has been reviewed by Kramer[1]. The first such reactor, the BORAX-I, was first operated in 1953 at the reactor testing station in Idaho. It is interesting to note that the BORAX-I, and the subsequent reactors in the BORAX series, were built primarily to study the dynamic characteristics of this type of reactor. This is the case also for the SPERT-I reactor which was built in Idaho a few years later.

The experiments with these reactors showed that the steam bubbles in the core had a negative effect on reactivity, and that this had an important self-regulating effect. Boiling water reactors proved to have a high degree of inherent safety in their ability to shut themselves down by expulsion of the

water from the core, even in the case of severe power excursions that were induced artificially for testing purposes.

Although these reactors proved easily controllable and highly stable at their design power level, they were all intentionally brought to higher and higher power levels until instabilities occured. The tests with SPERT-I, for instance, showed[2] that this reactor could go into sustained and even divergent oscillations under certain conditions.

Parallel to the reactor experiments, numerous investigations were carried out with natural circulation hydraulic loops, representative of boiling water reactor cores. Although this work was mainly of a steady state nature, it was shown[3,4,5] that these loops could oscillate also.

The realization that natural circulation systems could oscillate even without the driving force supplied by the reactivity feed-back effect present in reactors, brought up this question: Are the reactor oscillations due to the hydraulic effect, or to the reactivity feed-back effect?

For the SPERT-I reactor it has been shown[6] that the resonant frequencies for both effects are so close to the observed oscillation frequency of the reactor (approximately 1 cycle per second) that it must be clear that both effects play an important part.

Although it is of high interest in special cases to determine which of the two effects is the most important, the main issue is this: The physics involved in both effects mentioned must be fully understood. Next, the effects must be described mathematically in terms useful for stability analysis of complete reactor systems. The transfer function approach is the one most suitable for the purpose.

The present status as far as the meeting of these objectives is concerned will be reviewed in the sections to follow.

C. Theoretical Work Concerning Boiling Water Reactor Stability

Complete systems of equations describing the dynamical behaviour of boiling water reactors have been presented by Horning and Corben[7], Iriarte[8], Beckjord[9], Thie[10,11,12], Fleck and Huseby[13], Fleck[14], and Akcazu[15].

All authors calculate the variations in the total steam void population by the superposition principle, by adding linearly the effects on voids caused by changes in different variables. This allows the definition of: a power-to-void transfer function, a flow-to-void transfer function, a pressure-to-void transfer function, and an inlet temperature-to-void transfer function.

Because the present work is mainly concerned with the power-to-void transfer function, the treatment of this effect will be emphasized in the following discussion. Equations describing the power-to-void effect have been evaluated by all the authors mentioned, in various degrees of refinement. The main differences will now be pointed out. No attempt will be made to give a complete listing of the assumptions adopted in each case.

Some of the authors have lumped the reactor core parameters, and adopted a one-point model. The others have divided the core into two sharply defined sections:

1. The subcooled region, where the steam void fraction is taken equal to zero, and
2. The boiling region, where all the water is assumed to be at the saturation temperature.

Another assumption commonly adopted is that the pressure variations in the boiling section do not affect the rate of steam formation. Or, stated differently: It is assumed that no pressure variations take place in the boiling section, as far as the derivation of the power-to-void transfer function is concerned.

Horning and Corben[7] use the one-point model, and write one differential equation for the total steam volume. The heat capacity of the fuel is taken

into account, and a constant fractional removal rate of steam void is considered. These effects are described by two constants, the nature of which they did not discuss.

Iriarte[8] uses the one-point model also. He characterizes the power-to-void transfer function by two time constants and one time delay. The heat capacity of the fuel plates gives rise to one time constant. The other describes the steam bubble growth time. The time delay is the relaxation time for steam bubbles in the core. Iriarte calculates the closed loop transfer function for the Experimental Boiling Water Reactor. He finds close agreement with measured values, although this author finds that some of the constants mentioned above have been derived by methods less than satisfactory.

Beckjord[9] divides the fuel plate into several regions, and arrives at a three time-constant transfer function, linking power production in the fuel plate to power delivery to the coolant. The transfer function between the latter variable and the void volume in the boiling section is next derived by a difference method, and approximated by a one time-constant term. Beckjord does not take into account the contributions to the power-to-void transfer function from the non-boiling section.

The authors to be mentioned next, have taken care of this effect by letting the boundary line between the non-boiling and the boiling section be a function of time.

Thie[10,11,12] solves the distributed parameter equations for the heat transport in the fuel, and for bubble transport in the channel. The results are expanded in Taylor series', and the first term defines a single time constant for each of the two effects. Thie's very valuable work in this field is difficult to appreciate, because of some lack of clarity in the presentation.

Fleck and Huseby[13], and Fleck[14] assume that the conditions in the boiling section can be described by a linear variation with channel height of the

variables: void fraction, water velocity, and steam velocity. Lumped parameter equations describe the heat transport from fuel plate to liquid. For the transport of disturbances along the coolant channel, the distributed parameter equations are written. These are next integrated along the channel height to yield lumped parameter approximations. Fleck and Huseby are the only authors to account satisfactorily for the nuclear radiation heat deposited directly in the coolant. This has been shown[17] to have an important stabilizing effect in certain cases.

Akcazu[15] recognizes that perturbations in void volume may not propagate along the boiling section with a velocity equal to the steam velocity. This means that a perturbation in steam mass flow rate may cause the local steam velocity to change, so that the local void fraction changes less than would otherwise be expected.

Akcazu argues that the perturbation velocity should be taken greater than the steam velocity at atmospheric pressure. A delay effect associated with bubble growth must then be assumed to explain the data of Zivi and Wright[16]. At higher pressures Akcazu takes the perturbation velocity equal to the steam velocity. Akcazu assumes that the transient heat flow out into the coolant is a function of the fuel temperature only.

Zivi and Wright assume that perturbations in steam void fraction travel with the velocity of water, and that variations in the steam production in the boiling section is completely taken care of by an increase in steam velocity. This implies that the power-to-void transfer function is completely governed by heat perturbations in the non-boiling section. This very simple model agrees surprisingly well with the experimental results of Zivi and Wright, to be mentioned in the next section. It is questioned by this author whether the model will hold for different values of the subcooling temperature.

D. Recent Experimental Work

Reference will first be made to three experiments performed in reactors, and concerned with the effects of variable steam void concentrations. Next three selected experiments done on natural circulation loops will be discussed.

An attempt was made by Daavettila[18] to measure dynamic void effects in a critical assembly. The object was to measure the void volume by its reactivity worth. Steam was produced in the reactor core by boiling from rods which were heated electrically. This arrangement produced temperature changes which almost masked out the reactivity effect of the void variations.

Eriksen[19] used an oscillation technique to measure the reactivity effects of voids at different positions in a reactor. He showed that the worth of a void volume is a very strong function of its nearness to the fuel surface. This experiment was performed in a heavy water reactor with large lattice spacing. The effect must be expected to appear in light water reactors also.

The following conclusion can be drawn from the results of the two experiments mentioned above: A reactor is a very poor void detector for studies of dynamic boiling phenomena.

A series of very important experiments were carried out by DeShong and Lipinski[20] on the Experimental Boiling Water Reactor. The transfer function of the reactor was measured at several low powers by the rod oscillator technique. The measured curves were fitted to a theoretical model for the reactor system kinetics by means of an analog computer. The time constants in the different feed-back loops were adjusted to give the best fit to the experimental results for each run. The values thus obtained were plotted as functions of power and extrapolated to higher powers. Based on these extrapolations transfer functions at higher powers were calculated. The results predicted that the reactor would be stable at powers up to 65 Mw.

The EBWR was subsequently run safely at powers as high as 61.7 Mw, which compares to a design power of 20 Mw. The transfer functions measured at higher powers agreed well with the calculated curves. It has been pointed out by DeShong and Lipinski that some of the constants resulting from the fitting procedure varied with power in an inconsistent manner.

The importance of this work is to show that a system as complicated as a boiling water reactor can be well represented by a linearized, lumped parameter model. The inconsistencies mentioned point out the difficulty in assigning exact physical meanings to the different constants of such a simplified model.

As mentioned in Section B, natural circulation loops may exhibit hydrodynamic instabilities independently of any coupling between voids and power. The instability generally manifests itself as periodic variations in the flow rate at the test section inlet. In the majority of cases the variations of the system parameters can be well approximated by sinusoidal oscillations. These systems should therefore lend themselves well to stability analysis, by using the complex transfer function theory developed by workers in the servo field[21]. Yet very few attempts have been made to study hydrodynamic instabilities along these lines. Some notable exceptions will now be mentioned.

Wallis and Heasley[22] studied a natural circulation loop at atmospheric pressure with penthane as the working fluid. The differential equations for the system are presented, and solved in the complex frequency domain for small perturbations in the variables. This mathematical model shows the same mode of oscillations as were observed experimentally.

Beckjord[23] has studied the stability of a water loop at 68 Atm (1000 psi). The condition for stability was found through a mathematical method similar to the one used by Wallis and Heasley. Beckjord has focused attention on the riser section. **Steady state void fractions were measured.**

Through an averaging procedure the heated section has been reduced to a point model, and no heat storage effects in this section have been considered.

The only experiment known to this author where the heat input to a boiling test section has been varied sinusoidally, was carried out by Zivi and Wright[16,24,25]. The experiment was performed at atmospheric pressure in a natural circulation loop, representative of the core geometry of the SPERT-I reactor. The power-to-void and the power-to-flow transfer functions were measured as mentioned in the previous section. An analytical model predicts hydrodynamic instabilities in the absence of power oscillations.

To conclude this introductory chapter, the following statements seem to be justified:

1. It has been shown experimentally, especially through the work of DeShong and Lipinski, that the transfer function method is extremely useful in analyzing boiling water reactor stability.
2. The state of the art is now such that the dynamic characteristics of a boiling water reactor in operation can be determined fairly accurately, through use of the rod oscillator technique.
3. Much has been learned about the possible causes for instability. It is now possible to design a boiling water reactor with a high degree of stability.
4. However, it is still necessary to introduce very large safety margins, as the exact description of the several mechanisms involved is still lacking.
5. It is believed that the weakest links in all the mathematical models for boiling water reactor stability referred to, are the equations describing transient heat transfer to the boiling mixture, and the dynamic behaviour of steam bubbles in the channel.

CHAPTER II

OUTLINE OF THE PRESENT WORK

A. Possible Areas for Investigation

As a result of major efforts at numerous research laboratories during the last five to ten years, the steady state conditions in a boiling channel can now be fairly well described in terms of average values of the parameters involved. However, present day knowledge is to a large extent empirical. Much is to be desired in the understanding of such basic processes as: Heat removal from a wall in nuclear boiling, the collapse of steam bubbles in turbulent subcooled water, the relative velocity of steam and water in a vertical channel, to name a few.

It was brought out in Chapter I that in order to predict the dynamic behaviour of boiling water reactors, it is of utmost importance to fully understand the different effects which may alter the void distribution in the reactor core. This points to a whole field virtually untouched by experimenters. Most of the work done so far, has been on complete reactor systems. These are so complex that it becomes extremely difficult, if not impossible, to separate all the physical processes involved.

Any mathematical model describing transient boiling phenomena had, therefore, to be based on certain assumptions, the validity of which is difficult to ascertain. Careful experiments are needed to test these assumptions.

It was felt that to further the knowledge in the field of boiling water reactor dynamics, an experimental study of void transients in a boiling test channel would be of great value at the present time.

Because there are so many uncertainties regarding the boiling process, the experiment should be simple, with as many variables as possible kept constant.

B. The Purpose and the Procedures of the Present Work

The purpose of the present work was to test experimentally the assumptions upon which the derivation of the power-to-void transfer function for pressurized boiling water reactors is based.

A rectangular boiling test channel, comparable in size to the coolant channels of a boiling water power reactor, was studied at representative conditions. The direct aim of the experiment was to measure the power-to-void transfer function for the channel.

This was done by oscillating the heating power to the channel walls sinusoidally around an average value at various frequencies, and observing the variations in void fraction at different points along the channel.

Theoretical power-to-void transfer functions were derived, and compared with the experimental results. This was done for the main purpose of testing the validity of different assumptions, rather than to present formulas immediately useful to reactor designers.

The application of the present work is concerned with boiling water reactor stability. It is pointed out again, however, that the primary purpose of this investigation was to gain further insight into the transient behaviour of steam/water mixtures.

To simplify the interpretation of the results, these parameters were maintained at constant values:

1. Inlet water flow rate to the test channel.
2. Temperature of the inlet water.
3. Pressure at the outlet of the test section.
4. Average heating power.
5. Heating power per unit height of the test channel.

To meet these requirements, the experiment had to be carried out in a pressurized heat transfer loop with forced circulation. Such a loop was made available by the Reactor Engineering Division of Argonne National Laboratory, where the work was done.

PART II

DESCRIPTION OF EXPERIMENTAL EQUIPMENT AND TECHNIQUES

CHAPTER III

SHORT REVIEW OF THE EXPERIMENT

The purpose of the experiment was to oscillate sinusoidally the heating power to a boiling test channel, and observe the void oscillations which resulted. A short review of the experiment and the equipment used is given below. In the chapters to follow, more detailed descriptions will be given.

The test section was a rectangular tube of stainless steel. The heated height was 127 cm, and the inner channel dimensions were 4.44 x 1.11 cm. A rectangular channel was chosen, partly because of its importance to the EBWR program, and partly because this geometry is particularly well suited to the void detector system used.

The test tube was heated uniformly along its length by passing an AC current of several thousand Amps through the test section wall. The wall thickness was 0.09 cm.

The "Small Scale Loop" in the Heat Engineering Laboratory of Argonne National Laboratory was used for the experiment. A sketch of the loop has been given in Figure 1, and Figure 2 gives a view of the control panel. This loop was originally built for pressurized water studies, and had to be partly revised for this experiment. Forced circulation was provided by a canned rotor pump.

The water temperature at the inlet of the test section could be set at the desired value by opening partly for the flow through the heat exchanger, and by manipulating the four electric line heaters shown in Figure 1. The inlet and outlet temperatures were measured by bare Chromel-Alumel thermocouples in the stream. The wall temperature of the test section was measured

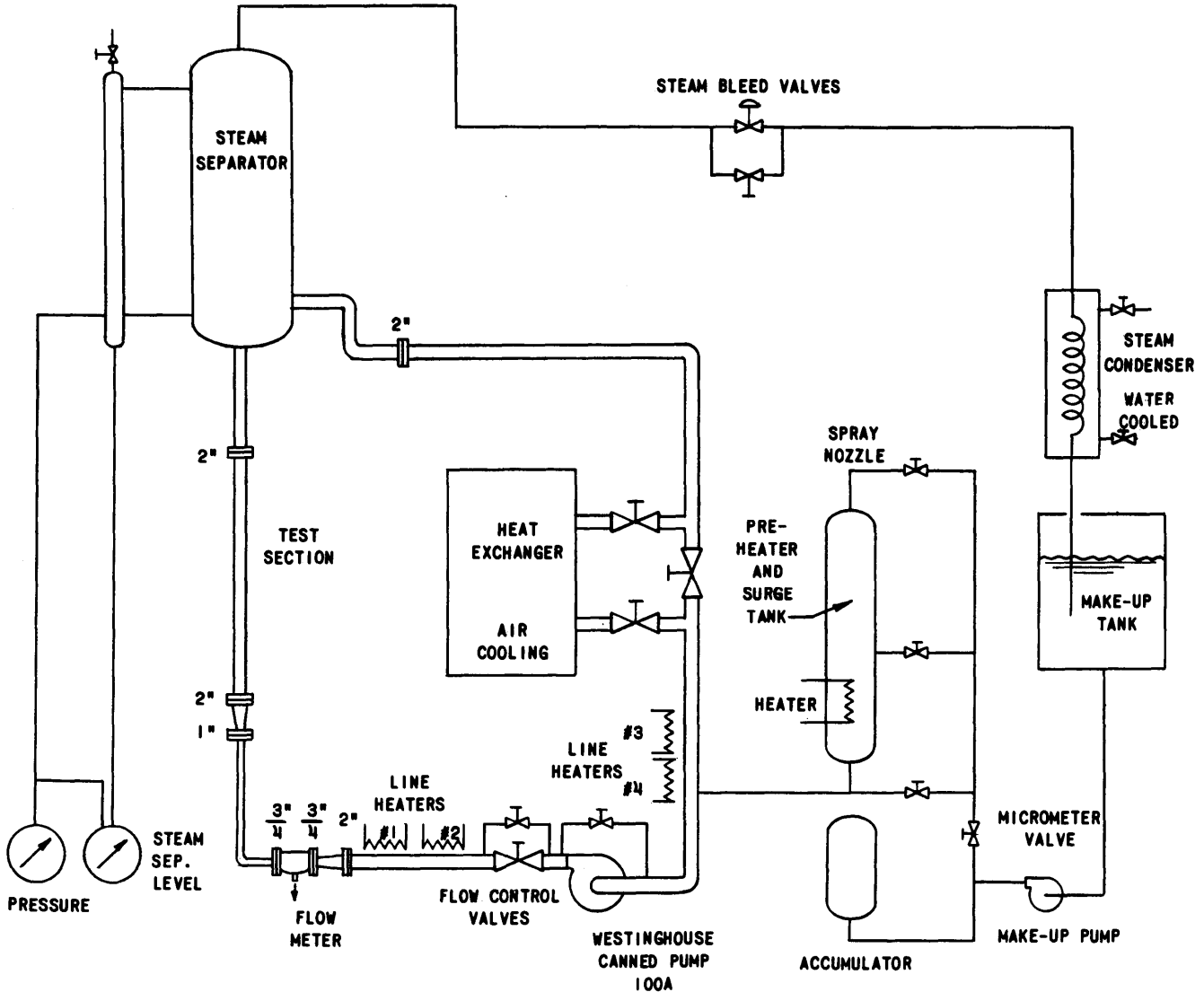

FIG. 1
DIAGRAM OF THE SMALL SCALE LOOP

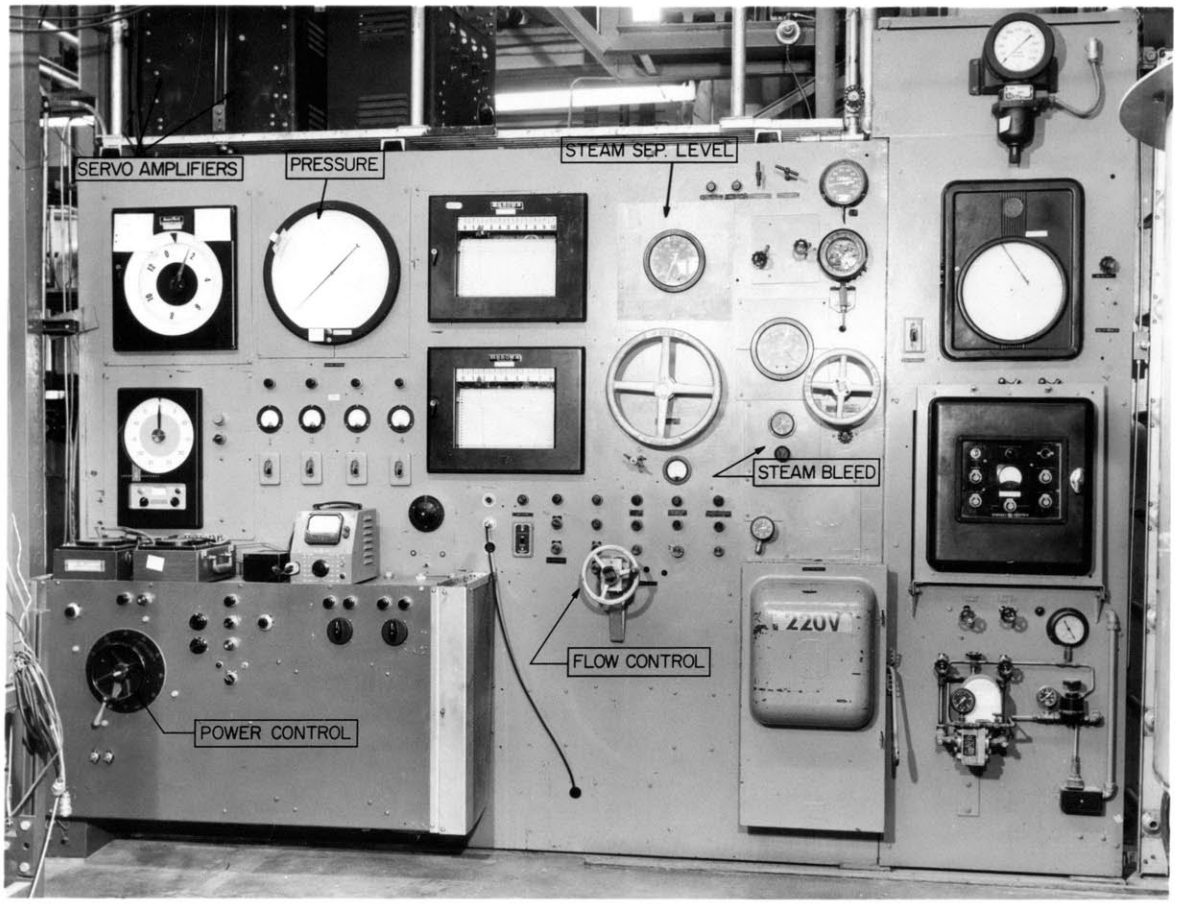

FIGURE 2

CONTROL PANEL FOR THE SMALL SCALE LOOP

at 12 different points along the height, by using Chromel-Alumel thermocouples welded to the outside of the tube.

The inlet water flow rate was measured by a flow meter of the propeller type in the lower leg of the loop. A block diagram of the instrumentation used for the experiment has been given in Figure 3.

The Small Scale Loop was powered by a 92 KVA transformer, and the average power level was controlled by a set of DC reactors in series with the primary transformer winding. This control system proved much too slow to be used for varying the test section power throughout the desired frequency range of 0.01 to 10 cycles per second. Therefore a separate control system for producing the sinusoidal power variation was built, based on the fact that the power transformer resembles a constant current generator. A current shunt with the total capacity of 400 Amps was built and connected in parallel with the test section. When the shunt current was varied sinusoidally, sinusoidal power variations were produced in the test section. The current in the shunt was controlled by an array of 20 silicon controlled rectifiers. These were triggered in sequence to produce the desired effect. This system, including the electronic triggering equipment for the rectifiers, was designed and built for this experiment.

To produce the primary driving signal for the power oscillator, a speed controlled servo system was used, see Figure 3. By adjusting the motor speed and the gear ratio, the output axel could be set to rotate at any speed in the interval 0.01 - 10 revolutions per second. A sine potentiometer, geared to the output axel, produced the driving signal to the power oscillator.

A steam void detector system was built, based on the gamma attenuation technique. Radiation from a Thulium-170 source was beamed through the test section to a scintillation crystal, photo multiplier detector. The signal current, which was an exponential function of the void fraction, was amplified

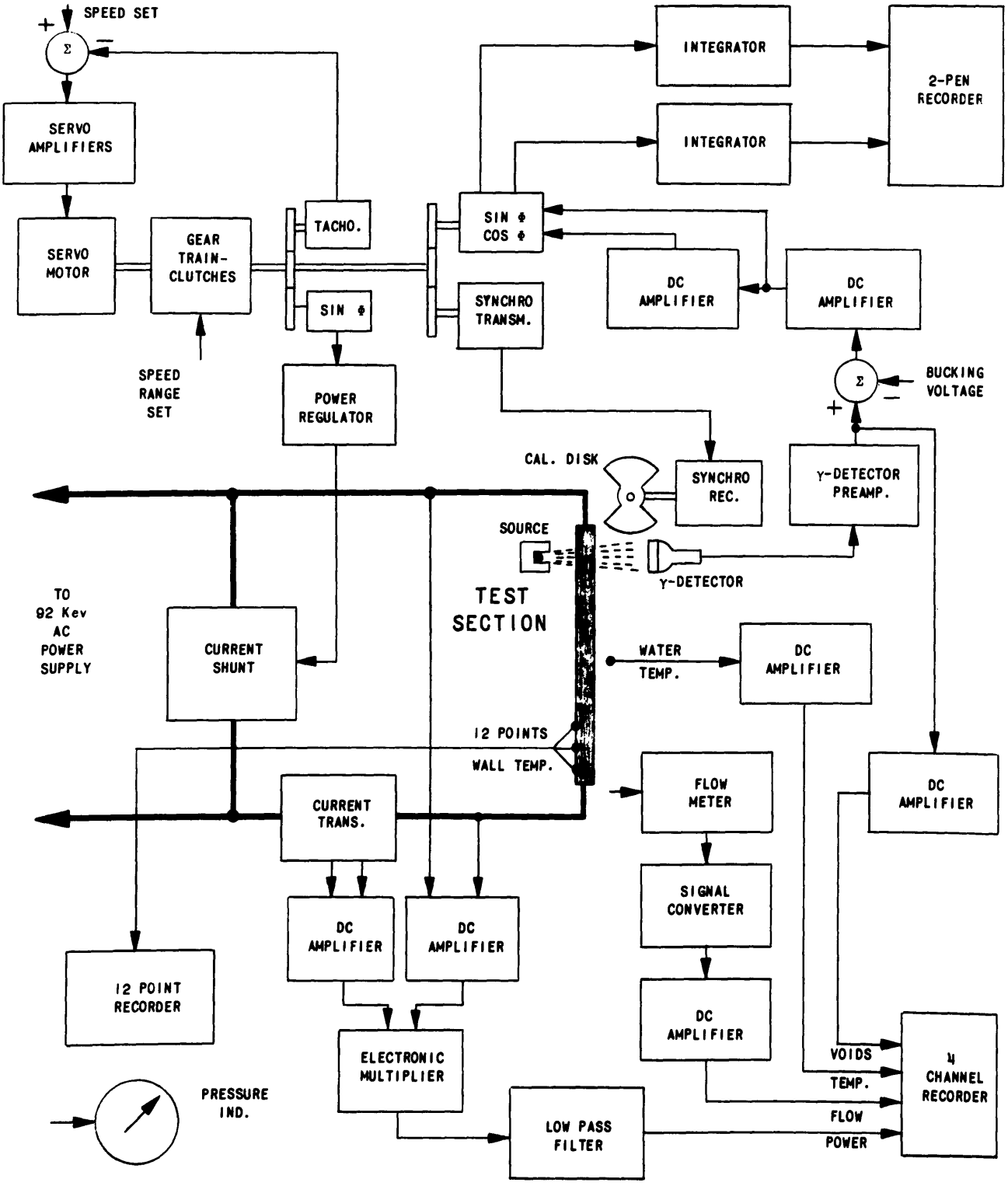

FIG. 3
INSTRUMENTATION BLOCK DIAGRAM

in a DC amplifier as shown in Figure 3. Here the signal path divides in two, one for the measurement of average void fraction, the other for the measurement of void oscillations. For the latter purpose, a wave analyzer - or harmonic analyzer - was built, which picks out the coherent void variations in a background of source noise and boiling noise.

A four channel recorder, shown in Figure 4, was used to take simultaneous readings of four important loop variables: the heating power, the inlet flow rate, the average void fraction, and the inlet water temperature. For accurate measurements of temperature, a potentiometer bridge was used. The recorder was convenient, however, to check that the inlet temperature did not drift during a run.

The other major loop parameter, the pressure in the steam separator, was read on an indicator instrument, and controlled manually by bleeding steam from the separator.

It would normally take about 3 hours to start up the loop and stabilize it at a given operating point, unless it was necessary to hunt for a specific value of the inlet temperature. In such cases it could take several hours more before the loop was ready for the start of oscillations. To complete a transfer function measurement at one height could take from 2 to 3 hours, depending upon the number of frequencies taken.

As it required an additional one hour to shut down the loop, a shift schedule was maintained for the taking of data in order to extend the useful part of the day.

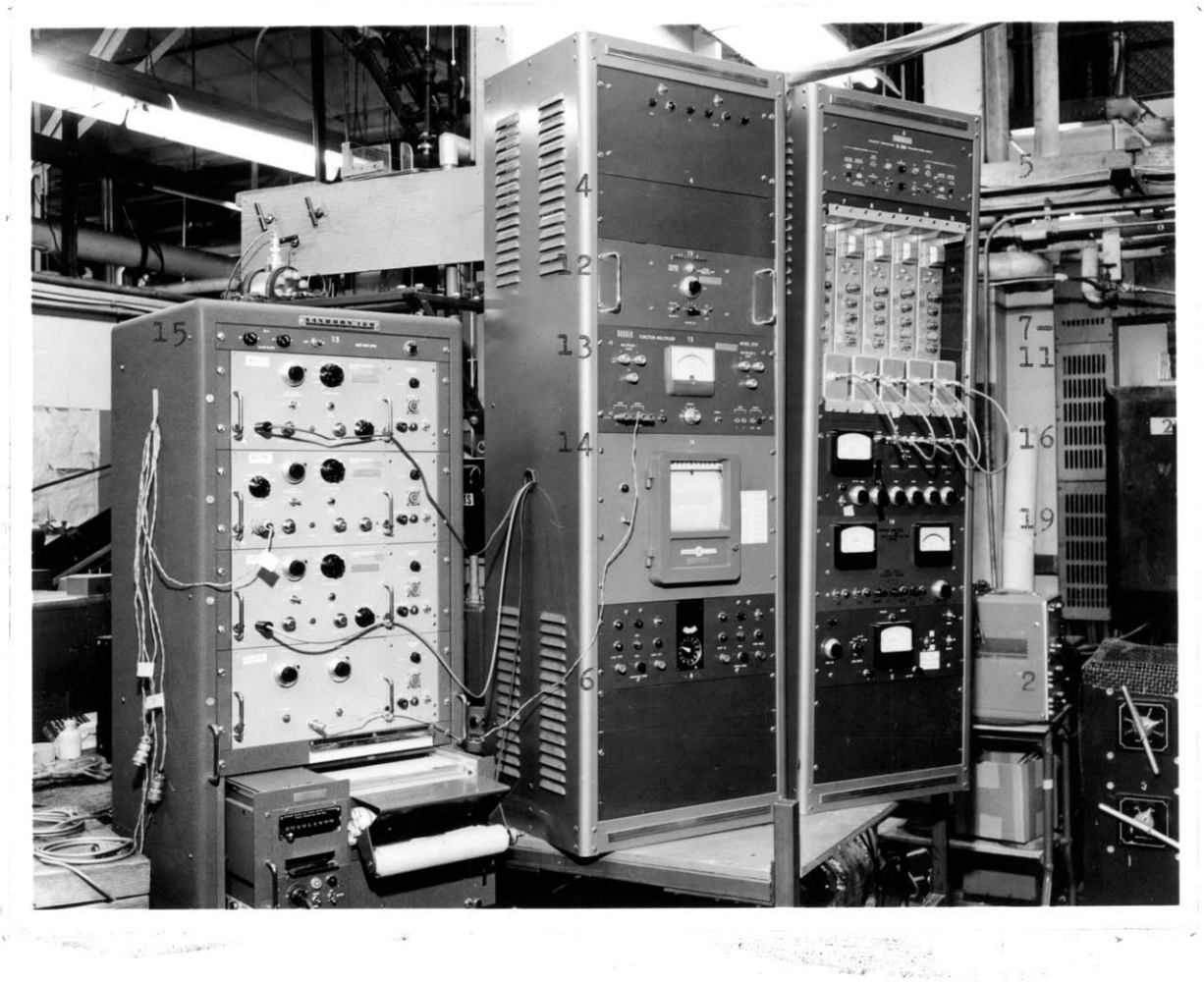

FIGURE 4

INSTRUMENT RACKS AND 4 CHANNEL RECORDER

2 SERVO CONTROL UNIT
4 POWER REGULATOR
5 REGULATED DC SUPPLY
6 TRAVERSE CONTROL
7 INVERTER AMPLIFIER
8 INTEGRATOR
9 INTEGRATOR
10 CURRENT SIGNAL AMP.
11 VOLTAGE SIGNAL AMP.
12 FLOW SIGNAL CONVERTER
13 ELECTRONIC MULTIPLIER
14 WAVE ANALYZER RECORDER
15 4 CHANNEL SANBORN RECORDER WITH PREAMPLIFIERS
16 γ-SIGNAL BUCKING VOLTAGE AMPLITUDE SETPOINTS FOR UNITS 7-11

CHAPTER IV

THE SMALL SCALE LOOP

A. General Description

The "Small Scale Loop" was considered the most suitable for this experiment, among the heat transfer loops in the Heat Engineering Laboratory at Argonne National Laboratory. It is a forced circulation loop, built for pressures up to 170 Atm (2500 psi) at water saturation temperature. A schematic of the loop is shown in Figure 1. Figure 2 gives a photograph of the loop control panel.

Water flow is maintained by a Westinghouse canned rotor pump, type A 100. The main water loop is made of 2 inch pipe. All pipes and flanges, and also the test section itself, were insulated thermally during runs.

Above the test section there is a steam separator, from which the steam is removed through a bleed valve. The steam condenseruns into a makeup tank.

A heat exchanger in the main flow loop can be valved all the way in or out, to give the desired temperature at the test section inlet. The heat exchanger is air cooled, and only a fraction of its cooling capacity was normally used. Four line heaters with a total capacity of 12 kilowatts can be used to make up for heat losses around the loop, in the case where an inlet temperature close to saturation is desired.

A high pressure feed water pump supplies make-up water to the loop. An accumulator system is used to give a continuous, smooth flow. The gas pressure in the accumulator, usually 5 to 10 atmospheres above the loop operating pressure, is regulated by an automatic on/off controller, which operates the pump. The make up flow rate is controlled by a micrometer valve. The return water can be piped into the lower leg of the loop, or through a preheater tank.

The Small Scale Loop was originally designed for pressurized water studies, and had to be revised to meet the requirements of this experiment. To facilitate

the close control of loop pressure, the steam bleed-off system was added. A steam separator and a steam condenser was built, and connected as shown in Figure 1. The make up system used belongs to the Armadilla Loop, which is located in the same laboratory. Provisions were made to allow alternative use of the system with both loops.

B. Operating Experience with the Loop

After the correct make up flow rate had been found, and the loop had stabilized thermally, the loop could normally be kept at constant conditions throughout the day, by small adjustments in heating power and steam bleed off rate.

The manual control system for the electrical heating power, which is described in the next chapter, was not well suited to maintain constant average power in the presence of changes in the power line voltage. The average heating power, therefore, had to be watched continuously and adjusted at relatively frequent intervals.

Mainly due to the drift in power, the loop pressure also had to be continuously regulated. The steam bleed valve, which was pneumatically operated from the loop control panel, was very accurate. At all but the highest heating powers used, the pressure in the steam separator was controlled to within $\pm$ 0.1 atmospheres.

The volume capacity of the steam separator proved to be too small at the lowest frequencies to completely quench pressure variations caused by the power oscillation. The effect was not seen above 0.1 cycles per second. It was first tried to keep the pressure constant by following the power cycle with the steam bleed valve. This however, resulted in too much scatter in the measurement of void amplitudes. Better results were obtained by just letting the pressure swing. The readings of void amplitude now proved to be quite consistent, but a reduction in amplitude at the very lowest frequencies was observed. The result of this effect on transfer function measurements, and possible means of correcting it, has been discussed in Part IV.

Most of the pressure drop around the loop was taken up by the main flow control valve. At the relatively low flow rates used, no measurable change in flow resulted from power oscillations. The flow was very easy to control, and changes in valve settings during a day's run were seldom needed.

The variable most difficult to control was the inlet water temperature. Because of the large heat capacities of the steel structure of the loop, and of the water in it, the best results were obtained by just leaving the settings alone after the loop had been stabilized at the desired point. Thiskept drifts in the temperature to within $\pm$ 1 degree C of the desired value.

CHAPTER V

THE BOILING TEST SECTION

Figure 5 shows a drawing of the test section used. The test tube itself was rectangular, made of 304 stainless steel. The wall thickness was 0.090 cm, and the flow cross section 1.11 x 4.44 cm. The design pressure in hot condition was 70 atmospheres. To keep the section from deforming, heavy back-up plates were used. These were insulated electrically and thermally from the test tube by 0.24 cm layers of Durabla. The back-up plates were held together by 2 x 17 bolts, spaced 7.62 cm (3 inches) apart.

Spacer rings and steel liner strips, both made to close tolerance, defined the distance between the back-up plates, which held the test tube firmly without crushing it. The purpose of the liner strips, which can be seen in one of the life size sections of Figure 5, as well as in Figure 6, was to prevent gamma leakage through the Durabla insulation.

The test tube was joined to end pieces by silver soldering along a 7 cm length. This facilitated the passage of heating current through the end pieces to the test tube itself. The heated length of the test tube was 127 cm. Copper bus bars were bolted to the end pieces. The test section ended in 2500 pounds, 2 inch, lap joint flanges, which fitted into the Small Scale Loop.

As shown schematically in Figure 1, there was an inlet section directly below the test element. A transition piece, located in this inlet section, and photographed in Figure 6, fitted into the spider shown at the bottom of the test section. This arrangement served to give a smooth flow transition from a one inch circular pipe to the rectangular test section. The flow areas of the two were the same.

The dimensions of the test section were arrived at as the best compromise between these requirements:

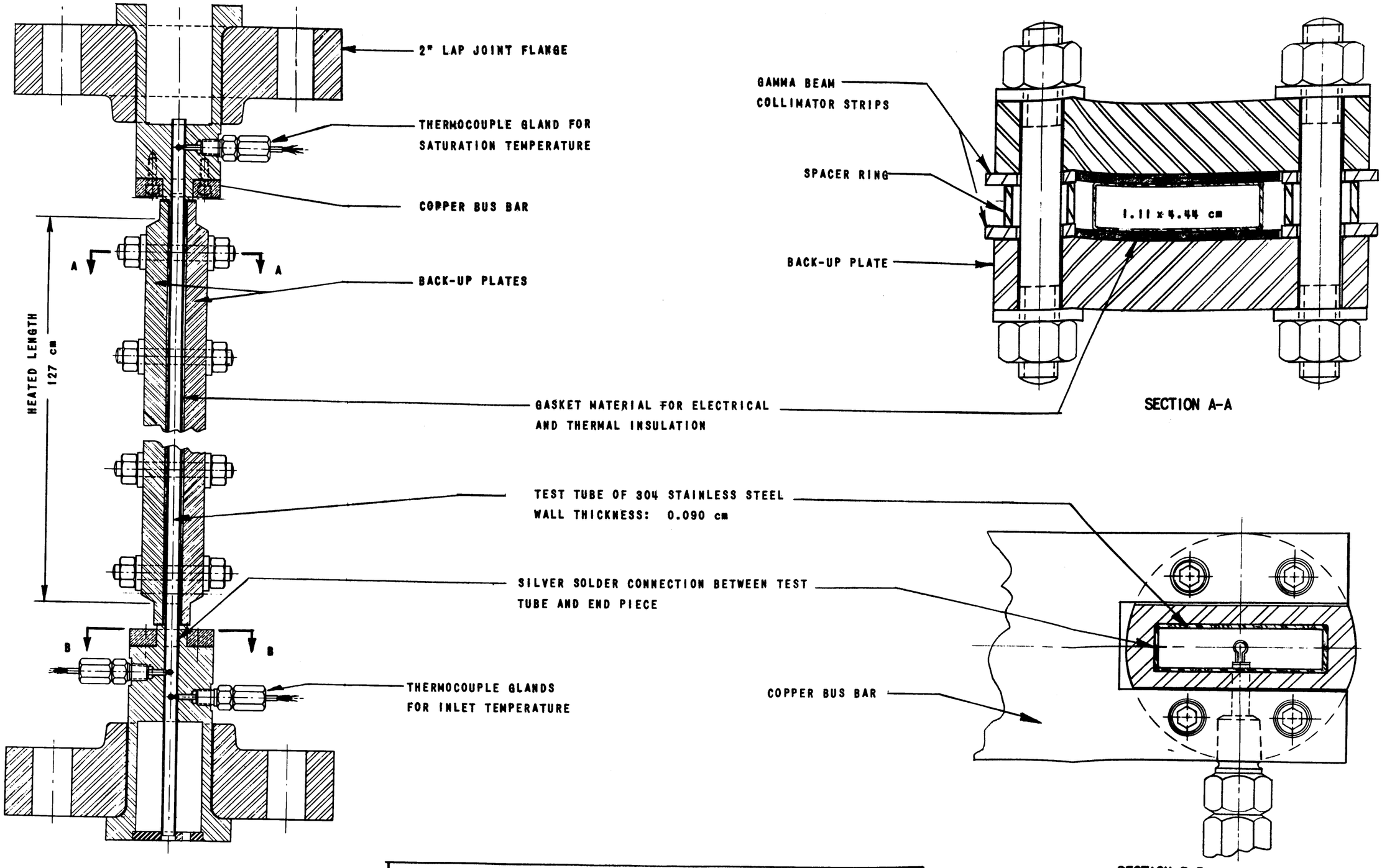

FIG. 5
BOILING TEST SECTION. VIEWS A AND B SHOWN TO ACTUAL SIZE

FIGURE 6

THE TEST SECTION

WITH BACK-UP PLATES REMOVED

1. The tube wall should be thin to give high gamma transmission.
2. The tube wall should be thin to give a small thermal time lag and enhance the boiling and the transport effects in the two-phase mixture.
3. The gamma ray water path should be long to give a large empty-to-full ratio (see Chapter VII).
4. The water cross section must be small enough to assure that the power supply is sufficient to give the desired void fractions at the flow rates wanted.
5. The ohmic resistance of the test section must match the power supply.
6. The back-up plates must be thermally insulated from the test section, to assure that no heat pulsates back and forth.
7. The test tube must be able to hold 70 atmospheres at 340° C.

The test tube was made from stainless steel plate. Two L-pieces were bent up and joined by weld seams in opposite corners. The tube was made in the Central Shops of Argonne National Laboratory, to tolerances of ± 5 mils (0.013 cm).

Figure 6 shows a photograph of the test section with the back-up plates removed. The positions of 12 thermocouples welded to the outside of the test tube can be seen. When in place, the ends of the back-up plates butted against stops in the two end pieces. During the assembly, the test tube was stressed lengthwise, to improve the mechanical stability of the test section. The back-up plates were packed with dry ice, and the test tube was heated by internal electric heaters. The test tube expanded a total of 0.1 cm compared to the back-up plates, and the gaps formed in both ends between the back-up plates and the stops were filled with Mica spacers.

The back-up plates were insulated electrically from the end pieces and from the test section. The plates were made of non-magnetic stainless steel, to eliminate induction heating from the test tube current.

As shown in Figure 5, screw fittings for thermocouples were supplied in both end pieces, two at the inlet and one at the outlet. These fittings were made for Conax Thermocouple Glands, type TG-24-A4, each of which carry two Chromel-Alumel couples. Pressure taps could also be inserted in these positions for pressure drop measurements.

CHAPTER VI

THE POWER OSCILLATOR

A. The Small Scale Loop Power Supply

The power supply normally used with the Small Scale Loop is a 60 cycle AC supply, capable of delivering a maximum of 92 kilowatts at 33.5 volts and 2750 amps. The power to the test section can be varied from zero to maximum value by the following arrangement: In series with the primary winding of the output transformer, there are three saturable reactors capable of taking up the full 220 V primary voltage. The DC control current to the saturable reactors is set by regulating the voltage to a full wave rectifier system by means of a powerstat, the location of which is shown in Figure 2.

For this experiment it was necessary to oscillate the power to the test section sinusoidally around the average value, with a peak to peak amplitude of 10%, or more if possible. The desired frequency range was 0.01 to 10 cycles per second.

B. Possible Oscillator Schemes

Three different possibilities for accomplishing this were considered.

1. Oscillating the DC control current to the saturable reactors.
2. Using a separate 10 kilowatt power supply, which could be oscillated.
3. Bypassing some of the test element current through a shunt of variable resistance.

It was quickly established that the components of the existing control system could not be used, as the time constants of these units were too large. As for the second method, a low frequency oscillator with a peak output of 10 kilowatts is hard to come by. Another difficulty was one of matching the impedances between the test section and the two power supplies, to avoid interaction between the latter.

It was felt that the third method only had real promise. An experiment was carried out to measure the step response of the power transformer. A shunt resistor of stainless steel strips was made. It was connected across the secondary side of the power transformer through a contactor capable of handling 300 amps. With the Armadillo test loop, which also uses this power supply, running at 30 kw, the contactor was closed, and the system voltages were recorded on a fast oscillograph. It was observed that the power in the Armadillo test element jumped to its new value within one cycle of the 60 cycle power. The percentage change in the test element power was found approximately equal to the percentage of the total current which flowed through the shunt resistance. The test showed that although the output transformer did not act as a true constant current device, the effect was large enough to be used for the purpose.

C. Description of the System Used

The difficulty of making a resistor which can be varied sinusoidally, and which has a current carrying capacity of several hundred amps is apparent. It was decided instead to make a unit consisting of 10 separate fixed resistors. These could be connected in parallel with the test element in a sequence designed to give the best approximation of a sine variation in the test element power.

A mechanical switching system was being designed when a new semiconductor component, the silicon controlled rectifier, was brought out on the market. This unit was particularly well suited for the purpose. Not only could each of the ten shunt rectifier subunits be fully connected at staggered intervals in order to simulate a sine curve by 10 steps, but each of the subunits could be gradually opened for current flow, to give a closer fit to the sine curve. Rectifier losses would be small, as the forward voltage drop across a silicon controlled rectifier is in the order of one volt, as compared to the arch voltage drop of about 10 volts in an ordinary thyratron.

The system built consisted of 10 subunits, each connected as shown in Figure 7. The current through the shunt resistor was governed by two silicon controlled rectifiers, type Transitron TCR-1020, in a full wave arrangement. The resistor was aircooled, made of nichrome strips, and as indicated in the diagram, the resistance can be set at any value between 1/2 and 2 Ohms. A photograph of the shunt resistor bank is given in Figure 8. The silicon controlled rectifiers mounted on cooling plates, can be seen along the top of the unit.

The rectifiers would not conduct unless trigger pulses were applied at the gate electrodes. Magnetic Trigger Units for this purpose are now commercially available. The units used were Avion Type 410-13. Variation of a DC control current from 0 to 2.5 milliamps, would delay the trigger pulses from 0 to 180 degrees.

This control current was supplied from a triode circuit as shown in Figure 7. The connections were such that with a zero control signal to the triode grid, both rectifiers would be fully conducting. With the control signal at its maximum value, both rectifiers would be completely cut off. The switching action took place in a relatively narrow voltage interval, as the control signal swept by the triode bias point. The potentiometer P-1 allowed adjustment of this bias level, and through the potentiometer P-2 the width of the switching interval could be adjusted. The bias signals to all 10 subunits were supplied from a ladder network as indicated on Figure 7. A series of 10 four volt Zener-diodes stabilized the voltages along the chain. The bias to the 10 cathodes were staggered approximately four volts, The switching interval for each subunit was approximately eight volts. The overlapping between units that resulted, gave better linearity in the relationship between control signal and total shunt current.

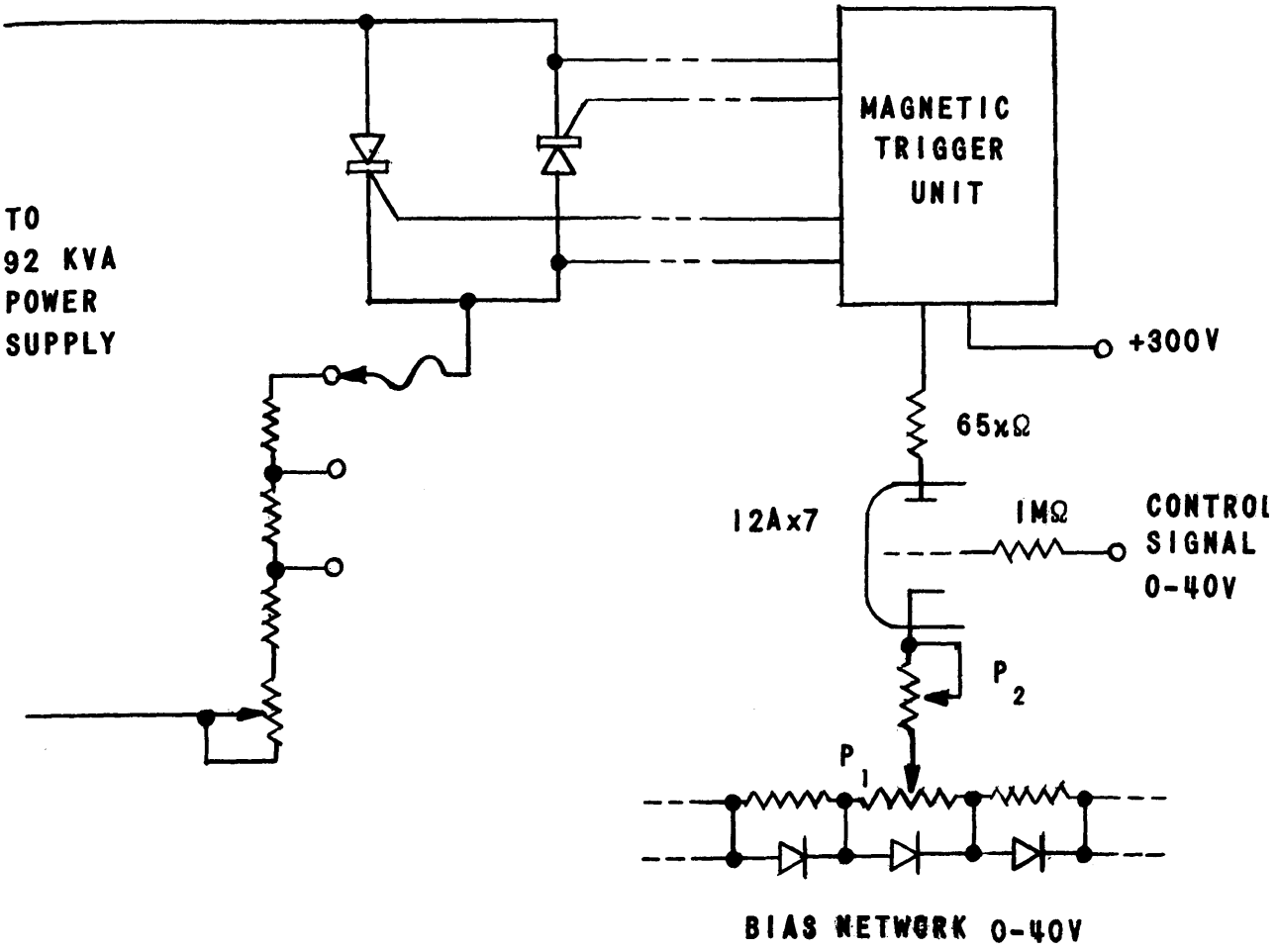

FIG. 7-
WIRING DIAGRAM FOR ONE OF 10 SUB-UNITS FOR THE POWER REGULATOR

FIGURE 8

THE SHUNT RESISTOR ASSEMBLY

The same control signal was supplied to all the 10 grids of the system. The power regulator was able to reproduce any wave form of a control signal input. For this experiment, however, a sinusoidal control signal was used.

The control circuits for all 10 subunits were contained in unit 4 of Figure 4. By removing the panel just below the number 4, access was gained to the 20 adjustment potentiometers. After the power regulator system was installed, these potentiometers were given a last adjustment, to make the recorded power trace conform to a sinusoid.

D. The Speed Servo

The control signal to the power regulator was supplied from a sine potentiometer, as shown in the block diagram Figure 3. The sine potentiometer was driven by a servo system, also shown. The servo motor and the servo amplifiers were found in storage. The gear unit which was built specially for this experiment is shown in Figure 9. The speed of the servo motor itself could be accurately controlled through a speed ratio of 10 to 1. A system of gears and clutches extended this range to 3 decades. Geared to the output axel of the unit were the sine potentiometer mentioned above, another sine potentiometer belonging to the wave analyzer, and a syncro transmitter which ran a calibration disk for the wave analyzer. The functions of the latter two units will be described more fully in the chapters to follow.

Panel 2 in Figure 4 contains the control unit for the servo system. From here, the servo speed could be set to the desired speed within an accuracy of 0.5%. A switch, which energized one of the three magnetic clutches, controlled the speed range. The error voltage in the servo loop was displayed on the meter shown. The calibration disk was controlled from this panel also.

E. Operating Experience with the Power Regulator

A feedback effect through the system controlling average power to the loop had not been anticipated, and reduced the efficiency of the power regulator as follows:

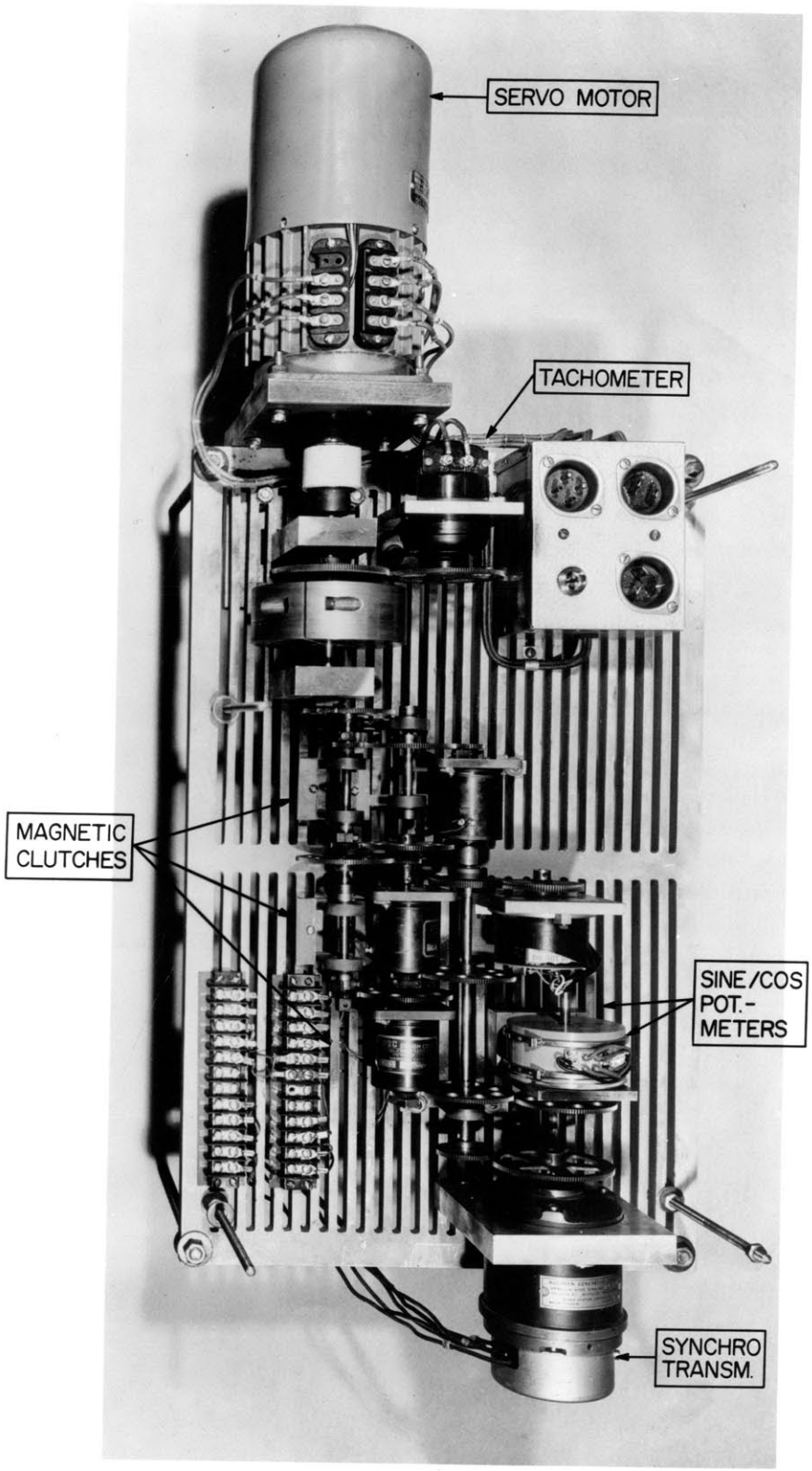

FIGURE 9

THE SERVO GEAR UNIT

1. When the system was being run at constant average power, and at a given setting of the shunt resistors, the oscillation amplitude would decrease with increasing oscillation frequency.
2. At a given oscillation frequency, and for a given shunt resistor setting, the oscillation amplitude would decrease with increasing average test element power.

These effects are shown in Figure 10. It was possible, butvery time consuming, to reset the shunt resistors for each new setting of the frequency, to obtain the same power amplitude throughout. Usually the amplitude was allowed to vary within limits. Gross adjustments were made by resetting the plugs shown in Figure 8.

The maximum shunt resistor current was 400 amps. This was sufficient to give the desired 10% peak to peak power swing at the lower average power levels utilized. At higher power levels, the shunt could carry only a smaller percentage of the total test element current, and a smaller relative oscillation amplitude resulted. The system was found satisfactory for the experiments described in this report. If necessary for future use, higher oscillation amplitudes could be obtained by exchanging the present silicon controlled rectifiers with 50 amp units.

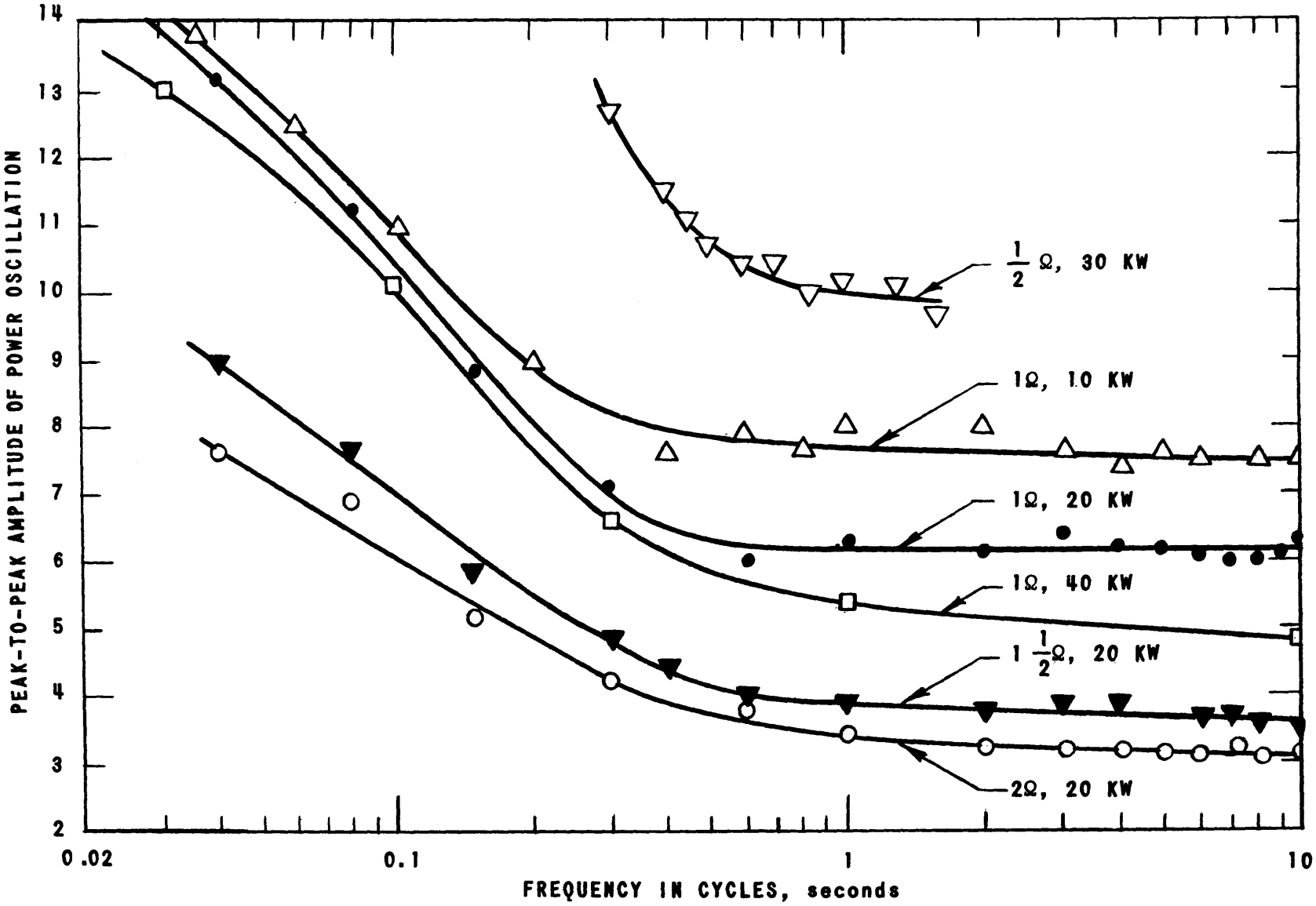

FIG. 10
OSCILLATION AMPLITUDES FOR DIFFERENT VALUES OF AVERAGE POWER AND OF SHUNT RESISTANCE

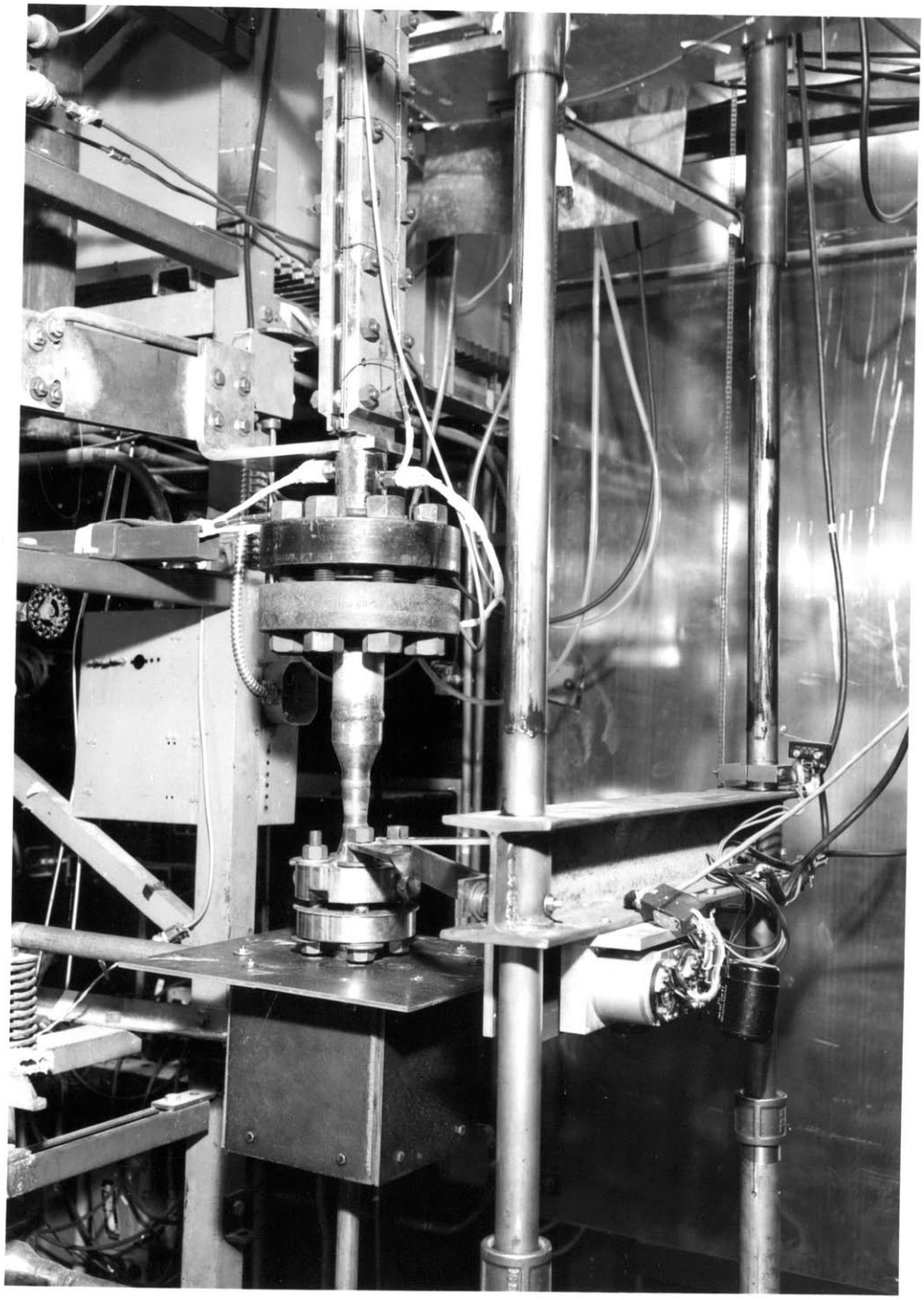

FIGURE 11

THE TEST SECTION IN PLACE
IN THE SMALL SCALE LOOP

CHAPTER VII

THE STEAM VOID DETECTOR

A. Choice of Detection Method

A detector was required for measuring the volume fraction of steam at different heights along the test section.

Two different detection methods were considered, both based upon the use of penetrating electromagnetic radiation. These were:

1. The Tracer Method

   A radioactive salt with low solubility in the steam phase is mixed with the water. The radiation intensity from a selected portion of the test section is then proportional to the amount of water in the section at that point.

2. The Gamma, or X-Ray Attenuation Technique

   A narrow beam of radiation is directed at the test section, and is attenuated by the amount of water in the section, as well as by the test section walls. The radiation intensity at the far side of the section is an exponential function of the void fraction.

The first method has been used successfully by Dengler and Addoms[26], and by Poletavkin and Shapkin[27]. It is especially advantageous for use with heavy walled, circular test sections. If the gamma rays from the salt used are sufficiently penetrating, the geometry of the test section would give no problems. Neither would inhomogeneties in steam void distribution inside the section be liable to give errors in void readings. (See section on errors). A further advantage is that the output signal from the gamma detector will be a linear function of the steam void fraction.

However, the disadvantages of the method are many. Some of the radioactive salt will be deposited on the inside test section wall, and give an unwanted background reading from the gamma detector. The complete loop must be shielded

during runs, and containment in case of leaks is also a problem. A tracer material with a short half life must be used. This necessitates corrections for the decrease in radiation intensity through the duration of a run. The tracer method has for these reasons, not been accepted for general use.

For the second method, both x-ray machines and gamma emitting isotopes have been used as a radiation source. With rectangular test sections, accuracies of better than 1% void fraction are within reach in both cases. Ball, Langmuir and Wright[28] have described a system using an x-ray machine. This instrument is claimed to be accurate to 0.3% voids, with a time resolution of 20 milliseconds. An instrument developed at the heat engineering laboratory at Argonne National Laboratory has been described by Hooker and Popper[29], and by Petrick and Swanson[30]. The radiation source used was the standard Thulium-170 sources developed at Argonne National Laboratory[31].

B. Description of the Present System

The design of the void detector used for this experiment was based on the latter of the two instruments described above. Some important changes were necessary as the main purpose was to measure accurately the transient void fraction, rather than the average value.

The block diagram for the system has been shown in Figure 3. The signal from the gamma detector is fed to a preamplifier of the type described by Hooker and Popper[29]. The zero to ten volt output from the gamma preamplifier has been utilized two ways. For the measurements of void oscillations, the average output signal is being bucked out. The difference is fed to the wave analyzer, which has been described in Chapter VIII.

The full signal goes to a DC amplifier (Sanborn 150 - 1300 Z), and is recorded by the 4-channel recorder (Sanborn 154 - 5460). The recorder gives a measure of the average void fraction, and the boiling noise can be studied as well.

Figure 12 shows the basic geometry of the void detector system. Because a high counting rate is essential to obtain rapid response, and because the signal to the wave analyzer must contain information from the full width of the section, it was decided to let the section itself collimate the gamma beam in the direction perpendicular to flow.

The collimation is taken care of by the back-up plates (see Figure 5), and by the tube wall itself. The purpose of the steel liners along the edges of the back-up plates is to block out gamma leakage through the insulation material between the plates and the test tube. An advantage of letting the test section itself collimate the beam is that small misalignments between the detector carriage and the test section will not affect the signal.

The source holder shown in Figure 12 contains two Thulium-170 sources, each of approximately 10 Curies. The two are aligned along the height of the test section, and are located at 8.5 cm depth at the bottom of the 2 cm diameter hole shown on the photograph.

The gamma detector assembly shown in Figure 13 consists of a detector package and a lead collimator housed in a heavy lead shield. The latter serves 3 purposes. First, as shielding against scattered gammas and cosmic radiation. Second, as a magnetic shield to keep out AC-fields from the test section heating current. Thirdly, it serves to keep the scintilation crystal and photo multiplier tube at constant temperature.

The lead collimator, which limits the width of the beam in the direction of flow, as well as the gamma detector package, has been shown in Figure 14. The light-tight package contains a sodium-iodide scintilation crystal, a Lucite light guide, and an EMI-9536 S photo multiplier tube. This type is not very sensitive to magnetic fields, but even so, the photo multiplier tube has a MU-metal shield around it.

The particular tube usedwas selected between half a dozen for the lowest dark current.

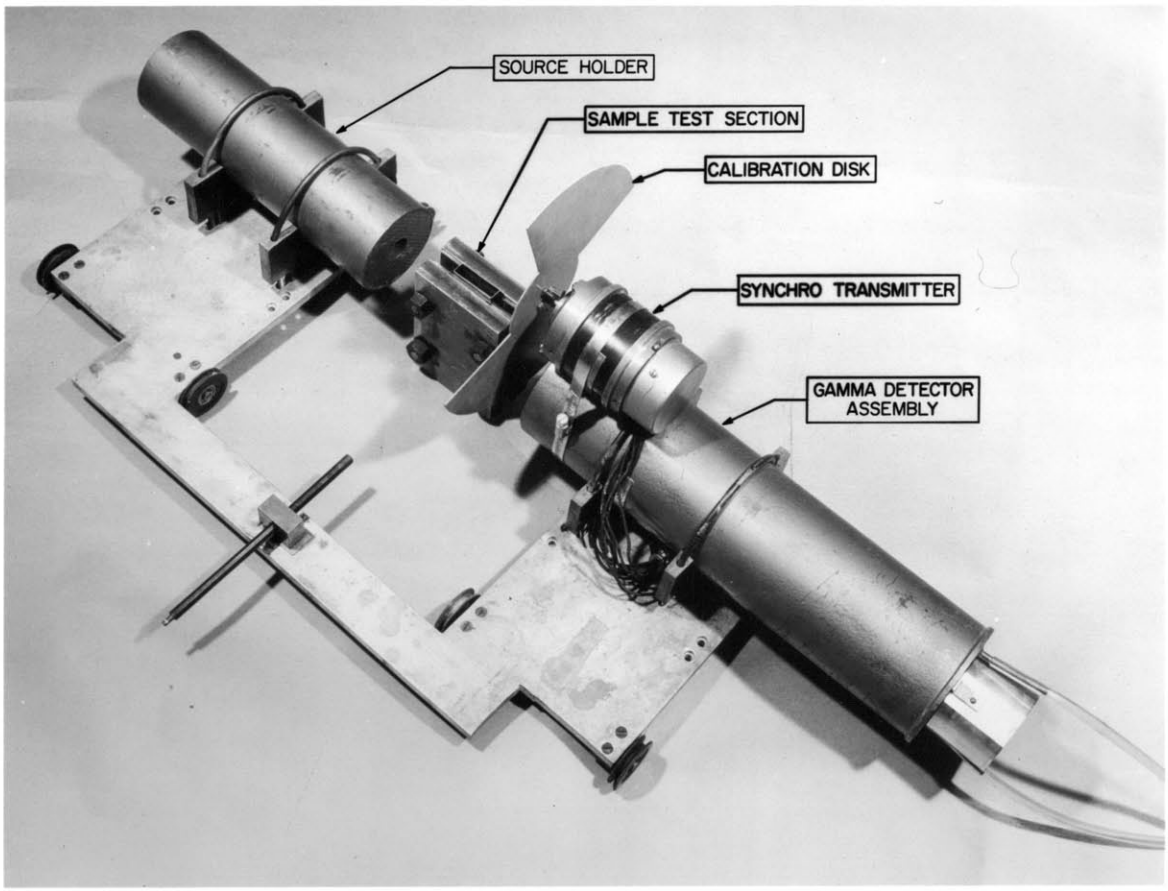

FIGURE 12

VOID DETECTOR CARRIAGE

WITH THE SAMPLE TEST SECTION

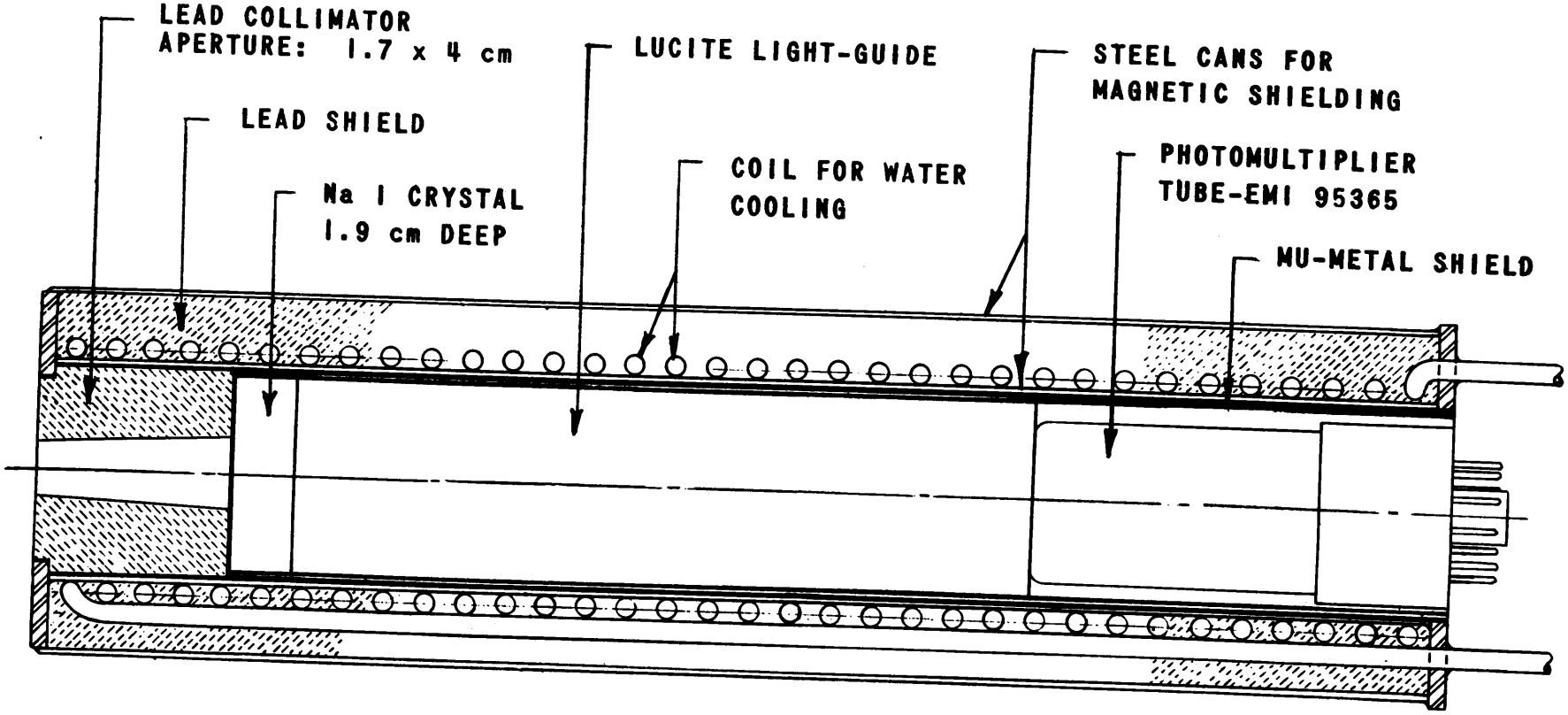

FIG. 13
THE GAMMA DETECTOR ASSEMBLY

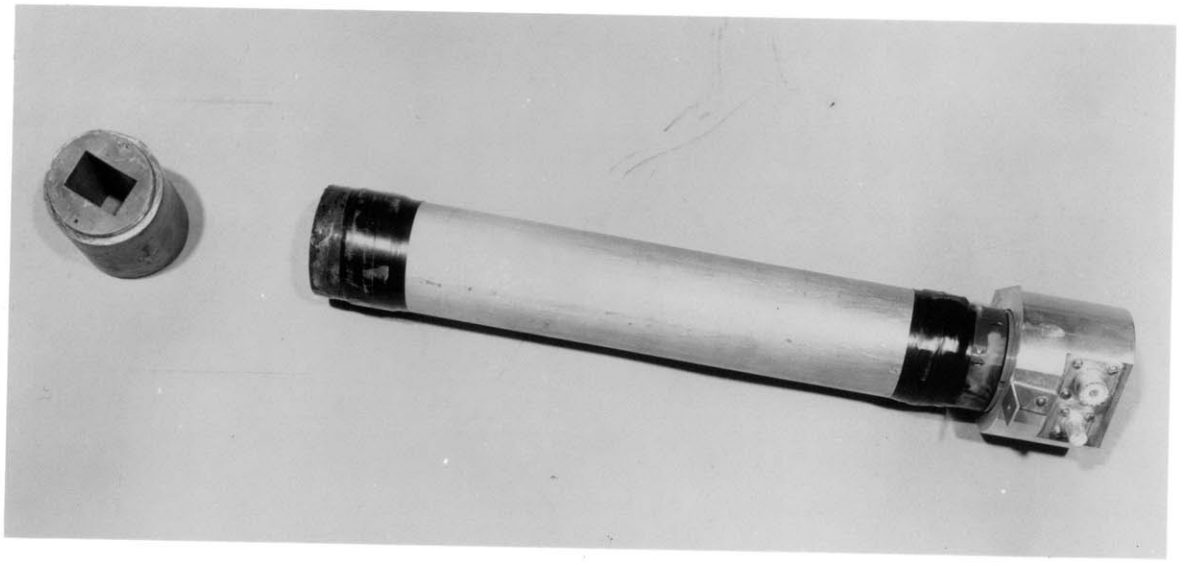

FIGURE 14

THE GAMMA DETECTOR PACKAGE

THE LEAD COLLIMATOR

The crystal is 1.9 cm thick, and 6 cm in diameter. The light guide is of the same diameter, and is 20 cm long. The light guide permits the photo multiplier tube to be retracted from the test section, to a region with lower magnetic fields.

Mounted on top of the detector shield can be seen a syncro repeater, carrying a disk the purpose of which will be described in Chapter VIII.

Figure 15 shows the void detector system in position at the Small Scale Loop. A traverse table, guided by two supporting rods, is connected to a chain drive. This table can be driven up and down along the height of the test element between limit switches in both ends. A fine and a coarse syncro indicate the table position on a control panel to within a few millimeters. The table has been counterbalanced by two lead weights, totalling approximately 150 kg. The support structure is fastened to the test section, and moves with the latter when thermal expansions take place.

The detector carriage runs on top of the traverse table. It is driven by a second motor between stops defined by micro switches. In the one end position, the test section, and in the other, a fixed gamma absorber will be in the beam. The fixed absorber corresponds to the waterfilled test section in cold condition, and is used as an absolute standard for the measurement of average void fraction. The control panel for the horizontal and vertical traverse drives is shown as Unit 6 of Figure 4. The synchros show the height of the detector above the test section inlet.

C. The Thulium Source

The gamma source used at Argonne National Laboratory for void detection measurements, consists of 200 mg of Thulium Oxide, contained in a small aluminum cylinder[31]. After 4 months in the MTR the activity of this source is approximately 20 Curies. The active element Thulium-170 has a half life of 129 days.

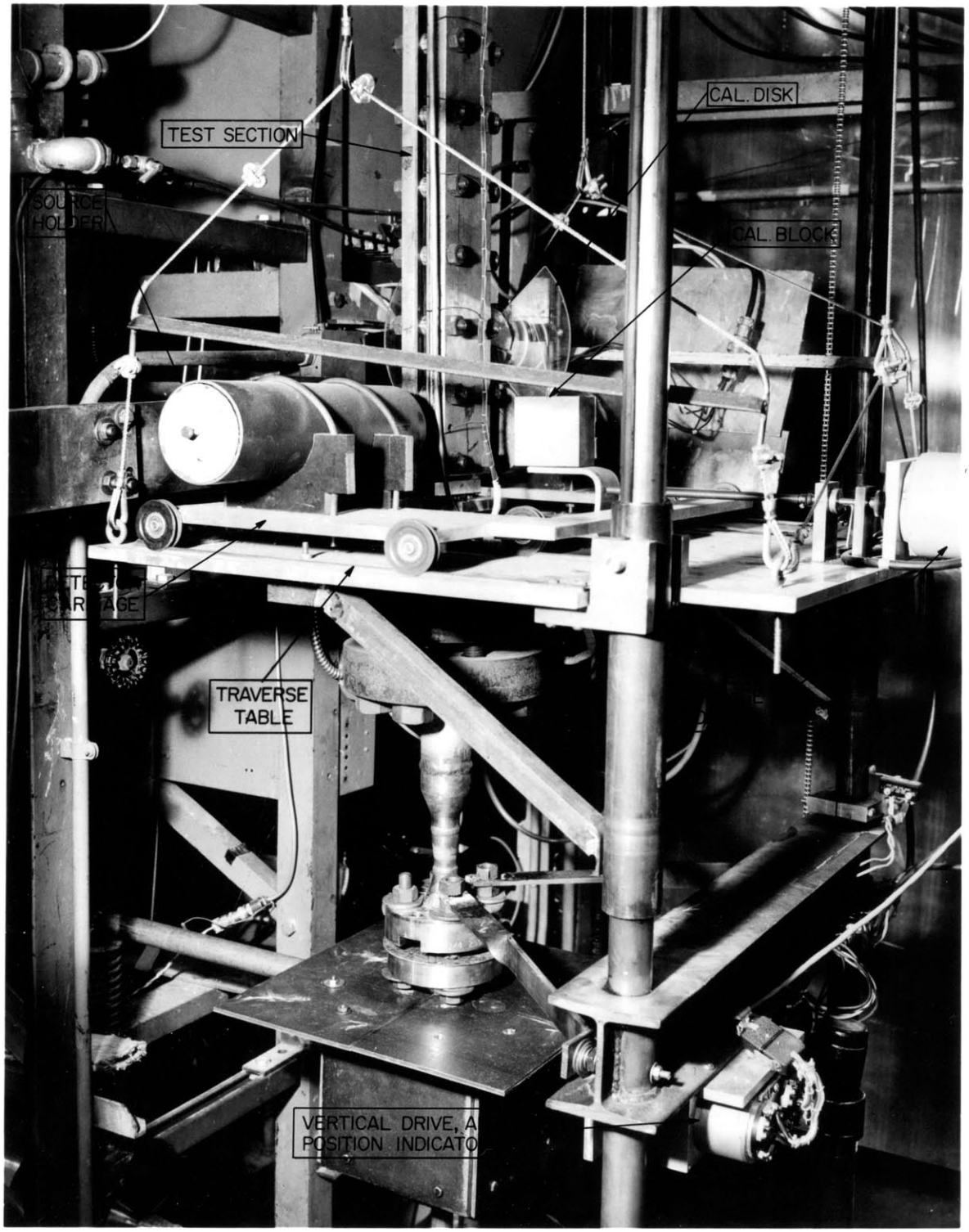

FIGURE 15

THE VOID DETECTOR SYSTEM IN POSITION

Thulium-170 gives off a line spectrum consisting of a primary 84 kev gamma ray, a 52 kev x-ray, both from the daughter product Yttrium, and a 24 kev escape peak[32].

For the detection of voids inside a steel tube, the higher energy is the most applicable. It has previously been the practice of this laboratory to filter out the lower peaks, in order to produce a monoenergetic beam. Lead is useful for this purpose, as it has a K-absorption edge at 88 kev.

However, when the spectrum for the source to be used for this experiment was measured, see Figure 16, it was found that a large part of the electromagnetic energy emitted from the source lies in the energy interval 100 to 300 KEV. This is due to Bremsstrahlung resulting from the stopping in aluminum and thulium oxide of beta particles (0.970 and 0.886 mev) emitted by Thulium-170. The continuous spectrum is more penetrating than the line spectrum, and counts, as shown in Figure 17, for most of the gammas reaching the detector. If this spectrum is weighed by the individual energy of the gammas, it will be realized that the signal from the void detector is almost entirely due to the high end of the spectrum. A filter is therefore useless, as it only tends to cut down the rate of arrival of gammas. Except for a 0.5 mm Al retainer plate, the bare source was used for this experiment.

D. The Accuracy of the Void Measurement

There are two different measurements to be considered: The measurement of void variations, and the measurement of average void fraction. The void detector equipment was optimized to give the best results in the former measurement. The different sources of errors to be listed will not affect the two measurements in equal degree, and the discussion that follows will, therefore, be split in two parts.

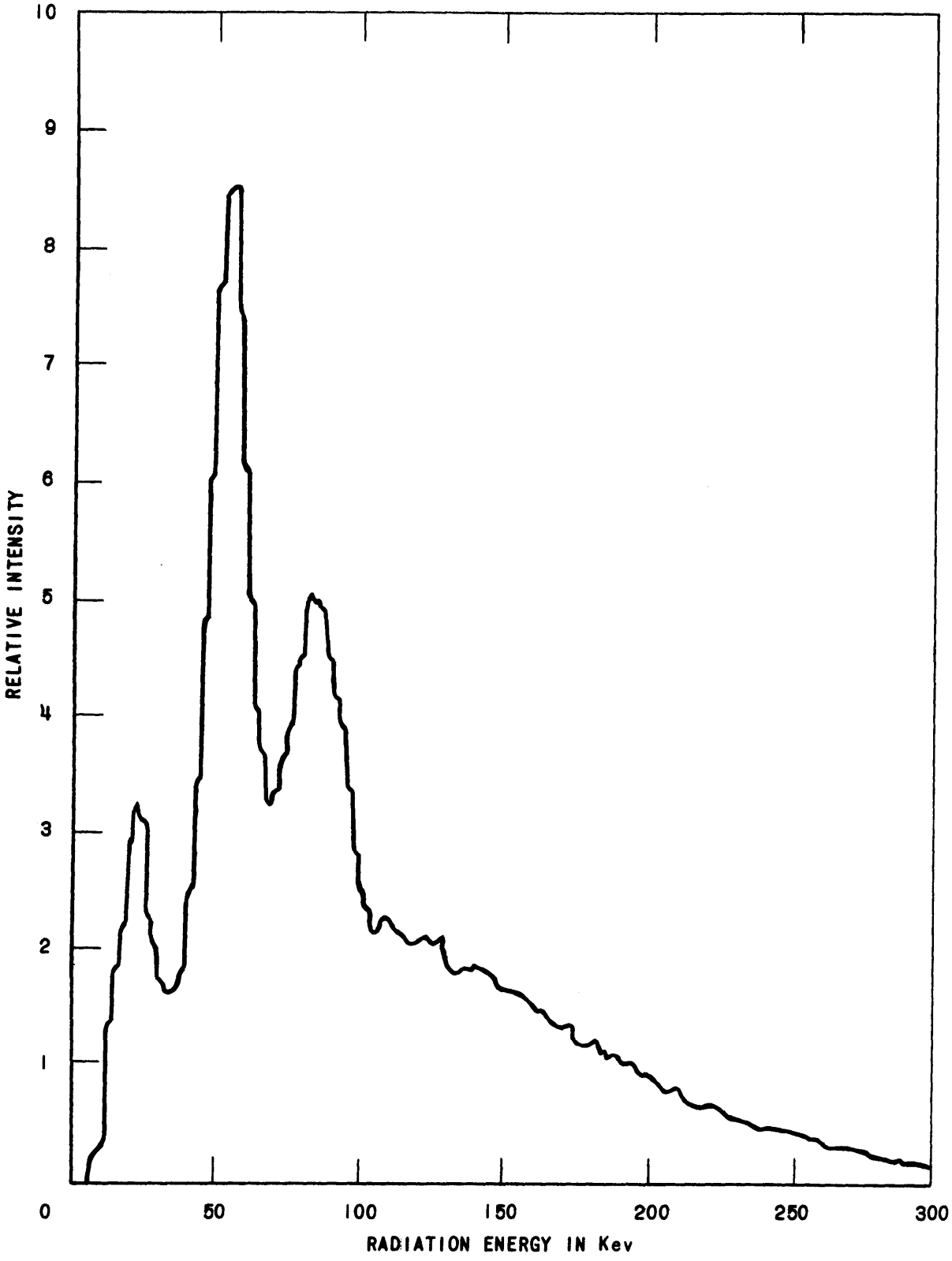

FIG. 16
SOURCE SPECTRUM TH-170 IN ALUMINUM CAPSULE

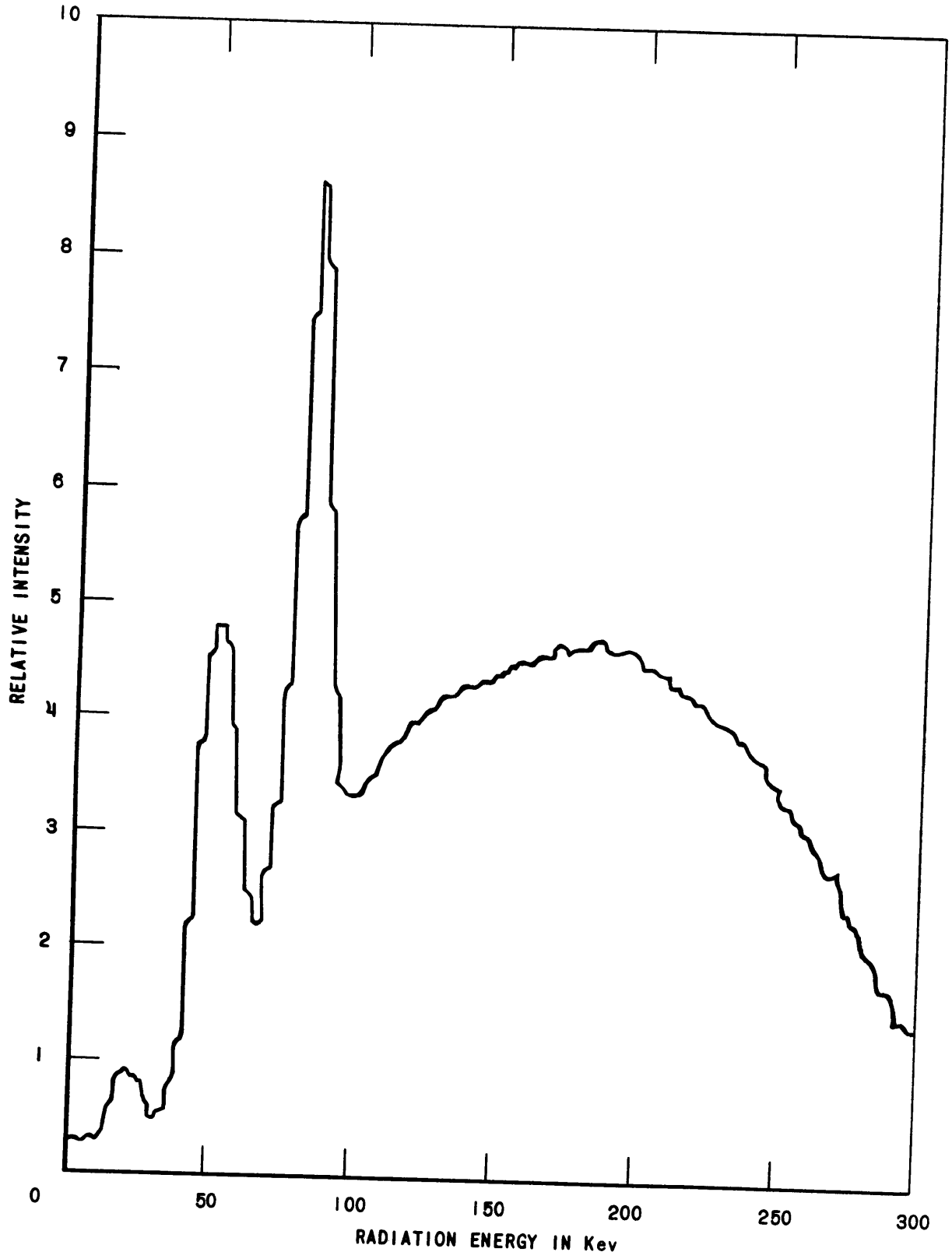

FIG. 17
SPECTRUM AT DETECTOR. WATER FILLED SECTION

The sources of error are:

1. Noise due to source statistics and boiling.
2. Gamma rays of different energies will be attenuated differently.
3. Inhomogeneous steam void distribution in the test element.
4. The difficulty of covering the full cross sectional area of the flow channel.
5. Drifts in the high voltage to the photo multiplier tube.
6. Changes in gain of the crystal and the photo tube due to changes in temperature.
7. Drifts in the recorder system.
8. The non-linearity of the void detector system.

Most of these points have been discussed by Hooker and Popper[29], Richardson[33], and Petrick[34]. Some measures to reduce the errors will be mentioned. Note that all void fraction errors will be given in percent of the total channel cross section.

a. The measurement of average void fraction

1. The effect of noise. With water filled test section, the arrival rate of gammas to the detector was approximately 1.7×10^6 per second. This resulted in a noise corresponding to ± 3% void variations when no filter was used at the output of the gamma preamplifier. The standard deviation in signal value to be expected with a given source, and the effect of using an RC-filter in the circuit, have been discussed in Appendix II.

In order to study the variations in void fraction at boiling conditions, several void traverses along the height of the section were taken without such a filter. It appears that slug flow always developed in the upper part of the test section. Variations in void fraction of ± 20% around the average value were frequently observed at "steady state" conditions. The

average was estimated by visual inspection of the recorder trace, and the error resulting from this procedure is estimated to ± 1.5% voids. It was found, however, that the recorder system could not handle a noisy input signal properly. A saturation effect, probably in the pen system, gave a consistent shift of the void signal towards higher void fractions. Errors in the range 5 - 15% were observed, and later measurements of average void fraction were always taken by filtering the signal. Errors due to noise were thereby eliminated.

2. The Effects of distributed source spectrum. The attenuation of a mono-energetic gamma beam is an exponential function of the absorber thickness. As shown in Figure 16, the spectrum reaching the detector is far from mono-energetic. An experiment was therefore carried out to see how the signal from the gamma detector varied with the void fraction in the test section. The sample test section shown in Figure 12 was used for this experiment. The results are given in Figure 18. The measured points form a straight line on semi-log paper, showing that the attenuation can be accounted for by a single absorption coefficient. Two tests were made, one with the source pointing up, the other with the source pointing down. It will be seen from the plot that there is a noticeable, but very small difference between the results in the two cases.

The experiment described allows the use of the following equation for the void detector output voltage:

$$V_\alpha = V_F \left[\frac{V_E}{V_F} \right]^{\alpha^\circ} \qquad (7.1)$$

α° is the volume void fraction, and subscripts F and E refer to full and empty channel, respectively. The empty-to-full ratio was measured from time to time, and remained constant at 1.75 throughout the series of data runs taken. The calibration block gave the value of V_F as described below. This number, how-

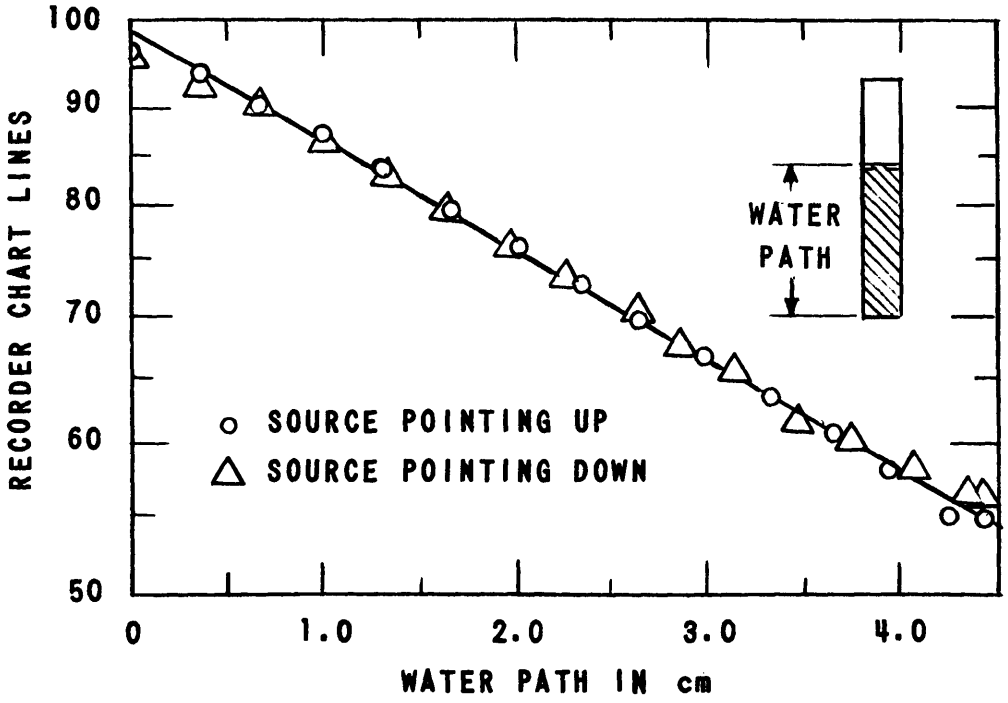

FIG. 18
VOID DETECTOR OUTPUT SIGNAL
AS A FUNCTION OF WATER PATH

ever, as well as the empty-to-full ratio, had to be corrected for changes in water density at higher temperatures. The corrected values, using water densities from Keenan and Keyes[35], checked perfectly the void detector output with full, hot channel.

If the spread in the measured points in Figure 18 can be taken as a measure of error (drift errors from points 4, 5, and 6 are included also), this effect adds 1% to the composite probable error in average void fraction.

3. The effects of inhomogeneous phase distribution. If the water in the channel was completely separated from the steam, and if the division was not as shown in the sketch on Figure 18 but along the sides of the tube, then the output signal from the void detector would be given by:

$$V_\alpha = \alpha^\circ V_E + (1 - \alpha^\circ) V_F \qquad (7.2)$$

It is seen that this result agrees with equation 7.1 for $\alpha^\circ = 0$, and for $\alpha^\circ = 1$. The deviation is the greatest when the channel is half empty, where the error may be as high as 5%. The exact number depends on the empty-to-full ratio. Phase distributions as radical as the one discussed will not be found during normal boiling conditions.

4. The effects of incomplete scanning. Although the effect discussed above cannot give rise to very large errors taken alone, that effect becomes extremely important if not all parts of the cross section are weighed with equal importance by the void detector system. At higher void fractions, the steam bubbles tend to concentrate in the middle of the channel. If the void detector does not "see" the areas close to the side walls, the void readings will tend to be too high. This problem was studied extensively by Richardson[33] and Petrick[34]. They found that accurate readings could only be obtained

by traversing across the width of the test section using a very narrow gamma beam, and then integrate the results.

In the present case, a wide beam covering the full width of the test section had to be used for the oscillation tests. When this equipment was tested by measuring the voids in some plastic models made for the studies of Richardson and Petrick, it was revealed that the areas near the side walls were not covered properly. After the completion of the oscillation tests, therefore, the traversing technique was used to obtain accurate void traverses at the same conditions at which oscillations had been taken. Because of the finite width of the gamma beam (a lead collimator with a 1/32" slit was used), and the difficulty of aligning the detector system perfectly with the test section, some uncertainty still remains regarding the areas extremely near to the walls. Probable error due to this effect is estimated to 2%.

5, 6, and 7. Drifts in the different components of the detector system can lead to appreciable errors unless frequent calibrations are carried out. Means for doing this was, therefore, provided. The void detector carriage could be driven to the side to a fixed calibration block which can be seen on Figure 15.

This block was made to give an attenuation effect exactly equal to the water filled test section at room temperature. To calibrate, the high voltage to the photo multiplier tube was adjusted to give a certain output voltage from the gamma detector preamplifier. The detector system, including the Sanborn recorder, was calibrated before and after the taking of each void traverse. The short term stability of the system proved to be very good. In rare cases, where the drift between the calibrations corresponded to 2% void fraction or more, the run was repeated. Therefore, the

probable error in void reading due to drifts, is less than 1%.

8. The effect of detector non-linearity. As mentioned above, the variations in void detector output signal due to boiling noise, may be considerable. Due to the non-linear relationship between voids and output signal, any averaging procedure used to find the mean signal value will result in errors. This has been considered in Appendix I. Assuming that the apparent slug flow results in a sinusoidal signal response, it has been shown that the maximum error is less than 1%, even for void variations as large as 20%.

The total composite error from all the sources listed is less than 2.5% in the case where the traversing technique was used, and when the signal was properly filtered.

b. The measurement of void variations

In this case the unfiltered output signal from the gamma preamplifier was fed to the wave analyzer which will be described in the following chapter. From the discussion to be given, it will appear that the errors due to noise (point 1 above), or to drifts (points 5, 6, and 7), will be negligible. It has been shown above that the spread in gamma energies is unimportant. The effect of detector non-linearity have been discussed in Appendix I for the present case also, and found to be negligible.

The only important sources of errors are points 3 and 4. With the system used, errors in the measurement of the <u>average</u> void fraction due to inhomogeneities in void distribution, and to the fact that the areas closest to the walls are not properly seen, may well be 10% in the upper parts of the test channel. It is apparent that these effects will give errors in the measurement of oscillation amplitudes also, but it is more difficult in this case to estimate the error involved. The fractional error in the oscillation amplitude will be less than 10%, but not very much less.

CHAPTER VIII

THE WAVE ANALYZER

A. Review of Possible Methods

When the heat production in the test section wall is oscillated, the signal from the gamma detector will contain these different components:

1. A steady state signal value which corresponds to the average void fraction.
2. A sinusoidally varying signal giving the void response to the sinusoidal power variation.
3. A component due to boiling noise.
4. A noise component due to the random arrival of gammas.

To be able to pick out the amplitude and the phase of the sinusoidal void response, the use of a wave analyzer is necessary.

Two different types of wave analyzers are in general use for transfer function measurements. These are:

1. The Integration Type Wave Analyzer. The signal is here multiplied by the sine and the cosine of the driving force angle, and the results integrated over a large number of cycles to give the inphase and quadrature components of the signal.
2. The Nulling Method Wave Analyzer. The AC-part of the signal is here nulled against a voltage of the same frequency as the driving force, but of variable phase and amplitude.

The last method, which is used for example in EBWR[36], and SPERT-I[37], has the advantage of not being affected by drifts in the average signal value. This method, however, becomes useless if the signal-to-noise ratio drops below 1. For the first method, good results can be obtained even for signal-to-noise ratios as low as 1/20. Drifts in average signal level appears as added noise

in the integrated output. This system, which is used with several reactors[38,39], is favoured for transfer function measurements on "out-of-reactor" experiments such as electrically heated boiling loops[16].

It is possible to eliminate the effect of drift in the average signal, even for the integration method wave analyzer. A system for doing this was first used in the Jeep Reactor, and has been described by Schmid[40].

In recent works[41] the use of digital computers to correlate the input and output signals from oscillator tests have been taken up. The inherent accuracy of this method is as good, or better, than the other methods. Advantages are that data can be collected faster, and that several variables can be recorded simultaneously, and later correlated one by one with the driving signal. Disadvantages are the considerable cost of the equipment needed, and also the difficulty of assessing on the spot whether useful data is being taken or not.

B. Description of the System Used

For the present investigation, a wave analyzer of the integration type was built. A block diagram of the system is shown in Figure 19. The signal from the gamma detector is amplified, and the steady state signal value bucked out. The signal voltage is now given by:

$$v(t) = v_o(t) + v_b(t) + v_s(t) \qquad (8.1)$$

v_o is the remaining DC-level due to small errors in bucking voltage setting, and to the fact that small drifts in the average signal value will take place during the run. v_b is due to boiling, and to source noise. This part of the signal is assumed to be random and completely uncorrelated with the power variation. v_s is the response due to the forced power oscillations. This is the signal component that is to be measured by the wave analyzer. The total signal as given by equation 8.1 is now, together with the inverted signal, fed

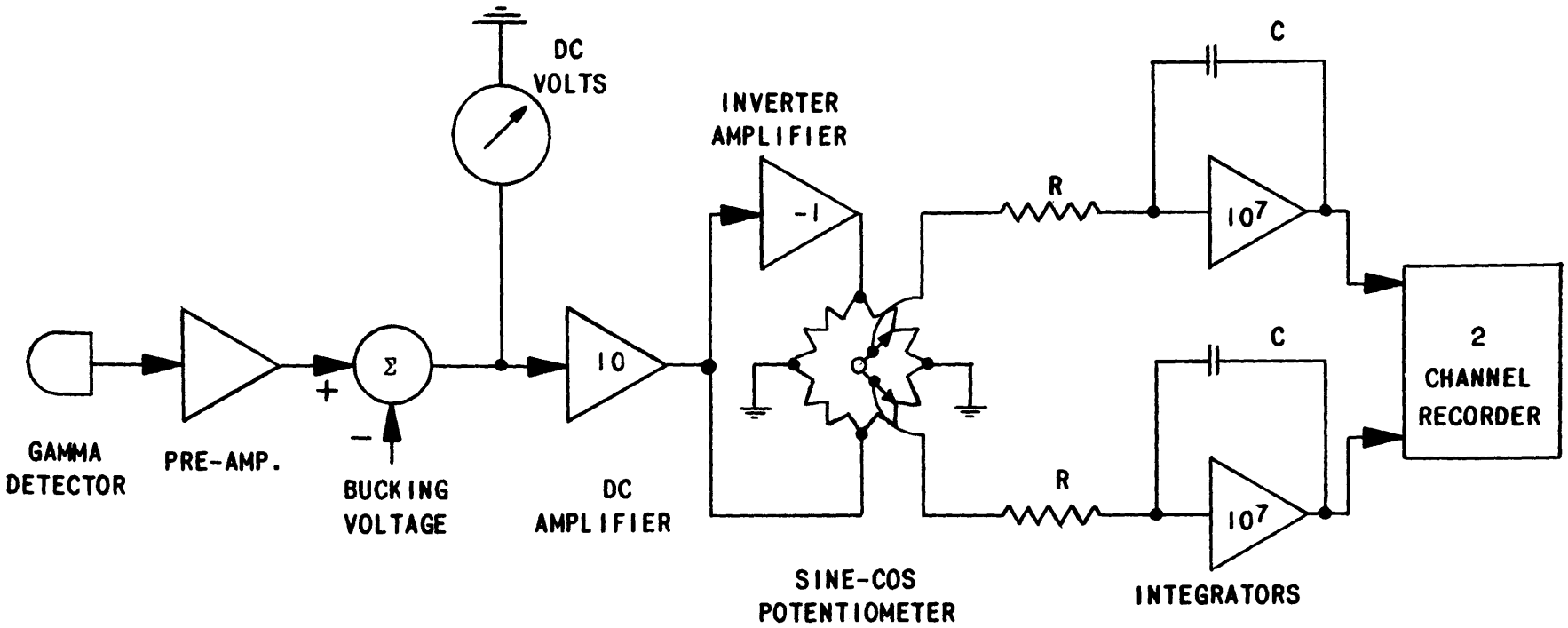

FIG. 19
BLOCK DIAGRAM OF THE WAVE ANALYZER

to the two sides of a sine-potentiometer, the midpoint of which is grounded. The potentiometer has 2 wipers spaced 90 degrees apart, and the input to the two integrators will be $v(t)\sin \omega t$, and $v(t)\cos \omega t$, respectively. The potentiometer, which is shown on Figure 9, is geared to the servo system which triggers the power oscillation, and the potentiometer runs exactly in phase with this oscillation.

Assuming that the wave analyzer had already been checked and calibrated, one data point was taken as follows. First, the power oscillator was set to run at the frequency desired. Next, the bucking voltage was set to give a zero reading on the DC voltmeter shown in Figure 19. Then the integrators were zeroed by shorting the condensers C, and this brought the two pens of the recorder to the mid chart position. This started the actual data run, and the system was now left for a time T, which should be long compared to $2\pi/\omega$. At the end of this time, the strip chart of the recorder would appear as shown in Figure 20.

To explain this result, the equations for the input voltage to the recorder will be considered.

$$-\frac{1}{RC}\int_0^T \left[v_o + v_b + v_s\right] \sin \omega t \, dt \quad = \quad \text{The Sine channel} \qquad (8.2)$$

$$-\frac{1}{RC}\int_0^T \left[v_o + v_b + v_s\right] \cos \omega t \, dt \quad = \quad \text{The Cosine channel} \qquad (8.3)$$

If v_o is constant with time, this term will add a sinusoidally varying signal to the recorder reading. If the test loop pressure, and other loop parameters, are controlled closely, v_o will be small, and the resulting "noise" in the recorder output will be insignificant. v_b is a random signal with zero average, and multiplied with either a sine or a cosine, it still gives zero average. The effect of v_b will be some added noise to the chart reading, but

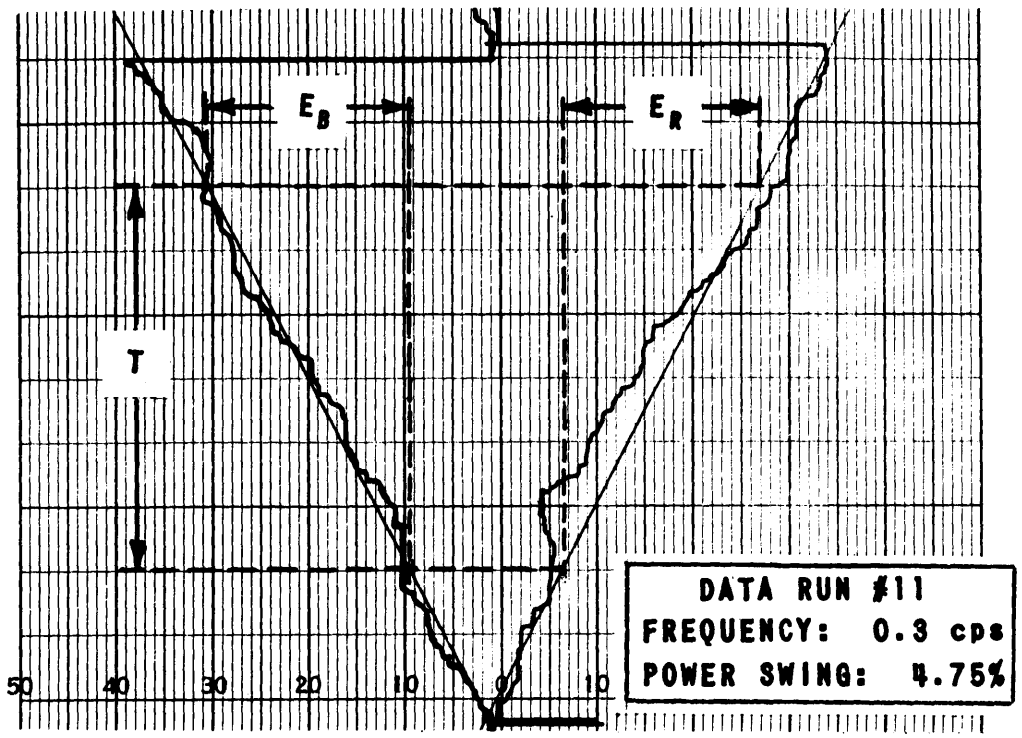

FIG. 20
TYPICAL OUTPUT RECORD FROM THE WAVE ANALYZER

no DC-error. v_s is a periodic signal, with period $2\pi/\omega$, and v_s can be expanded in a Fourier series, as follows:

$$v_s(t) = \sum_{n=1}^{\infty} A_n \sin (n\omega t - \varphi_n) \tag{8.4}$$

When this is inserted in equations 8.2 and 8.3 and the integration is carried out, the following results (now neglecting the contributions from the terms v_o and v_b):

Sine channel: $$E_R = -A_1 \frac{T}{2RC} \cos \varphi_1 \tag{8.5}$$

Cosine channel: $$E_B = +A_1 \frac{T}{2RC} \sin \varphi_1 \tag{8.6}$$

A_1 is the amplitude and φ_1 is the phase lag of the first harmonic of v_s. If higher harmonics are present in v_s, they will not be detected. E_R and E_B are the deflections of the two pens after time T. Solving equations 8.5 and 8.6 for A_1 and φ_1:

$$A_1 = K\sqrt{\left(\frac{E_B}{T}\right)^2 + \left(\frac{E_R}{T}\right)^2} \tag{8.7}$$

$$\varphi_1 = \arctan\left(-\frac{E_B}{E_R}\right) \tag{8.8}$$

K, which has replaced 2 RC, can be considered as a scale factor, relating void amplitude to units of slope for the lines on the recorder chart.

The value of K was determined by the calibration process described below. Then φ_1 and A_1 could be found from the formulas by measuring the slopes of the two lines in Figure 20. The slopes should be taken for the best straight lines which can be drawn through the pen traces.

By recording the integrator output instead of simply using two voltmeters, one gets the advantage of being able to get a picture of the drift and the noise at a particular data point, and to estimate the error in the slopes.

The two channel recorder used is shown as Unit 14 in Figure 4 . Units 7, 8, and 9 are also part of the wave analyzer.

Bucking voltage set-point potentiometer, amplifier gain controls, and means for zeroing and calibrating the wave analyzer, are incorporated in Unit 16 directly below the amplifiers.

C. Calibration of the Wave Analyzer

Checks were made daily to ensure that the gains were the same in the two channels of the wave analyzer, and that the gain of the inverter amplifier was exactly one, so that DC-components of the input signal would be rejected.

Next, the value of the constant K was determined. For this purpose, a calibration disk of Lucite, and another of Micarta, were made. The disks had two quadrants cut away, and produced a square wave modulation in the void signal if rotated in the gamma beam. The disk was driven by a syncro repeater, mounted on the gamma detector carriage, as shown in Figure 12, and linked to a syncro transmitter on the servo unit output shaft. Lucite is close to having the same gamma absorption characteristics as water. The insertion of the Lucite disk in the beam will correspond to the collapse of a certain amount of steam bubbles in the section. The equivalent change $\Delta\alpha$ in void fraction, is determined once and for all by a separate calibration.

Before calibration, the power oscillation was turned off. The disk was started, and would run at the frequency for which the servo, and therefore the wave analyzer, currently was set. The resulting square wave in the void detector signal contained a first harmonic of amplitude $4\Delta\alpha/\pi$. This signal was detected by the wave analyzer, and resulted in a recording similar to Figure 20. Using equation 8.7, this would determine K as:

$$K = \frac{4\,\Delta\alpha}{\pi\sqrt{\left(\frac{E_B}{T}\right)^2 + \left(\frac{E_R}{T}\right)^2}} \qquad (8.9)$$

Because of the nonlinearity of the void detector, the value of K depends upon the average void fraction. Therefore, K is measured again every time the

void detector is moved to a different point along the channel, or after changes in the steam conditions in the test section. It can be shown from equation 7.1 that K and α^{o} at two different conditions will be related by:

$$K_1 = K_2 \left(\frac{V_E}{V_F}\right)^{\alpha_1^{o} - \alpha_2^{o}} \qquad (8.10)$$

D. Errors in Measurements with the Wave Analyzer

There are 4 possible sources of error that can be readily distinguished:

1. Errors due to drifts in the test loop parameters.
2. Errors due to the non-linearity of the gamma detector.
3. Errors due to drifts in the wave analyzer.
4. Errors due to an inhomogeneous phase distribution in the test tube.

The first of these is not due to the limitations of the wave analyzer, and will not be discussed here. The second has been treated in Appendix I, and is shown to be negligible. The main sources of error are the last two points, and they will now be discussed in some detail.

3. Errors due to drifts in the wave analyzer: Extreme care was taken at the start of every data run to ensure that the wave analyzer was functioning properly. Because of the low power amplitude used, however, the system has a relatively high gain, and could not be made completely drift free.

The integrator amplifiers and the converter were all Philbrich UPA-2 Operational Amplifiers. A precision DC amplifier, Electro Instrument Co. Type A-12, provided the gain of x10. Drifts in these amplifiers as a possible cause of the drift has been ruled out.

The sine/cosine potentiometer was a Fairchild Type 753, with 45k Ω per quadrant. The cause of the drift was noise developed in this unit. Voltage spikes occurred as the wipers hit rough spots along the slide wire. The resulting noise was periodic, and gave an error signal after the integration.

To check for drifts, the power oscillator was turned off, and the signal from the void detector, which then contained the noise from boiling and source only, was fed to the wave analyzer. Drift checks through the full range of frequencies were taken on two subsequent days. These runs were taken after the other data runs had been completed, and the sine/cosine potentiometer was rather worn. Odd drift checks in the middle of data runs were also taken, and based on the results, a probable error of $\pm$ 0.35% void fraction must be assigned to the actual data points. It was noted that there is a large spread around this figure, and that conditions may be more favorable one day than the next.

The error in the phase measurement is more difficult to estimate. The drifts are not completely random, but tend to negative values of E_R and E_B. Thus, the drift can be expected to give systematic deviations in phase reading, rather than random deviations from the true results.

The errors due to drift are most important near the node point in the transfer functions measured. Here the signal value drops to near zero, and it is difficult to obtain conclusive information about the phase changes as the node is approached from both sides.

4. Errors due to inhomogeneous phase distribution in the test tube: In section D of Chapter VII errors in average void fraction in the order of 5 to 10% channel volume are shown to be possible due to this effect. The error in the measurements of transient void fraction is even more difficult to estimate. However, as a first approximation it must be expected that it should be comparable to the error in the steady state reading. Thus, if the latter is given by:

$$\alpha^{\circ} = 50\% \begin{matrix} +0\% \\ -5\% \end{matrix}$$

the void amplitude should be written:

$$\alpha \pm 0.05\,\alpha \tag{8.12}$$

This effect should not give any error in the phase reading.

In summary: Errors are caused by sine potentiometer noise, and by possible phase inhomogeneities in the coolant flow. Unfortunately, both causes tend to give systematic errors, and both are difficult to assess.

The errors in the measurement of void amplitude and void phase for Run No. 13 has been estimated, and shown on Figure 43.

CHAPTER IX

THE MEASUREMENT OF LOOP PARAMETERS

A. The Pressure Measurement

The saturation pressure in the steam separator was read by a Heise Gauge, Type H 3192, to be seen in Figure 2. This instrument was calibrated 3 times: before, during and after the completion of the data runs. There was no change in calibration, but the gauge had a hysteresis effect of about 0.15 atmospheres. This effect was the major cause of error in the pressure reading.

At prolonged operation at a constant pressure, the loop pressure could be controlled to better than $\pm$ 0.1 atmospheres as indicated by the meter scale. At all but the lowest oscillation frequencies (see Chapter B) the standard deviation in the pressure is estimated to be $\pm$ 0.15 atmospheres. This includes drift as well as meter errors.

B. The Temperature Measurements

Thermocouples were used for all temperature measurements. As described in Chapter V and shown in Figure 5, 3 Conax Glands were used to insert thermocouples into the coolant stream at the inlet and the outlet of the test section. These glands contained 2 bare Chromel-Alumel couples each, which were carried to an ice junction, and each pair was connected to form a thermopile. Another couple, also double, was inserted into the steam zone of the steam separator. These 4 double couples, plus a spare used alternatively at the inlet, were calibrated before and after the data runs. Deviations between the two calibrations were within 0.5 degrees C. Readings on all 4 thermocouples were taken periodically during a data run, and for this a Leeds & Northrup Portable Precision Potentiometer No. 8662 was used. Either of the couples could be connected as shown in Figure 3 to the Sanborn recorder.

Although the recorder system proved valuable to check for drifts in inlet water temperature, it was not accurate enough as a measurement of the temperature itself. This was due to the large 60 cycle noise voltage induced in the couples by the test section heating current. The potentiometer proved to be a very effective filter because of its low input impedance, and of the inertia of the galvanometer. As measured by the potentiometer, any 2 of the 3 thermocouples used at the inlet agreed to within 0.5 degrees C.

By using the calibration curves mentioned above, the probable error in the measurement of inlet temperature is estimated to be $\pm$ 0.5 degrees C. Although this was not as good as had originally been hoped for, it proved sufficient in the presence of the drifts in inlet temperature described in Chapter IV.

C. The Flow Measurement

The water flow rate was measured below the inlet of the test element by means of a Potter turbine type flow meter, model No. 3/4 - 885. Its principle of operation is the following: The turbine carries a permanent magnet, and variations in magnetic field as the turbine rotates, are sensed by a pick-up coil placed outside the pressure region. The output voltage is a sinusoid, with a frequency and a voltage amplitude proportional to the flow. This signal is converted to a DC voltage in a Potter Frequency Converter, type 3 C-1, and recorded as shown in Figure 3.

For the flow range used, the output frequency from the Potter meter ranged from 0 to 100 cycles per second. Extreme care had to be taken to shield the pick-up coil from the 60 cycle AC field from the heating current. By moving the flow meter as far away from the test section as was convenient, by magnetic shielding of the pick-up coil, and by proper orientation of this coil, the problem of pick-up was finally eliminated.

The flow meter was a new one, and came freshly calibrated from the factory. The accuracy of these instruments are guaranteed to ± 1%. The frequency converter and the Sanborn recorder were calibrated at frequent intervals during a data run. The loop itself was so stable that a change in flow reading normally indicated that it was time to recalibrate the electronic measuring circuits. After the completion of the data runs, the flowmeter, together with the electronic measuring circuits, was calibrated outside of the loop. The results checked the factory calibration to within 1%.

D. The Measurement of Heating Power

To be able to measure accurately the amplitude of the power oscillations, it was necessary to produce a power signal which would be suitable for recording. The system used is shown in the block diagram in Figure 3.

A signal voltage proportional to the test element current as measured by a current transformer, was amplified by a Philbrick UPA-2 operational amplifier. The voltage drop across the test element was amplified in an identical unit. The current and voltage signal outputs were multiplied together in a Donner Function Multiplier, model 3731. The output from the multiplier contained a DC signal proportional to the average test element power, and an AC component which is mainly 120 cycles. Before the signal could be recorded, the AC component had to be filtered out.

A two stage low pass filter with M-derived end sections was designed for this purpose. The filter, which is shown in Figure 21, was built in a preamplifier chassis which plugged directly into the Sanborn recorder. The amplitude response of the filter was measured with the Sanborn recorder, and thus includes the response of the latter. It will be seen that the frequency band used for power oscillations will pass the filter undamped, while the 60 and 120 cycle noise components will be cut off.

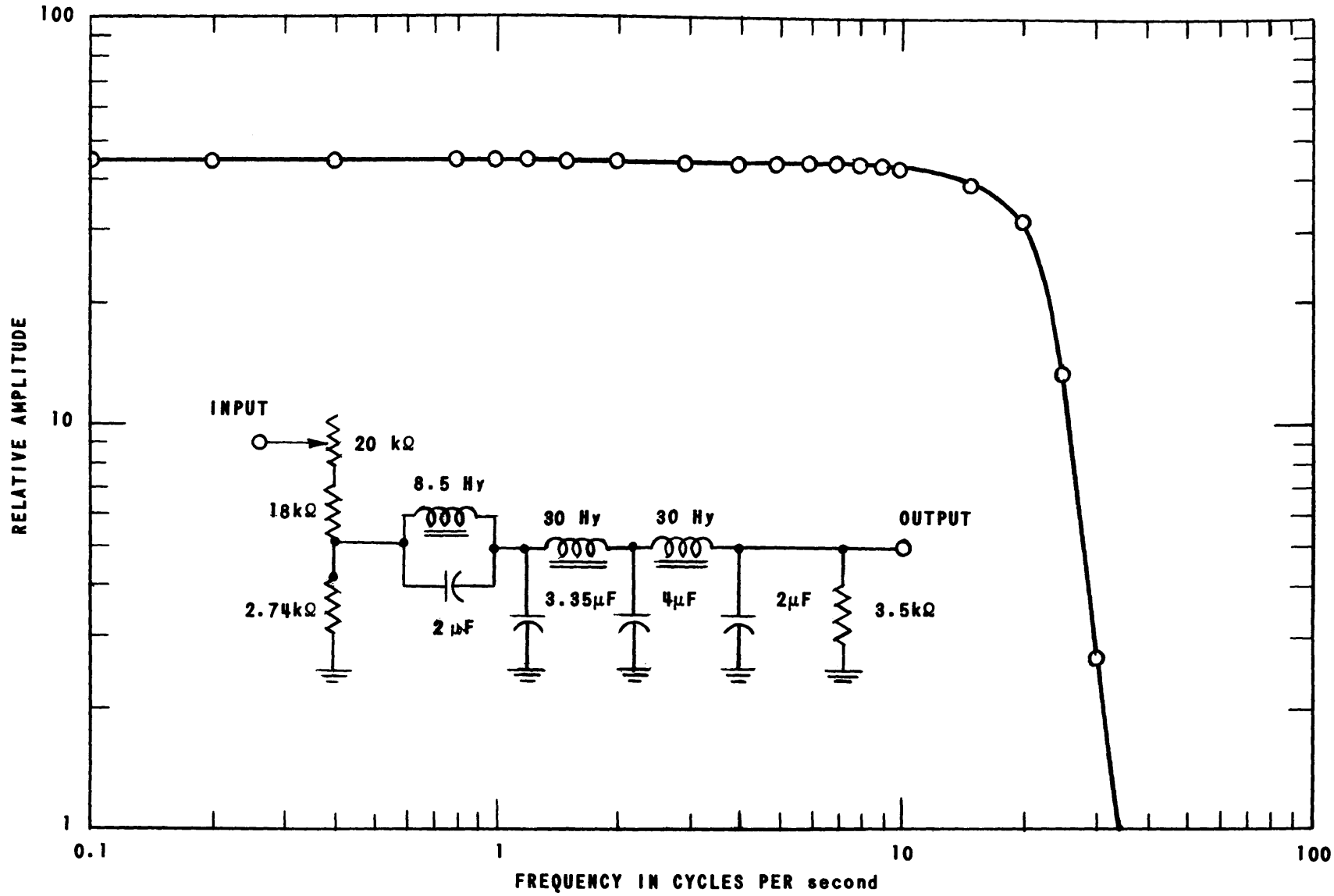

FIG. 21
AMPLITUDE RESPONSE OF M-DERIVED LOW PASS FILTER, MEASURED TOGETHER WITH THE RECORDER.

The system just described was used for the measurement of relative oscillation amplitudes only. The main source of error in this measurement was not due to the system itself, but to noise in the average heating power due to power line voltage fluctuations. This effect, mentioned in Chapter IV, was most bothersome at the low frequencies used, and is estimated to cause a probable error of $\pm$ 0.2% amplitude in the measurement of a 10% power oscillation amplitude.

The average loop power was read on an indicating watt meter type Weston, Model 310. The error in this measurement is mainly due to the current transformer, and is estimated to $\pm$ 1%.

PART III

THE THEORY OF THE EXPERIMENT

CHAPTER X

THE BOILING MECHANISM

A. A Short Review of the Theory of Nuclear Boiling

In this chapter, a short review of those aspects of boiling which have a bearing upon the present investigation will be given.

When boiling takes place at a heated surface, the bubbles originate from specific nucleating centers. It is now generally accepted that these are microscopic pits in the surface. Due to the liquid surface tension σ, the pressure inside a steam bubble must be:

$$\Delta P = \frac{2\sigma}{r} \tag{10.1}$$

greater than the pressure of the water outside, in order to keep the bubble from collapsing. It is seen that ΔP goes to infinity, as the bubble radius r goes to 0. It can be shown that if a surface cavity of radius r contains water superheated corresponding to a saturation pressure of $\Delta P + P$, where P is the pressure of the coolant, and ΔP is given by equation 10.1, then a bubble may form inside the cavity and grow out of it. The reader is referred to Zuber's work[42] for full details.

The larger the cavity, the smaller the superheat needed to form a bubble. If the heat flux is increased, the frequency and the size of the bubbles from the established nucleation centers will remain approximately constant. The surface temperature will increase sufficiently to activate additional nucleation centers, which accommodates the increased heat flux. This microscopic theory of nucleate boiling has been based mainly upon low flux experiments. Zuber[42] cites evidence to show that the specific condition of the boiling surface becomes

less important at heat fluxes close to critical. Nevertheless, the picture briefly sketched above will be used as a basis for the discussion of pressure effects on nuclear boiling which is given in Section B of this Chapter.

Jacob[43] states that only a very small part of the heat produced is directly transferred to the interior of the bubbles adhering to the surface, and that most of the heat is removed from the wall in the form of superheated liquid. In the case of subcooled boiling, this heat will be transferred directly to the cooler liquid in the middle of the channel. Or, in the case of bulk boiling, the heat will make a detour through the liquid into bubbles which grow as they flow away from the wall.

This statement was based on photographic observations at atmospheric pressure, where the latent heat of evaporation carried by the bubbles leaving the wall could only account for some 2% of the heat flux.

Experiments by Gunther and Kreith[44] gave the same results. This led Engelberg-Forster and Greif[45] to propose the following mechanism to account for the high heat transfer rates in subcooled nuclear boiling.

The surface will be covered by a thin, superheated boundary layer. As the steam bubbles grow on the surface, they will push their way through this superheated water layer. Although the growing bubble will grow partly by taking heat from the hot water outside it, some of this water will be pushed out into the cooler stream. As the bubble moves away, the space left vacant by the wall will be filled with cooler liquid. If it is assumed that the bubble will effect an exchange of water equal to its own volume, then the ratio of the heat removed from the wall in form of hot water to the heat removed as steam, can be given by:

$$J_a = \frac{c_f \ \rho_f \ (T^o_w - T^o_f)}{h_{fg} \ \rho_g} \qquad (10.2)$$

This ratio, named the Jacob's Number by Zuber[42], will attain values which agree reasonably well with experimental data taken at atmospheric pressure.

It may not be expected that the mechanism just described should give close results at very high heat fluxes and higher pressures. However, it is significant to note that at the conditions of the present experiment, the Jacob Number will be of magnitude 1. This certainly shows that now a large part of the heat removed from the surface is carried away in the form of steam.

The heat transfer rate in subcooled nuclear boiling does not depend upon the subcooling temperature of the liquid. Heat transfer data are therefore normally correlated in terms of the variable:

$$\Delta T^{o}_{sat} = T^{o}_{wall} - T^{o}_{sat} \tag{10.3}$$

Several such correlations have appeared in the literature, and a short review has been given by Lottes[46]. One of the simpler correlations is the one by Jens and Lottes[47], which can be written in the following form:

$$\frac{Q^{o}}{A_w} = K_1 \ (\Delta T^{o}_{sat})^4 e^{K_2 P^{o}} \tag{10.4}$$

The numerical values of the constants K_1 and K_2 have been given in Reference 47. The correlation was derived for subcooled boiling in water cooled channels, but agreement is also good for channels containing saturated water. The actual value of ΔT^{o}_{sat} in high pressure boiling water reactors is so low (10 - 20 degrees C), as to be of little importance to steady state reactor calculations. For the present study, however, it is of prime importance to evaluate how the heat transfer rate changes with changing conditions. This will be discussed further in the section to follow.

It should be pointed out that the concept of a heat transfer coefficient is not related to the physics of nuclear boiling, and is, therefore, of little help in understanding the mechanisms involved. This concept was arrived at during studies of convection cooling, where there is a linear relationship

between heat flux and temperature difference. In the case of nuclear boiling, one can always define a heat transfer coefficient by:

$$\frac{Q^o}{A_w} = h\Delta T^o_{sat} \tag{10.5}$$

but h will no longer be constant.

B. Pressure Effects on Nuclear Boiling

Consider a boiling channel, initially in steady state conditions, where the pressure suddenly is being raised. If the heat production rate in the channel wall is kept constant, the effect on heat transfer rate and temperatures will be as sketched in Figure 22. ΔT^o_{sat} will drop sharply, and this will render a number of nucleation centers inoperative. The heat transfer to the coolant will also drop, and heat corresponding to the cross-hatched area will be stored in the channel wall. This causes the wall temperature to rise, until enough nucleation centers have been reactivated to bring the heat transfer rate back to the original value. ΔT^o_{sat} will also increase, almost to its original value. According to Equation 10.4, the higher pressure should give a slightly lower value of ΔT^o_{sat}. This can be loosely explained by assuming that bubble size and bubble frequency from active sites remain constant. As more heat is carried away per bubble at the slightly higher pressure, some nucleation sites become superfluous, and lower ΔT^o_{sat} will suffice.

The above discussion should show that for a given channel the heat transfer rate is a function mainly of wall temperature and channel pressure. Next an attempt will be made to estimate the quantitative effect of small changes in these variables. Although the Jens-Lottes correlation, given in equation 10.4, is based on steady state boiling data, it will be assumed to give a valid picture at transient conditions as well. No other alternative is available at present.

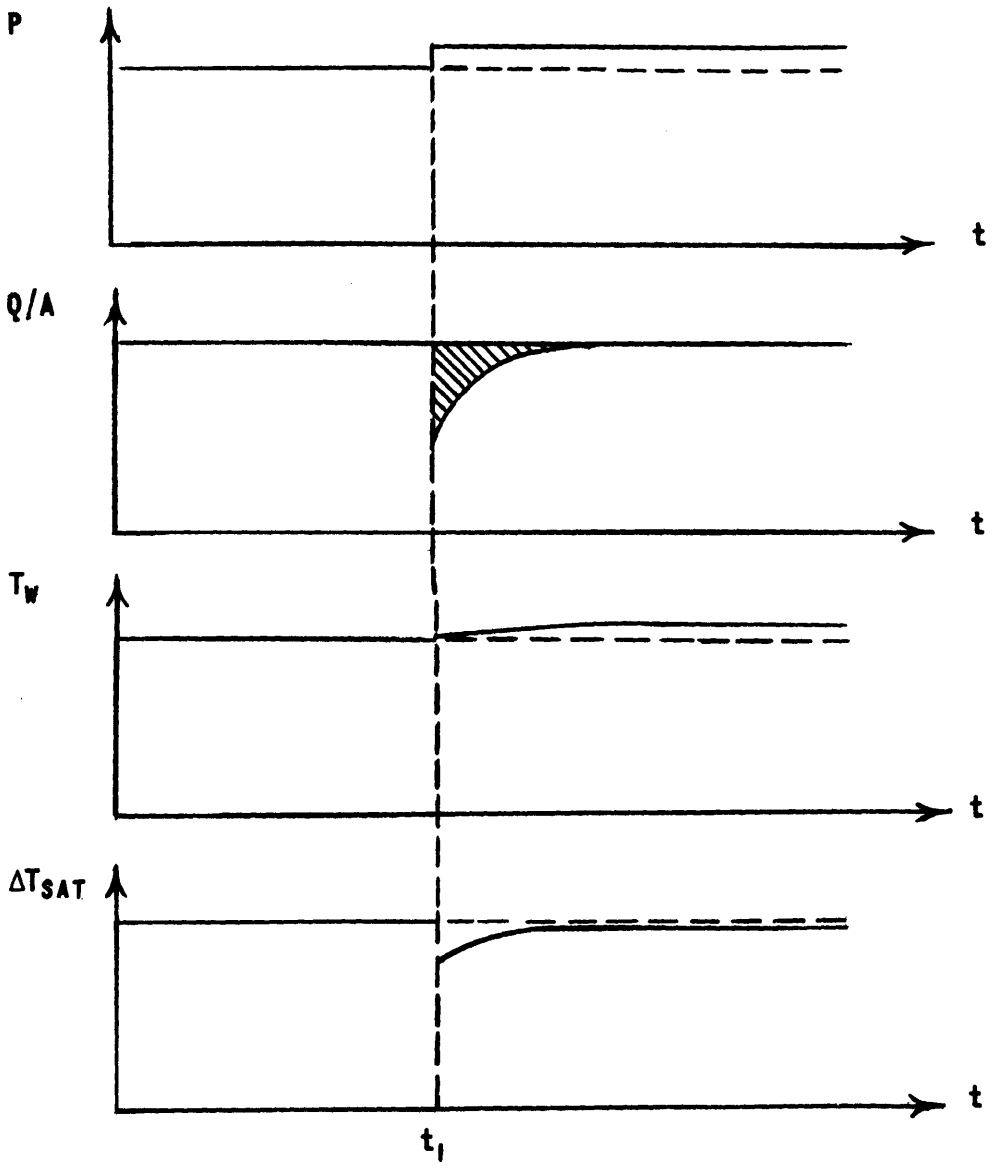

FIG. 22
THE EFFECT OF A SUDDEN PRESSURE CHANGE IN A BOILING CHANNEL

A note about the nomenclature used must be made at this point. The variables Q (heating rate), T (temperature), P (pressure) and α (void fraction), carry superscript o if the total values of the parameters are to be indicated. Without superscript, the same variables indicate differential values, or rather: the variation from mean values.

Now, considering T^{o}_{sat} to be a function of pressure, the differential of the heat transfer rate can be found from equation 10.4:

$$\frac{Q}{A_w} = 4h\, T_w + h \left[K_2\, \Delta T^{o}_{sat} - 4\, \frac{T_{sat}}{P} \right] P \qquad (10.6)$$

h has been defined by equation 10.5. $\frac{T_{sat}}{P}$ can be evaluated directly from the steam tables[35].

The negative term in the bracket is always predominant. The transient heat transfer will therefore decrease with increasing pressure, as would be expected.

If the pressure in the channel is kept constant, and only the wall temperature varies, an "incremental heat transfer coefficient" can be defined from equation 10.6, as follows:

$$h_i \triangleq \frac{\frac{Q}{A}}{T_w} = 4\, h \qquad (10.7)$$

The correct heat transfer coefficient to use in a model describing transient phenomena should be 4 times the "average" value as defined by equation 10.5, because of the 4'th order relationship given in equation 10.4.

C. The Growth of Steam Bubbles

It was stated earlier that only part of the heat is carried away from the wall as steam. The rest is removed in the form of superheated water, and in the region of bulk boiling will be converted into steam bubbles at a later time. This delay effect may be of importance to the power-to-void transfer function, and will now be discussed further.

At atmospheric pressure bubble growth times as large as several tenth's of a second have been observed[43]. These were very large bubbles, studied under conditions very different from the ones of the present experiment. To the knowledge of this writer, no bubble growth studies in water close to the present conditions have been published. Several theoretical studies have been carried out, two of which will be referred to in the following.

Zuber[42] has shown that in bulk boiling a bubble, after having been released from the wall, will stop growing when the bubble diameter is given by:

$$D_{max} = d_s \ J_a \tag{10.8}$$

where d_s, the thickness of the superheated film at the wall is given by:

$$d_s = \kappa_2 \frac{\Delta T^o_{sat}}{Q^o/A_w} \tag{10.9}$$

κ_2 is the thermal conductivity of water.

For the conditions of the present experiment, the value of the Jacob Number is of the order 1, and the magnitude of d_s will in all cases be less than 0.1 cm[50]. The following observations can be made:

1. The growth of a bubble after its detachment from the surface will be very limited.
2. The maximum size of newborn bubbles will be in the order of 0.1 cm or less.

Griffith[48] studied bubble growth rates experimentally in saturated boiling at atmospheric pressure, and derived a model which was extrapolated to higher pressures. In water, at pressures in the neighborhood of 40 atmospheres, characteristic bubble growth times from 0.5 to 1 millisecond was predicted. Bubble delays as short as this will be of no importance whatsoever in the present transfer function study.

In the following, it will be assumed that steam bubbles are formed with no delay.

The time taken for a steam bubble to reach equilibrium velocity after being released from the wall, has been studied in Reference 50. It is concluded that this time is in the order of1-2 milliseconds at the conditions of the present experiment. This time delay also will be neglected in the chapters to follow.

D. The Collapse of Steam Bubbles

The assumption of complete mixing in any section transverse to the flow direction is frequently made in the study of boiling channels. As mentioned in Chapter I, all reactor transfer function models previously published have adopted this assumption, which leads to the division of the channel in two parts:

1. The "non-boiling section" with subcooled boiling, where all steam bubbles rapidly collapse after release from the wall.
2. The "boiling section", where the coolant temperature throughout is T^{o}_{sat}. The heat added all goes to build up additional steam, and no collapse of bubbles takes place.

Unfortunately, this simple picture does not conform to the conditions in high pressure boiling water reactors. Especially in natural convection reactors, where the subcooling is low, and the inlet velocity limited, steam voids build up rapidly all the way from the inlet[49]. At the point of division (this is the bulk boiling point defined in Chapter XI), the steam void fraction may well be 10 - 20%. This can only be accounted for by the existence of subcooled water above this point. This has been explained[50] by the presence of a "cold spike" of subcooled water in the middle of the channel. The point where no subcooled water remains is difficult to determine with certainty. Marchaterre and Petrick[51] predict that this point is to be found at vapour fractions of about 30%, while Maurer[52] gives 40% for high pressure Bettis data.

Lottes[53] observed steam bubbles in a stream of subcooled water in a horizontal tube, and noted bubble lifetimes up to several tenth's of a second.

This question will now be raised: How large a fraction of the steam bubbles produced in the subcooled region actually do collapse? An indication of the answer should be given by the derivation to follow.

Consider a volume element of height dx, and of cross sectional area equal to the test channel. At steady state conditions, the inflow and boil-off rate of steam is balanced by steam outflow and bubble collapse. In the subcooled region it will be assumed:

$$\frac{1}{1+J_a} = \frac{\text{Heat used in bubble formation}}{\text{Total heat production}} \tag{10.10}$$

This first order approximation follows from the discussion related to equation 10.0.2.

If λ is the fraction of the total steam volume which collapses in the volume element per unit time, a steam balance gives:

$$dt\, A\, \alpha^o(x)\, Cg(x) + \frac{1}{1+J_a}\, \frac{\frac{Q^o}{L}\, dx\, dt}{h_{fg}\, \rho_g} = A\, \alpha^o(x+dx)\, Cg(x+dx)\, dt + \lambda(x)\, A\, \alpha^o(x)\, dx\, dt \tag{10.11}$$

Solving for $\lambda(x)$:

$$\lambda(x) = \frac{1}{\alpha^o}\, \frac{1}{1+J_a}\, \frac{Q^o}{h_{fg}\, \rho_g V} - \frac{dC_g}{dx} - \frac{C_g}{\alpha^o}\, \frac{d\alpha^o}{dx} \tag{10.12}$$

With increasing height, more heat goes to form steam bubbles, and the fraction in equation 10.10 will eventually reach 1. This should correspond to the point where no subcooled water remains, and where we must have $\lambda \to 0$. Therefore:

$$\text{For } x \gg x_s: \quad \frac{d\alpha^o}{dx} = \frac{Q^o}{C_g\, h_{fg}\, \rho_g\, V} - \frac{\alpha^o}{C_g}\, \frac{dC_g}{dx} \tag{10.13}$$

Except for the use of an average steam velocity C_g over the cross sectional area, this relation is exact, and can be used to check experimental data.

The steam bubble half life defined by

$$\tau_{1/2}(x) = \frac{\ln 2}{\lambda(x)} \tag{10.14}$$

have been plotted in Figure 23 for a traverse as part of Run No. 10. The equations for calculating steam and water velocities will be given in Chapter XI. At this point attention is drawn to the curves for $\tau_{1/2}(x)$. Two such curves, calculated from equation 10.12 using 10.14, have been given. One for the value J_a calculated for the conditions of the run by equation 10.2, and the other by taking $J_a = 0$. The last case corresponds to the assumption that all the heat is turned into steam, and will give the minimum limit for $\tau_{1/2}$. The dotted line between the two curves is sketched in. It shows roughly the half life to be expected in this region, where less and less of the heat is passed directly to the subcooled water in the channel without going through intermediary steam bubbles.

The exact value of the fraction defined in equation 10.10 is not known, and there are also errors in Cg and α. This precludes a high degree of confidence in the results as far as numerical values are concerned. However, it is believed that these conclusions can be drawn:

1. Steam bubbles in the subcooled region have a relatively long life expectancy.
2. As these bubbles are continuously flowing into regions of increasing $\tau_{1/2}$, a large fraction of bubbles created near the inlet will "make it" through the section outlet.
3. The curves show evidence that subcooled pockets of water may exist at very high values of the steam void fraction.

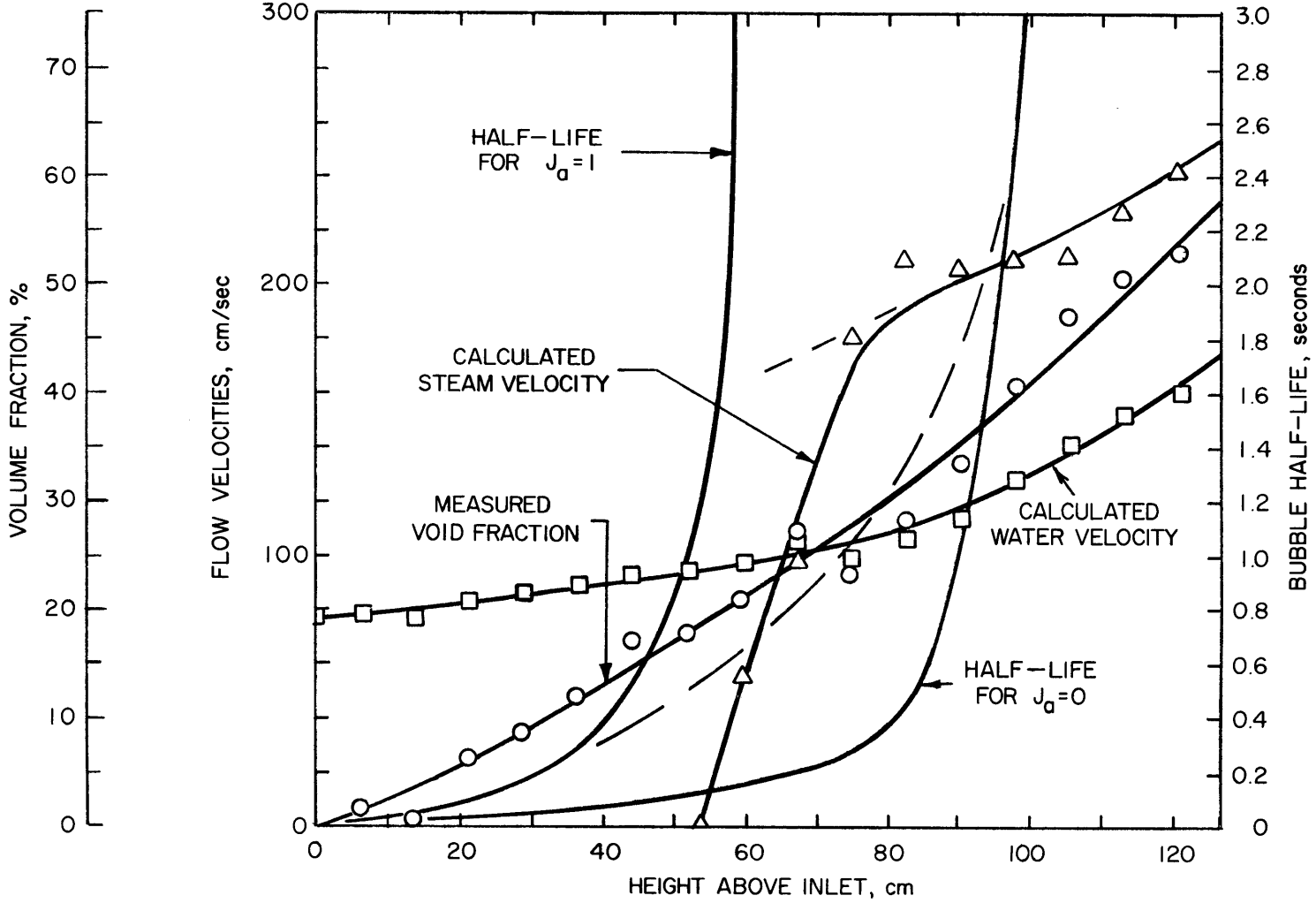

FIGURE 23
LIFE EXPECTANCY OF STEAM BUBBLES
RUN NO. 10*, 27.2 Ata, 47.9 kw/l
ΔT_{sub} = 8.6 °C

CHAPTER XI

THE CHARACTERISTIC VELOCITIES IN THE TEST CHANNEL

A. Calculation of Water and Steam Velocity

It is of interest for the interpretation of the transfer function measurements to know what the steam and water velocities are in the test channel. No satisfactory method exists for measuring these variables as functions of height in pressurized channels, although Popper[54] has used turbine type flowmeters to measure the water velocity at the exist of the test element.

A measurement of the steam volume fraction at a particular position gives the relative cross sectional areas occupied by steam and water. The flow velocities can then be computed if the mass flow rates of steam and water are known. The latter quantities can be calculated in the upper part of the test channel where it can be assumed that no subcooled water remains. This approach will be used here.

Assume for the time being that the mixing transverse to the flow direction is complete. The heating rate Q^o is uniform over the height of the test channel. Inlet flow rate W_o, inlet temperature T^o_o and saturation temperature T^o_{sat} are all known.

We can now divide the test channel into a "non-boiling" and a "boiling" section, as mentioned in Chapter X. The dividing point - the bulk boiling point x_s - is given by:

$$x_s = L \frac{W_o c_f \Delta T^o_{sub}}{Q^o} \tag{11.1}$$

This formula is easily arrived at by assuming that all heat produced in the channel wall from inlet to x_s goes to raise the water temperature the amount:

$$\Delta T^o_{sub} = T^o_{sat} - T^o_o \tag{11.2}$$

Above x_s, all heat goes to produce steam. The steam mass flow rate as a function of x ($x > x_s$), is then given by:

$$W_g = C_g \alpha^o A \rho_g = \frac{(x - x_s)Q^o}{Lh_{fg}} \tag{11.3}$$

In this equation we have neglected the contribution from steam flashing due to the pressure drop along the channel. This is important at low pressures. But at the lowest pressure used in this experiment, 27.2 Ata, the maximum error in C_g (at the exit, at $\Delta T_{sub} = 0$) due to the approximation in equation 11.3, has been calculated to be 2% only.

Solving equation 11.3 for the steam velocity:

$$C_g = \frac{(x - x_s)Q^o}{V\alpha^o \rho_g h_{fg}} \tag{11.4}$$

The water mass flow rate:

$$W_f = C_f(1 - \alpha^o)A_f = W_o - W_g \tag{11.5}$$

giving the water velocity:

$$C_f = \frac{W_o - W_g}{(1 - \alpha^o)A \rho_f} \tag{11.6}$$

It was stressed in Chapter X that the mixing in the channel is not complete, and that subcooled water may be present far above x_s. Near the outlet, however, where all the water will have reached T^o_{sat}, the formulas above will give correct average values for C_g and C_f.

Equation 11.6 for C_f can be used all the way from the inlet. Although the correct value of W_g is not accurately known, only small errors will result as we have $W_g \ll W_o$ in the lower region.

Equations 11.1, 11.2, and 11.3 have been used[50] to calculate C_g for all x-values above x_s. Although correct steam velocities are not obtained in the lower end of the range, the results can give valuable information when plotted as a function of x. From the shape of the curve it is possible to judge where all of the water finally reaches the saturation temperature. (Knee in C_g-curve).

B. The Uncertainty in the Calculation of Flow Velocities

From equation 11.4, there results:

$$\frac{\Delta C_g}{C_g} = \left[\left(\frac{\Delta \alpha}{\alpha^o} \right)^2 + \left(\frac{\Delta Q}{Q^o} \right)^2 + \left(\frac{\Delta x_s}{x - x_s} \right)^2 \right]^{1/2} \qquad (11.7)$$

where the contribution from Δx_s can be computed from equation 11.1. Near the outlet, the uncertainty in α^o is the dominating factor. For a $\Delta\alpha$ of 5% of tube cross section:

$$\frac{\Delta C_g}{C_g} \simeq \frac{\Delta \alpha}{\alpha^o} = \frac{5}{0.5} = \underline{10\%}$$

if an average void fraction of 50% is assumed.

Similarly for the water velocity:

$$\frac{\Delta C_f}{C_f} = \left[\left(\frac{\Delta W_g}{W_o - W_g} \right)^2 + \left(\frac{\Delta \alpha}{1 - \alpha^o} \right)^2 \right]^{1/2} \simeq \frac{\Delta \alpha}{1 - \alpha^o} \qquad (11.8)$$

$$\frac{\Delta C_f}{C_f} \simeq \frac{5}{0.5} = \underline{10\%}$$

Errors in α^o will result in larger errors in C_g and C_f.

C. Steam Slip Ratio. Flow Regimes

The purpose of this and the following section is to present some background information which will be of value later. This material should help in the appraisal of the assumptions on which the derivation of the transfer functions is based.

It has been established through the work of several experimenters (see for instance the review given by Marchaterre[46]), that the average steam velocity in a vertical channel generally is greater than the average water velocity.

The steam slip ratio S is defined by:

$$S = \frac{C_g}{C_f} \tag{11.9}$$

For test channels similar to the present one, and at comparable conditions, slip ratios at the outlet in the order of 1.5 to 2.5 have been measured.

Theoretical studies[50] indicate that the relative rise velocity of an isolated bubble surrounded by water is much too small to account for the slip ratios measured. The phenomenon of slip is explained by the tendency of the steam bubbles to assemble in the middle of the channel, where the general flow velocity is higher than near the wall. There is reason to believe that slip ratios of the order mentioned cannot exist unless the steam and water phases are unevenly distributed over the channel cross section.

This points out the importance of knowing what the flow is like in the channel. Four different "flow regimes" are generally recognized:

1. Separate Bubble Flow. With the bubbles distributed more or less evenly over the cross section, slip ratios close to 1 would be expected.
2. Slug Flow. Bubbles conglomerate in the middle of the channel to form clusters. These are spaced apart fairly regularly along the direction of flow. The separate bubbles in each cluster will gradually grow into a single bubble which almost fills the channel cross section. These large bubbles move faster than the slugs of water separating them, and slips in the order 1.5 to 2.5 may result.
3. Annular Flow. In this case there is a continuous steam passage up the middle of the channel. Very high steam slips can be expected.

4. Froth Flow. Small droplets of water are suspended in the steam and mixed homogenously over the cross section. Slips close to 1 result.

The flow regimes have been listed in the order of increasing steam void fraction, and more than one regime would generally be seen along a single heated section. A more detailed discussion on the subject of flow patterns is given by Isbin, Moen, and Vohr[55]. A literature survey on the general subject of two-phase flow has been given by Maung Maung-Myint[56].

There are reasons to believe (see Part IV) that the flow in the upper part of the test section used in this experiment should be classified as slug flow for most of the conditions studied. This type of flow has been described by Griffith and Wallis[57], and by Moissis and Griffith[58]. Experiments were carried out at atmospheric pressure in tubes where no boiling was taking place along the walls. The theory presented predicts well the slips observed.

On the assumption that slug flow does exist in the present test channel, the theory mentioned above can be applied. Slip ratios in the order of 1.5 to 2 are predicted.

D. The Velocity of Sound in Two-Phase Mixtures

In order to evaluate how perturbations in steam volume propagate along a boiling channel, it is of great interest to know the velocity of a pressure wave in a steam/water mixture. Unfortunately, no experiment giving direct measurements of this quantity has been found in the literature. Some measurements of critical flow velocities have been made[59]. These measurements were taken at low pressures and very high void fractions, and the bearing of the results upon the present discussion is somewhat doubtful.

The velocity of sound in an air/water mixture was studied experimentally and theoretically by Karplus[60]. At atmospheric pressure he found a minimum velocity of 20 m/sec at 50% air volume concentration. This compares with a sound velocity of 1500 m/sec in water, and 340 m/sec in air. The velocity was

found to be less than 30 m/sec for the volume fraction range of 10 - 90%. The damping of the sound energy with distance was found to be extremely large. Similar theoretical results have been presented by Heinrich[61].

These results show that the velocity of sound may be extremely low in steam/water mixtures, where the processes of condensation and evaporation provide another damping effect.

Karplus[62] has given a theoretical study of the velocity of sound in steam/water mixtures also. For the assumption of complete homogenity of the mixture, the velocity becomes a strong function of steam quality (steam-to-water mass ratio), and of pressure. The sound velocity increases with both parameters in the region of interest. The theory predicts velocities as low as a few meters per second at atmospheric pressure at steam qualities comparable with the conditions in boiling channels. For the conditions of the present experiment, velocities in the order of 20 - 30 m/sec are predicted.

CHAPTER XII

The Power-to-Temperature Transfer Function in Highly Subcooled Boiling

A. The General Equations

As an introduction to the derivation of the power-to-void transfer function we will discuss this simpler case.

A boiling section with parallel plate geometry is considered. d_2 is the halfwidth of the coolant channel as shown in Figure 24. d_1 is the full wall thickness for the present experiment, or the half thickness in case the heated plate is cooled on both sides.

For constant inlet flow and inlet temperature, the transfer function for the outlet temperature will be found. The heating rate is assumed uniform throughout the channel wall.

There is no buildup of steam along the tube, as we assume that steam bubbles collapse immediately upon release from the wall. The channel pressure is assumed constant as the power varies, and the heat transfer rate from wall to coolant will then be a function of wall temperature only.

The solution for this simpler problem will be presented fully, to illustrate the methods used in the following chapters also. It is important to note that below, T_1 and T_2 are perturbed values, giving the temperature differences from average temperatures.

The wall temperature:

$$\frac{\partial^2 T_1(y,t)}{\partial y^2} + \frac{Q(t)}{A_w d_1 K_1} = \frac{\rho_1 c_1}{K_1} \frac{\partial T_1(y,t)}{\partial t} \tag{12.1}$$

Q/A_w gives the perturbed heat flux per unit surface area. The other symbols are defined in the Nomenclature. No heat transport in the wall along the x-axis is considered.

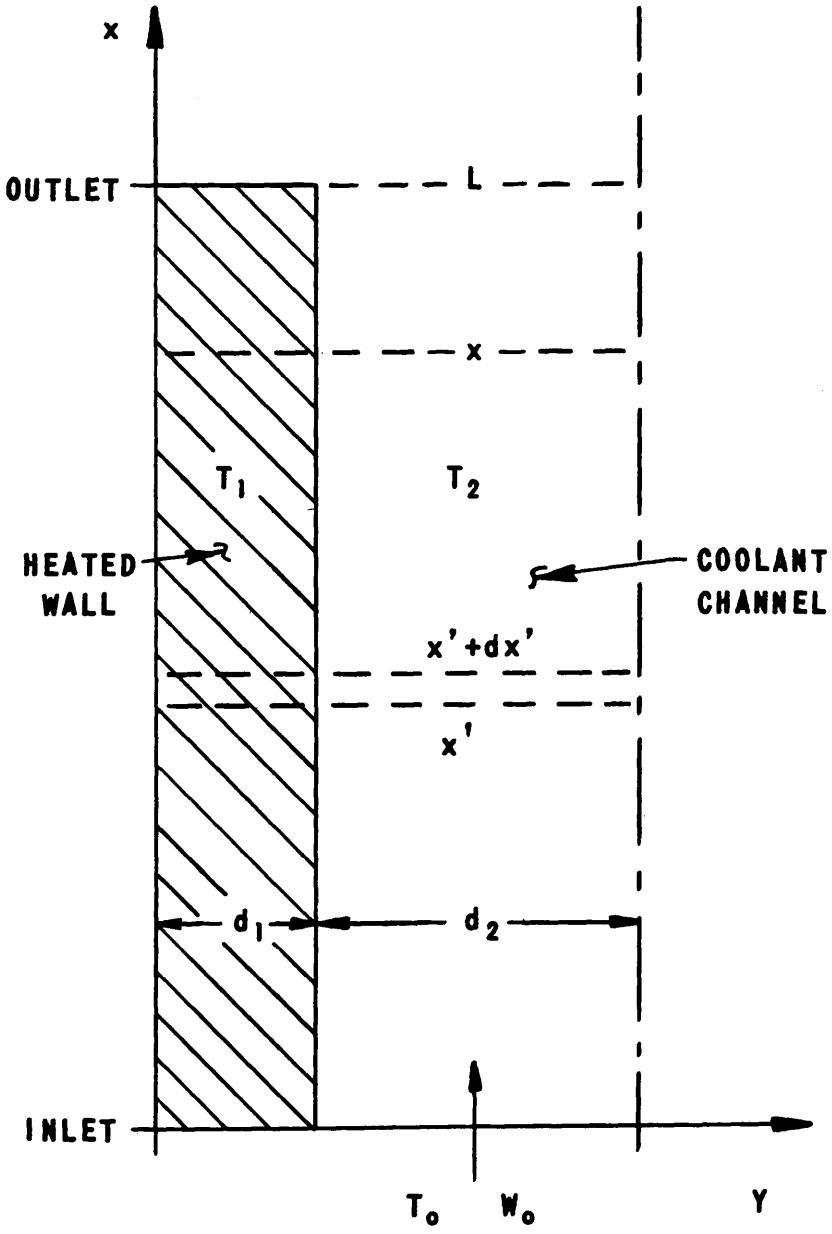

FIG. 24
TEST CHANNEL GEOMETRY

Initial condition:

$$T_1(y,0) = 0 \tag{12.2}$$

Boundary conditions:

$$\frac{\partial T_1(0,\ t)}{\partial y} = 0 \tag{12.3}$$

$$\frac{\mathbf{Q}_1(d_1, t)}{\mathbf{A}_w} = h_i\ T_1(d_1,t) = -\kappa_1 \frac{\partial T_1(d_1,t)}{\partial y} \tag{12.4}$$

The water temperature:

$$p\ h_i T_1(d_1,t) - \rho_2 A C_0 c_2 \frac{\partial T_2(x,t)}{\partial x} = \rho_2 A\ c_2 \frac{\partial T_2(x,t)}{\partial t} \tag{12.5}$$

T_2 is an average water temperature defined by complete mixing in the y-direction.

Initial, and boundary conditions:

$$T_2(x,0) = 0 \tag{12.6}$$

$$T_2(0,t) = 0 \tag{12.7}$$

The equations 12.1 through 12.4 form a complete set which will now be solved for $\bar{T}_1(y,s)$, by the Laplace transform technique. This solution will next be substituted into equation 12.5 which then can be solved for $\bar{\bar{T}}_2(x,s)$.

Note that barred symbols indicate Laplace transforms. A double bar is used if a function has been transformed with respect to two independent variables. The Laplace transform of the time t will be denoted s according to usual practice.

B. The Wall-Temperature Transfer Function

The transform of the equations 12.1, 12.3 and 12.4 with respect to time:

$$\frac{\partial^2 \bar{T}_1(y,s)}{\partial y^2} + \frac{\bar{Q}(s)}{A_w d_1 K_1} = \frac{\rho_1 c_1}{K_1} \; s\bar{T}_1(y,s) \tag{12.8}$$

$$\frac{\partial \bar{T}_1(0,s)}{\partial y} = 0 \tag{12.9}$$

$$h_i \; \bar{T}_1(d_1,s) = -K_1 \frac{\partial \bar{T}_1(d_1,s)}{\partial y} \tag{12.10}$$

The transform of equation 12.8 with respect to y, making use of equation 12.9:

$$\bar{y}^2 \; \bar{\bar{T}}_1(\bar{y},s) - \bar{y} \; \bar{T}_1(0,s) + \frac{1}{\bar{y}} \frac{\bar{Q}(s)}{A_w d_1 K_1} = \frac{\rho_1 c_1}{K_1} \; s \; \bar{\bar{T}}_1(\bar{y},s) \tag{12.11}$$

Solving for $\bar{\bar{T}}_1(\bar{y},s)$:

$$\bar{\bar{T}}_1(\bar{y},s) = \frac{\bar{y}}{\bar{y}^2 - \gamma^2} \; \bar{T}_1(0,s) - \frac{1}{\bar{y}(\bar{y}^2 - \gamma^2)} \; \frac{\bar{Q}(s)}{A_w d_1 K_1} \tag{12.12}$$

where, by definition:

$$\gamma^2 \triangleq \frac{\rho_1 c_1}{K_1} \; s \tag{12.13}$$

Taking the inverse transform with respect to y:

$$\bar{T}_1(y,s) = \bar{T}_1(o,s) \cosh y\gamma + \frac{1}{\gamma^2} \frac{\bar{Q}(s)}{A_w d_1 K_1} \left[1 - \cosh y\gamma\right] \tag{12.14}$$

Inserting this into equation 12.10 and solving for $\bar{T}_1(0,s)$:

$$\bar{T}_1(0,s) = \frac{\bar{Q}(s)}{\rho_1 c_1 d_1 A_w s} \left[1 - \frac{1}{\cosh d_1\gamma + \frac{\gamma \kappa_1}{h_i} \sinh d_1\gamma} \right] \tag{12.15}$$

Finally, inserting equation 12.15 into 12.14, and taking $y = d_1$:

$$\bar{T}_1(d_1,s) = \frac{\bar{Q}(s)}{\rho_1 c_1 d_1 A_w s} \frac{1}{\frac{h_i}{\gamma \kappa_1} \coth d_1\gamma + 1} \tag{12.16}$$

or:

$$\bar{T}_1(d_1,s) = \frac{\bar{Q}(s)}{h_i A_w} \frac{1}{\sqrt{\tau_1 s} \coth \sqrt{\tau_1 s} + \tau_i s} = \frac{\bar{Q}(s)}{h_i A_w} G(s) \tag{12.17}$$

where we have defined:

1) The wall time constant

$$\tau_1 \triangleq \frac{c_1 \rho_1 d_1^2}{\kappa_1} \tag{12.18}$$

formed by the heat capacity of the wall together with the heat flow resistance through the wall, and

2) The heat transfer time constant

$$\tau_i \triangleq \frac{c_1 \rho_1 d_1}{h_i} \tag{12.19}$$

formed by the heat capacity of the wall, together with the incremental "film resistance."

In a given case τ_1 can be calculated accurately. It will be realized from the discussion in Chapter X, that this is not the case with τ_i, as it is not possible at present to obtain accurate values for h_i. The possibility of measuring h_i through the use of equations 12.15, or 12.17 will be discussed further in Part IV.

The function

$$G(s) \triangleq \frac{1}{\sqrt{\tau_1 s}\ \coth \sqrt{\tau_1 s} + \tau_i s} = \frac{\bar{Q}_1(d_1,s)}{\bar{Q}(s)} \tag{12.20}$$

has been plotted in Figure 25 for several different values of h_i. In all cases we have taken $\tau_1 = 0.183$ sec, which is the correct value for the test tube used in this experiment at a saturation pressure of 41 Ata. The curves show that G(s) can be fairly well represented by a single time constant for the frequency interval used in the present experiment.

It should be pointed out that the one time-constant approximation is less good for larger values of τ_1.

The power-to-surface temperature transfer function for clad fuel elements have been given by several authors, see for instance Jacobs[63], or Narin and Langford[64].

C. The Outlet Temperature Transfer Function

The Laplace transform of equation 12.5 with respect to time:

$$\frac{p\, h_i}{\rho_2 A C_0 c_2}\ \bar{T}_1(d_1,s) - \frac{\partial \bar{T}_2(x,s)}{\partial x} = \frac{s}{C_0}\ \bar{T}_2(x,s) \tag{12.21}$$

The transform of this with respect to x:

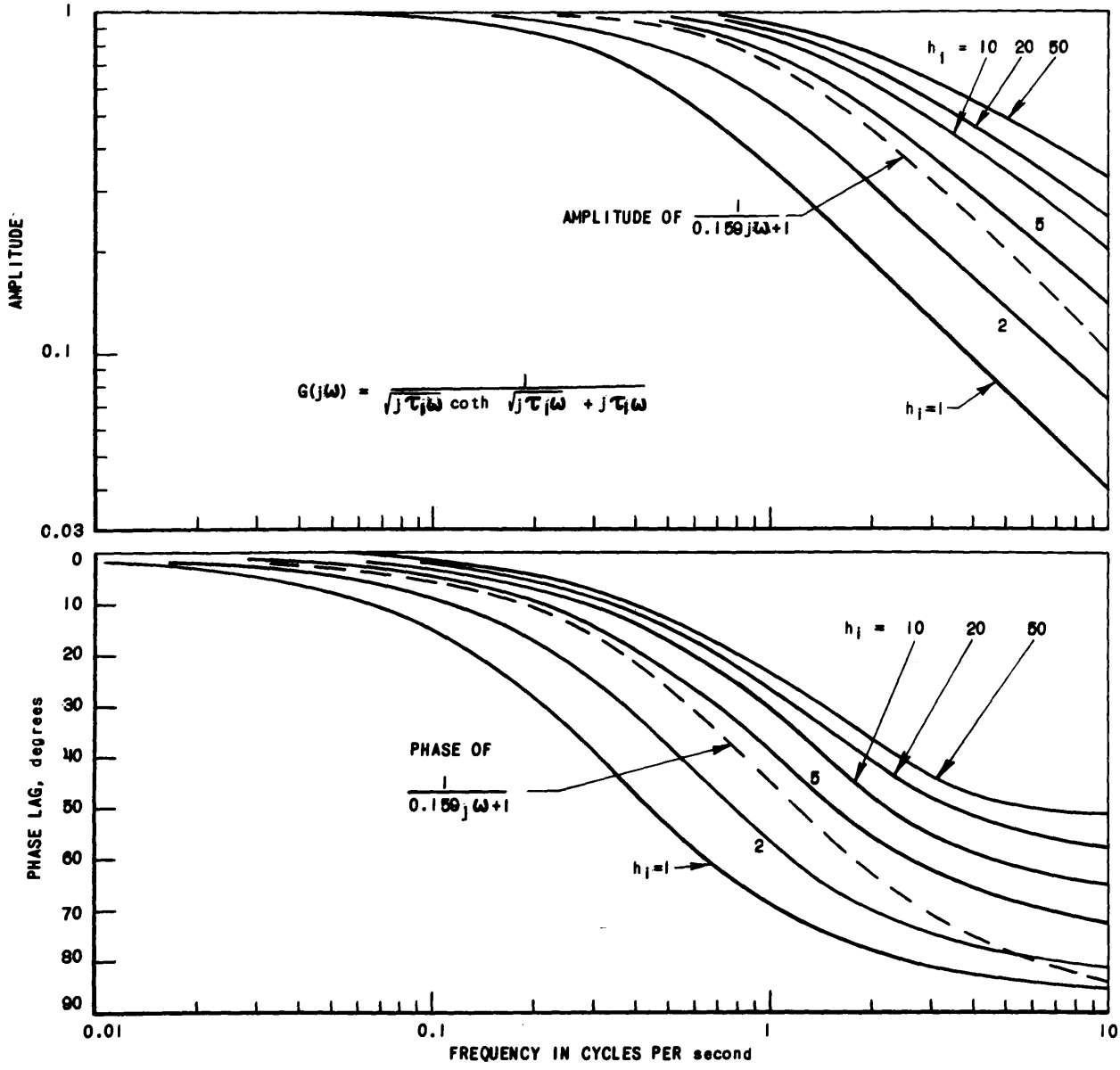

FIG. 25
AMPLITUDE AND PHASE OF THE FUNCTION $G(s)_2$
FOR DIFFERENT VALUES OF h_i (GIVEN IN watt/cm^2°C)

$$\frac{1}{\bar{x}} \frac{ph_i}{\rho_2 AC_0 c_2} \bar{T}_1(d_1,s) - \bar{x}\,\bar{\bar{T}}_2(\bar{x},s) = \frac{s}{C_0}\,\bar{\bar{T}}_2(\bar{x},s) \tag{12.22}$$

Solving for $\bar{\bar{T}}_2(\bar{x},s)$:

$$\bar{\bar{T}}_2(\bar{x},s) = \frac{1}{\bar{x}\left[\bar{x} + \frac{s}{C_0}\right]} \frac{p\,h_i}{\rho_2 AC_0 c_2}\,\bar{T}_1(d_1,s) \tag{12.23}$$

Taking the inverse transform with respect to x, and using equation 12.17, we get:

$$\bar{T}_2(x,s) = \frac{\bar{Q}(s)}{LA} \frac{1}{\rho_2 c_2}\, G(s)\, \frac{1-e^{-\frac{sx}{C_0}}}{s} \tag{12.24}$$

This can be written:

$$\bar{T}_2(x,s) = \frac{\bar{Q}(s)}{V} \frac{x}{\rho_2 C_0 c_2}\, G(s)\, \frac{1-e^{-st_x}}{st_x} \tag{12.25}$$

where we have defined

$$t_x = \frac{x}{C_0} \tag{12.26}$$

which is the water flow time from the inlet to the position x.

Equation 12.25 can be written in a different form which will be of use later. If $Q_2(x,t)$ denotes the perturbations in heat flowing past point x, we have:

$$Q_2(x,t) = T_2(x,t)\; C_0 A \rho_0 c_2 \tag{12.27}$$

If this is Laplace transformed, and inserted into equation 12.25, we get:

$$\overline{Q}_2(x,s) = \overline{Q}(s)\,\frac{x}{L}\,G(s)\,\frac{1-e^{-st_x}}{st_x} \qquad (12.28)$$

This simple expression gives the transfer function between heat produced in the wall, and heat transported past the point x. Three factors appear:

1) An amplitude factor x/L

2) A heat transfer delay factor G(s) given by equation 12.20

3) A heat transport delay factor $(1-e^{-st_x})/st_x$.

Most previous workers (see Section B, Chapter I) have used a single time-constant term to represent the transport delay. A time constant equal to $t_x/2$ have generally been used. A series expansion of the exponential in the expression above will lead to this result.

Akcazu[15] has presented the transport delay factor given, and discussed the validity of different approximations. He has further estimated the effect on the transport delay factor of spread in transport times around the value t_x. His result will be discussed further at the end of Chapter XIII.

CHAPTER XIII

The Power-to-Outlet Temperature Transfer Function with No Boiling

A. Derivation

In a channel where the water is highly subcooled, and where the heat flux is low, the heat transfer from wall to coolant is given by:

$$\frac{Q_1(x,d_1,t)}{A_w} = h_i \left[T_1(x,d_1,t) - T_2(x,t)\right] \tag{13.1}$$

This equation can be assumed to hold for average as well as perturbed values of the parameters, as we have $h_i = h$.

Contrary to the case treated in Chapter XII, the heat transfer rate from wall to coolant now depends upon the water temperature. With all other assumptions unchanged, the differential equations become (note the analogy to equations 12.1 through 12.7):

The wall temperature:

$$\frac{\partial^2 T_1(x,y,t)}{\partial y^2} + \frac{Q(t)}{A_w d_1 \kappa_1} = \frac{\rho_1 c_1}{\kappa_1} \frac{\partial T_1(x,y,t)}{\partial t} \tag{13.2}$$

Initial, and boundary conditions:

$$T_1(x,y,0) = 0 \tag{13.3}$$

$$\frac{\partial T_1(x,0,t)}{\partial y} = 0 \tag{13.4}$$

$$h_i \left[T_1(x,d_1,t) - T_2(x,t)\right] = -\kappa_1 \frac{\partial T_1(x,d_1,t)}{\partial y} \tag{13.5}$$

The water temperature:

$$ph_i \left[T_1(x,d_1,t) - T_2(x,t)\right] - \rho_2 AC_0 c_2 \frac{\partial T_2(x,t)}{\partial x} = \rho_2 Ac_2 \frac{\partial T_2(x,t)}{\partial t} \qquad (13.6)$$

Initial, and boundary conditions:

$$T_2(x,0) = 0 \qquad (13.7)$$

$$T_2(0,t) = 0 \qquad (13.8)$$

These equations can be solved by the double Laplace transform method illustrated in Chapter XII. Because equation 13.5 contains T_2 as well as T_1, the procedure becomes more involved in this case. The derivation will not be carried out here, only the results will be given.

The transfer function for the water temperature at height x, becomes:

$$\overline{T}_2(x,s) = \frac{\overline{Q}(s)}{AC_o\rho_2 c_2} \frac{x}{L} G(s) \frac{1-e^{-\left[1+\delta G(s)\right] st_x}}{\left[1+\delta G(s)\right] st_x} \qquad (13.9)$$

where G(s) is the wall transfer function given by equation 12.20, and where δ is defined by:

$$\delta \triangleq \frac{pd_2}{A} \frac{c_1\rho_1 d_1}{c_2\rho_2 d_2} \qquad (13.10)$$

For an MTR-type reactor fuel element, the factor pd_2/A will be equal to 1. In the present case, the end walls of the rectangular tube were heated also, and we find:

$$\frac{pd_2}{A} = 1.25$$

The product $c\rho$, the heat capacity per unit volume, is a very weak function of temperature for most materials. For saturated water this number varies less than 1% between 7 and 70 Ata (100 - 1000 psia). For a water filled test tube, therefore, δ can be considered a constant through a very wide range. For the test tube used in this experiment:

$$\delta = 1.25 \times 0.164 = 0.205$$

The transfer function for heat flow past the point x, can now be written:

$$\overline{Q}_2(x,s) = \overline{Q}(s) \; \frac{x}{L} \; G(s) \; \frac{1-e^{-\left[1+\delta G(s)\right] st_x}}{\left[1+\delta\, G(s)\right] st_x} \tag{13.11}$$

This result reduces to equation 12.28 if δ is taken equal to zero. This is realized when:

$$c_1\rho_1 d_1 << c_2\rho_2 d_2 \tag{13.12}$$

that is when the heat capacity of the wall is very small compared to that of the coolant.

The general solution for the outlet coolant-temperature transfer-function for clad fuel plates has been given by Gyftopoulos and Smets[65] . Storrer[66] has treated the same problem for clad cylindrical fuel pins, using a different approach.

The solution to the present problem has not previously been presented in the form of equation 13.11, which so clearly brings out the "δ -effect" in the heat exchange mechanism between coolant and wall. This effect will be discussed in the following section.

B. The Change in the Transport Factor due to Heat Exchange between Coolant and Wall.

The results of the previous section will now be discussed and compared

with the results of Chapter XII. It will be shown that the main difference introduced by letting the heat transfer from wall to coolant vary with the water temperature, has been to increase the transport time t_x a factor $(1 + \delta)$.

The following discussion is of high general interest, and in Chapter XIV it will be shown that the "δ-effect" is present in a boiling channel also.

In the following we will simplify G(s), by writing:

$$G(s) \cong \frac{1}{\tau s + 1} \tag{13.13}$$

It was shown in Chapter XII that this is a valid approximation for the present thin walled test tube in the frequency range of interest.

Equation 13.11 can now be written:

$$H(s) = \frac{x}{L} \; \frac{1}{\frac{\tau}{1+\delta}\, s + 1} \; \frac{1 - e^{-\frac{\tau}{1+\delta}\, s+1 \; s(1+\delta)t_x}}{s(1+\delta)t_x} \tag{13.14}$$

Equation 12.28:

$$H'(s) = \frac{x}{L} \; \frac{1}{\tau s+1} \; \frac{1-e^{-st_x}}{st_x} \tag{13.15}$$

By comparing these two equations it will be appreciated that the added complexity introduced through equation 13.1, has these effects on the results derived in the previous chapter:

1) There is no change in zero frequency amplitude.
2) The effective wall time constant has been reduced from τ to $\frac{\tau}{1+\delta}$.
3) The flow time for perturbations has been increased from t_x to $(1+\delta)t_x$.

4) The effect of the factor

$$\frac{\frac{\tau}{1+\delta}s+1}{\tau s+1} \tag{13.16}$$

is mainly to make the amplitude of the exponential less than 1. A study of the vector diagram of Figure 26 will show how this results in a smoother amplitude and phase behaviors of H(s). The function H'(s) exhibits discontinuities at the frequencies

$$\omega'_c = N\frac{2\pi}{t_x} \; ; \quad N = 1,2,3, \ldots. \tag{13.17}$$

H(s), however, is continuous at the corresponding frequencies, which is approximately given by:

$$\omega_c \tilde{=} N\frac{2\pi}{(1+\delta)t_x} \; ; \quad N = 1,2,3 \ldots. \tag{13.18}$$

Nodes will still be present, as will be shown by the theoretical curves in Part IV.

A physical explanation for the delay effect which is manifested in terms of δ, will now be given. Consider again the channel shown in Figure 24. The heating rate is assumed constant, except for a single impulse of heat delivered at time t=0 to a water element close to the inlet. We will now follow the history of this amount of heat. Thinking in terms of perturbations, the volume element just ahead of the heated one, will not receive any heat on its way to the outlet, which will be reached at time t_L. The volume element that received the heat impulse, will loose most of the heat to the

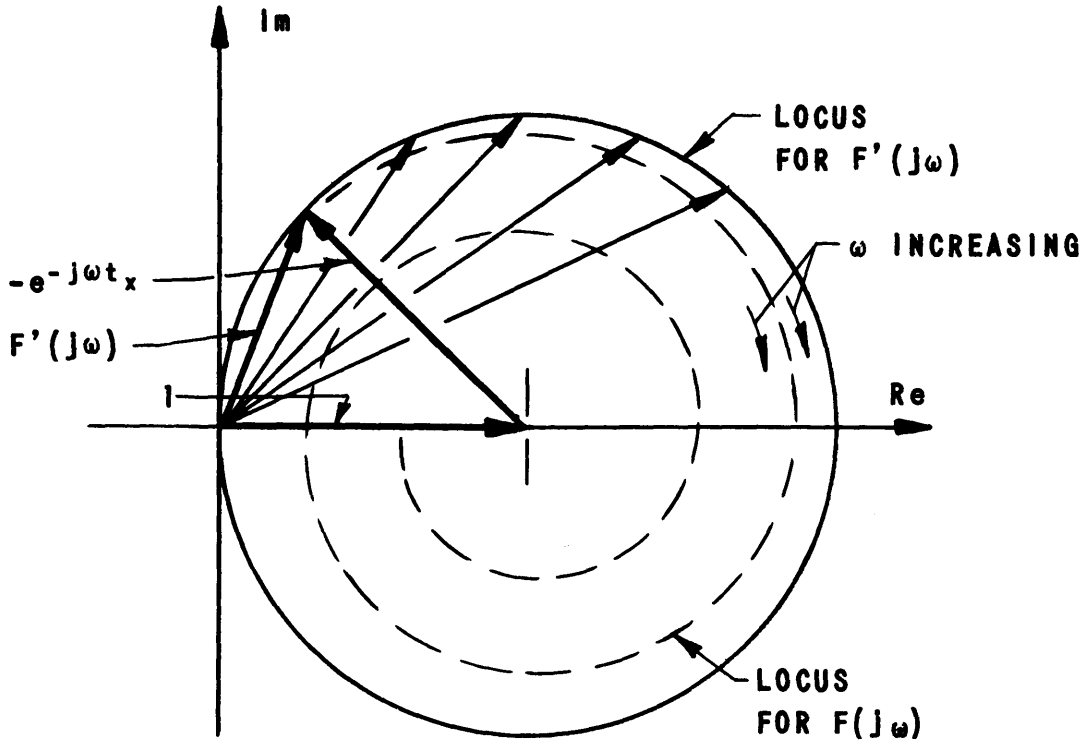

$$F'(s)=1-\exp\left[-st_x\right] \qquad F(s) = 1-\exp\left[-\frac{\frac{\tau}{1+\delta}s+1}{\tau s+1}(1+\delta)st_x\right]$$

FIG. 26
EFFECT OF δ ON SHARPNESS OF NODES.
INCREASED δ GIVES A SPIRAL THAT CONVERGES MORE RAPIDLY.

wall as it flows along. The following element will pick some of this heat up in the lower part of the channel. Some heat will again be lost to the wall in the upper part, but as the wall is now warmer than before, this element will reach the outlet at a little higher temperature than the preceding volume element. And so forth---. The outlet temperature will vary with time approximately as sketched in Figure 27, from which it should be clear that a delay, as well as a smoothing out of sharp features, will result.

Akcazu[15] investigated the effect on H'(s) of turbulent mixing as the coolant water flows up along the channel. He assumed that this will cause a spread in flow times around the average value t_x. This results in a smoothing effect similar to the one discussed in point 4 above. The mixing will not change the node frequencies, however.

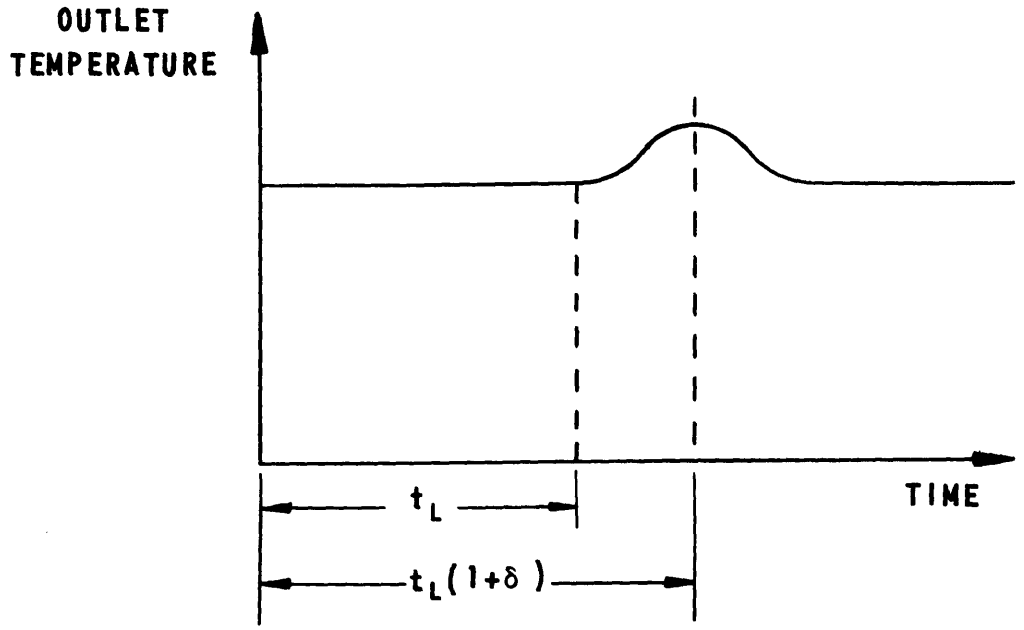

FIG. 27
THE EFFECT OF AN IMPULSE PERTURBATION
IN THE INLET TEMPERATURE

CHAPTER XIV

The Power-to-Void Transfer Function

A. Introductory Remarks

In this chapter, the transfer function for the void fraction at different heights will be derived for two sets of assumptions.

It will be shown that the resulting functions will contain frequency dependent parts which are analogous to the functions derived in Chapters XII and XIII.

Two new difficulties arise because of the build-up of steam voids along the section:

1. The steam velocity C_g and the water velocity C_f will be functions of height.
2. The propagation velocity C_d of perturbations in void fraction may differ from C_g and C_f.

In section B, these points will be considered in a simplified case, where the assumption of constant channel pressure will be made. Next, in Section C, the effects of pressure perturbations will be discussed.

The assumption of time invariant channel pressure, and therefore saturation temperature, has been adopted by all previous workers in the field, without question. The best justification for the assumption is that the derivations otherwise become extremely complicated.

Throughout this chapter, the following assumptions (all believed to be appropriate), will be made:

1. The bubble growth time is negligible.
2. The time taken for a bubble to reach the equilibrium velocity is negligible.
3. Disturbances in steam concentration travel with a velocity $C_d(x)$ which is a function of height, but not of time.

4. The production of heat is uniform throughout the tube wall.
5. Heat conduction in the wall in the x-direction is negligible.
6. Water flow rate and temperature at the inlet are not functions of time.
7. The effect of perturbations in $Q^{o}_{1}(x,d_1,t)$ - the flow rate of heat into the coolant - on the local void fraction, will not differ in the upper and the lower part of the test section.

Assumptions 1 and 2 have been justified in Chapter X. Three will discussed later in this chapter. Assumptions 4, 5 and 6 should not quire further comments, but a few words need to be said about 7.

In Section C of Chapter X, it was shown that the division of the annel into a boiling and a non-boiling part is a poor representation of the tual conditions at higher pressures. It has become customary[52] to predict erage void fraction curves by an empirical method which recognizes an inter- diate section between the two mentioned above. An attempt was made to fit e data of the present experiment by basing the transfer function calculations a similar three-section model. This led to a rather complicated expression, d as the numerical results were no better than those of the model to be scussed presently, assumption 7 was adopted. It should be pointed out that is assumption does not hold for the SPERT-I conditions simulated in the periment by Zivi and Wright[16].

Nuclear Boiling at Constant Pressure

The heat flux into the coolant is given by the solution to equations .1 through 12.4. As shown in Chapter XII, the solution is:

$$\frac{\overline{Q}_1(d_1,s)}{\overline{Q}(s)} = G(s) \qquad (14.1)$$

ere G(s) is defined by equation 12.20.

Exact solution of the transport problem by the methods used in Chapter XI is difficult, because of the x-dependance in C_d. The following approach gives a better physical feeling for the problem, and is preferred.

Consider the channel geometry sketched in Figure 24. The time it takes a perturbation in steam production at x' to reach x, is given by:

$$t_{x'x} = \int_{x'}^{x} \frac{dx}{C_d(x)} \tag{14.2}$$

The total perturbation in steam mass flow rate at point x at time t, will be made up of contributions from volume elements Adx' which were perturbed at the time:

$$t' = t - t_{x'x} \tag{14.3}$$

Differentiation yields:

$$dt' = dt \tag{14.4}$$

The mass of steam produced in Adx' from t' to t'+dt':

$$dw_g dt' = \frac{Q_l(d_l,t')}{Ih_{fg}} \, dx'dt' \tag{14.5}$$

This flows by point x from time t to t+dt. The total steam mass flow rate at x at time t:

$$w_g(x,t) = \frac{1}{Ih_{fg}} \int_0^x Q_l(d_l,t') \, dx' \tag{14.6}$$

Taking the Laplace transform with respect to t:

$$\bar{w}_g(x,s) = \frac{1}{Ih_{fg}} \int_0^x e^{-t_{x'x}s} \, \bar{Q}_l(d_l,s)dx' \tag{14.7}$$

If the solution is to be carried any further, an assumption regarding the variation of C_d with x must be made. The exact nature of C_d is not known, but two different assumptions will be studied:

a) C_d varies linearly with x.

b) C_d does not vary with x.

Assumption a):

$$C_d(x) \cong C_d(0) + ax \tag{14.8}$$

From the experimental data to be presented in Part IV, it will be seen that the steam and the water velocities vary linearly with x in most cases. Assumption a), therefore, seems a reasonable one to choose.

By equation 14.2:

$$t_{x'x} = \frac{1}{a} \ln \frac{C_d(0) + ax}{C_d(0) + ax'} \tag{14.9}$$

Equation 14.7 now becomes:

$$\overline{w}_g(x,s) = \frac{C_d(x)\ \overline{Q}_1(d_1,s)}{Lh_{fg}} \quad \frac{1-e^{-(s+a)t_x}}{s+a} \tag{14.10}$$

where t_x is given by:

$$t_x = \frac{1}{a} \ln \frac{C_d(x)}{C_d(0)} \tag{14.11}$$

Assumption b):

$$C_d(x) = C_0 \tag{14.12}$$

Equation 14.2 yields:

$$t_{x'x} = \frac{x - x'}{C_0} \tag{14.13}$$

Equation 14.7 becomes:

$$\bar{w}_g(x,s) = \frac{\bar{Q}_1(d_1,x)}{h_{fg}} \frac{x}{L} \frac{1-e^{-t_x s}}{t_x s} \tag{14.14}$$

Assumption b) brings the present problem in line with the case treated in Chapter XII, and the above result corresponds to equation 12.28. The value of t_x to be used in equation 14.14 should be obtained from equation 14.13 by taking $x' = 0$, and C_o equal to the mean value of $C_d(x)$ in the interval 0 - x. Or, better still, t_x could be computed from equation 14.11.

Comparing equations 14.10 and 14.14, it can easily be shown that the zero frequency response is the same in both cases. The difference in the frequency dependent parts can best be demonstrated through Figure 28. These points should be noted:

1. The node frequencies are the same in both formulas, if t_x is computed by equation 14.11 in both cases.
2. Assumption a), which is believed to be the most appropriate, leads to a transfer function without discontinuities.
3. The nodes in equation 14.10 will be sharper for smaller values of x.

Up to this point, the voids have been expressed in terms of mass flow rate of steam. This variable is related to the volume void fraction by:

$$W_g(x,t) = \rho_g A C_g(x,t)\, \alpha^o(x,t) \tag{14.15}$$

where it has been realized that the steam velocity may be a function of time.

We can write:

$$W_g(x,t) = W_g(x) + w_g(x,t) \tag{14.16}$$

$$C_g(x,t) = C_g(x) + c_g(x,t) \tag{14.17}$$

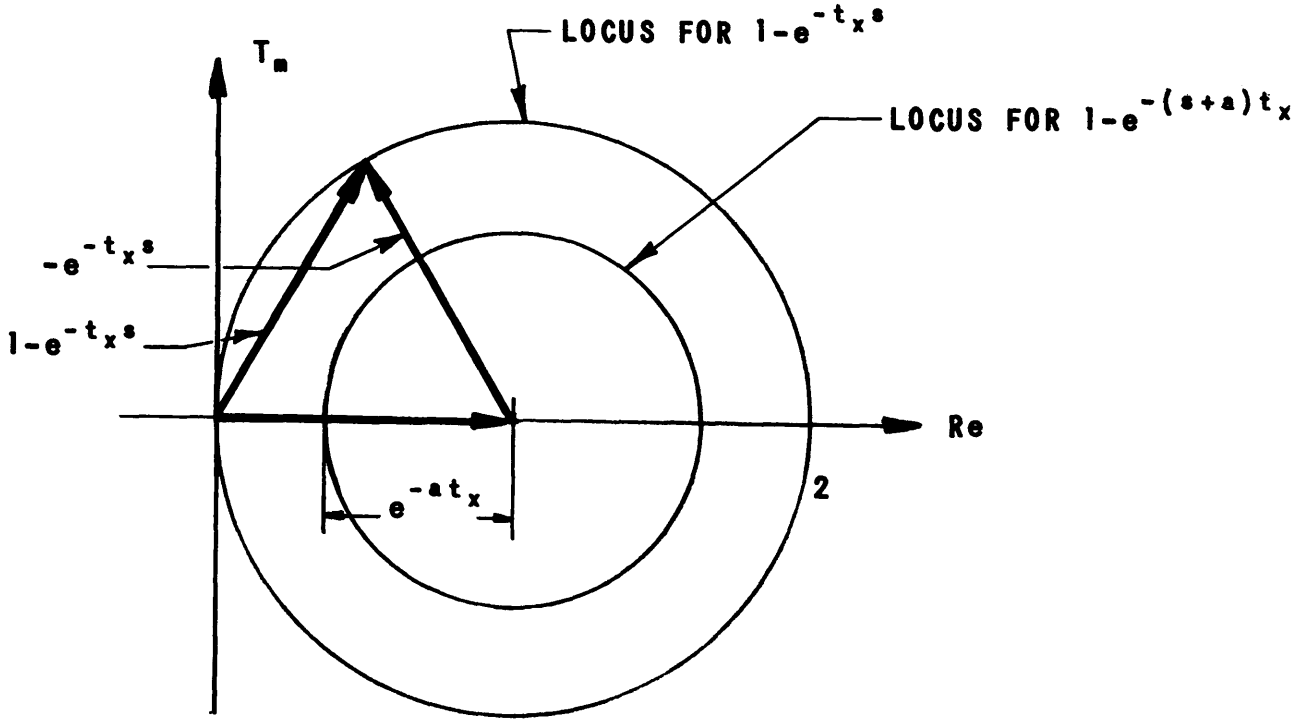

FIG. 28
COMPARISON BETWEEN ASSUMPTIONS a AND b
FOR THE VOID PERTURBATION VELOCITY

$$\alpha^{o}(x,t) = \alpha^{o}(x) + \alpha(x,t) \tag{14.18}$$

When these equations are inserted into equation 14.15, steady state terms cancel. Neglecting second order terms in the perturbed variables, we get:

$$w_g(x,t) = \rho_g A \left[\alpha^{o}(x)\ c_g(x,t) + C_g(x)\ \alpha(x,t)\right] \tag{14.19}$$

At this point, the derivation can be carried on along three different roads:

1. Using the law of conservation of momentum, it is theoretically possible to eliminate $c_g(x,t)$.
2. It can be assumed that the steam velocity is not a function of time, i.e.: $c_g(x,t) = 0$.
3. Some other simplifying assumption can be made that allows elimination of $c_g(x,t)$.

If a closed-form expression for the power-to-void transfer function is wanted, method 1 cannot be used. The exact equations become so complicated as to require solution by a difference method on a computer, digital or analog.

Method 2 has been adopted by all workers previous to Zivi and Wright[16], and Akcazu[15]. Taking $c_g = 0$, equation 14.19 can be Laplace transformed and solved for $\bar{\alpha}$:

$$\bar{\alpha}(x,s) = \frac{\bar{w}_g(x,s)}{\rho_g A\ C_g(x)} \tag{14.20}$$

Implicit in the derivation of Zivi and Wright[16] is the assumption that, as far as the contributions from the boiling section are concerned, $\alpha(x,t)$ can be taken equal to zero. This gives good results in their special case.

Akcazu's considerations[15] are rather involved, and will not be reviewed in full. In essence, his method is to define:

$$f \triangleq \frac{c_g(x,t)}{\alpha(x,t)} \tag{14.21}$$

and assume that f is a function of x, but not of time. This allows the definition of a modified steam velocity:

$$C_g'(x) = \alpha^o(x)f(x) + C_g(x) \tag{14.22}$$

Equation 14.19 can now be written:

$$w_g(x,t) = \rho_g A C_g'(x)\, \alpha(x,t) \tag{14.23}$$

Taking the Laplace transform with respect to time, and solving for α:

$$\bar{\alpha}(x,s) = \frac{\bar{w}_g(x,s)}{\rho_g A C_g'(x)} \tag{14.24}$$

Formally, this equation is equal to equation 14.20. Rather than using the latter, we will in the following carry the primed C_g' as a reminder that an assumption is involved. The test of the assumption will be the ability of equation 14.24 to match the experimental values of the zero frequency amplitude of the void oscillations.

The complete power-to-void transfer function can now be written for the present case.

Combining equations 14.1, 14.10, and 14.24:

$$\frac{\bar{\alpha}(x,s)}{\bar{Q}(s)} = \frac{C_d(x)}{V\rho_g h_{fg} C'_g(x)}\; G(s)\; \frac{1-e^{-(s+a)t_x}}{s+a} \tag{14.25}$$

for the assumption that $C_d(x)$ varies linearly with x.

Combining equations 14.1, 14.14 and 14.24:

$$\frac{\bar{\alpha}(x,s)}{\bar{Q}(s)} = \frac{x}{V\rho_g h_{fg} C'_g(x)} \; G(s) \; \frac{1-e^{-t_{xs}}}{t_{xs}} \qquad (14.26)$$

for the assumption that an average value from 0 to x can be taken for $C_d(x)$. For both equations above, t_x should be calculated from equation 14.11.

C. The Power-to-Void Transfer Function with Channel Pressure Variations Considered.

In this section, the formula to be used to correlate the experimental data in Part IV will be arrived at. It should be kept in mind that the derivation to follow is nothing more than a first order attempt to a solution. A more rigorous treatment will have to wait until means have been found to handle the difficulties pointed out below.

Let us consider an impulse of heat delivered from the heated wall to a coolant volume element close to it. If the volume element previously contained only saturated water and saturated steam, the extra heat will be accommodated by an increase in the temperature and also in the pressure of the volume element. This originates a pressure wave. Any attempt to express these processes mathematically will meet with two difficulties:

1. Because of the incomplete mixing in the channel, we do not know how large a part of the two-phase mixture in a cross-section take direct part in the transient heat exchange with the wall.
2. The present knowledge about the propagation of pressure waves in steam/water mixtures is not sufficient to permit a rigorous treatment of the problem.

In Chapter X, the following equation (10.6) was derived for the differential heat transfer rate to a boiling channel where the saturation pressure was varying:

$$\frac{Q_1(x,d_1,t)}{A_w} = h_i T_1(x,d_1,t) + h_i \left[\frac{K_2}{4} \Delta T_{sat}^{o} - \frac{T_{sat}(x,t)}{P(x,t)}\right] P(x,t) \qquad (14.27)$$

Through the use of Clapeyrons formula:

$$\frac{P}{T_{sat}} = \frac{h_{fg}}{T_{sat}^{o} v_{fg}} \qquad (14.28)$$

P(x,t) can be eliminated from equation 14.27 to yield:

$$\frac{Q_1(x,d_1,t)}{A_w} = h_i \left[T_1(x,d_1,t) - K_3 T_{sat}(x,t)\right] \qquad (14.29)$$

where we have defined:

$$K_3 \triangleq 1 - \frac{K_2}{4} \frac{\Delta T_{sat}^{o}}{T_{sat}^{o}} \frac{h_{fg}}{v_{fg}} \qquad (14.30)$$

K_3 is a dimensionless constant, which depends on average channel pressure and average heating power. K_3 is not a function of x.

Attention is now drawn to the analogy between equation 14.29 and equation 13.1. The differential equations for the wall temperature in the present case will closely resemble equations 13.2 through 13.5. We have:

$$\frac{\partial^2 T_1(x,y,t)}{\partial y^2} + \frac{Q(t)}{A_w d_1 K_1} = \frac{\rho_1 c_1}{K_1} \frac{\partial T_1(x,y,t)}{\partial t} \qquad (14.31)$$

$$T_1(x,y,0) = 0 \qquad (14.32)$$

$$\frac{\partial T_1(x,0,t)}{\partial y} = 0 \tag{14.33}$$

$$h_i \left[T_1(x,d_1,t) - K_3 T_{sat}(x,t)\right] = -\kappa_1 \frac{\partial T_1(x,d_1,t)}{\partial y} \tag{14.34}$$

It would now be very convenient if the saturation temperature were given by a differential equation analogous to equation 13.6. This can be accomplished by adopting the following set of assumptions:

1. The contents of the test section at a given height can be divided into:
   a) Saturated steam as given by the volume void fraction α^o.
   b) Saturated water as given by the volume fraction β^o.
   c) Subcooled water fill the rest of the channel volume.
   It is now assumed that part c is not affected by the heat perturbations. Parts a and b are assumed always to be in equilibrium along the steam/water saturation line.

2. Pressure disturbances are assumed to propagate <u>up</u> the channel with the velocity $C_d(x)$. It is further assumed that none of the energy contained in the pressure wave will travel <u>down</u> the channel. (Note that <u>up</u> is the "down-stream" direction for the present experiment).

The saturation temperature is now given by:

$$ph_i \left[T_1(x,d_1,t) - K_3 T_{sat}(x,t)\right] = \rho'_2 A C_d c'_2 \frac{\partial T_{sat}(x,t)}{\partial x} + \rho'_2 A c'_2 \frac{\partial T_{sat}(x,t)}{\partial t} \tag{14.35}$$

$$T_{sat}(x,0) = 0 \tag{14.36}$$

$$T_{sat}(0,t) = 0 \tag{14.37}$$

where the product $\rho'_2 c'_2$ can be found as follows:

$$\rho'_2 c'_2 = \frac{\Delta U/\Delta V}{T_{2_{sat}} - T_{1_{sat}}} \tag{14.38}$$

$\Delta U/\Delta V$ is the change in internal energy per unit volume corresponding to a temperature increase $T_{2_{sat}} - T_{1_{sat}}$ for a steam/water mixture at volume ratio α^o/β^o. Formulas by which $\rho'_2 c'_2$ can be calculated in a given case havebeen presented in Appendix III.

Equations 14.31 through 14.37 form a complete set. Except for the presence of the constant K_3, and for the fact that ρ'_2, c'_2, and C_d are functions of x, the equations are the same as the set treated in Chapter XIII.

We will assume that the three variables can be approximated by average values. The solution then becomes analogous to equation 13.11:

$$\bar{Q}_2(x,s) = \bar{Q}(s) \frac{x}{L} G(s) \frac{1-e^{-\left[1+\delta' G(s)\right] st_x}}{\left[1+\delta' G(s)\right] st_x} \tag{14.39}$$

where:

$$\delta' \triangleq K_3 \frac{pd_2}{A} \frac{c_1 \rho_1 d_1}{c'_2 \rho'_2 d_2} \tag{14.40}$$

and

$$t_x = \int_0^x \frac{dx}{C_d} \tag{14.41}$$

Assuming that:

$$\bar{w}_g(x,s) = \frac{\bar{Q}_2(x,s)}{h_{fg}} \tag{14.42}$$

the final answer can be arrived at by the use of equation 14.20:

$$\frac{\bar{\alpha}(x,s)}{\bar{Q}(s)} = \frac{x}{V\rho_g h_{fg} C'_g(x)}\, G(s)\, \frac{1-e^{-\left[1+\delta' G(s)\right] st_x}}{\left[1+\delta' G(s)\right] st_x} \tag{14.43}$$

$$\simeq \frac{x}{V\rho_g h_{fg} C'_g(x)}\, \frac{1}{\frac{\tau}{1+\delta'}s+1}\, \frac{1-e^{-\frac{\frac{\tau}{1+\delta'}s+1}{\tau s+1} s(1+\delta')t_x}}{s(1+\delta')t_x} \tag{14.44}$$

In equation 14.44, G(s) has been replaced by a single time-constant term as given in equation 13.13.

PART IV

EXPERIMENTAL RESULTS. CONCLUSIONS

CHAPTER XV

SECONDARY VARIABLES

A. Measurement of Average Void Fraction

The instrumentation and procedures for this measurement has been described in Chapter VII.

One or more void traverses were measured in connection with every one of the void oscillation runs. These traverses were taken before or in the middle of the oscillations, but always at constant power. The void detector was equipped with the wide beam collimator shown, (Figure 14), which was essential for the void oscillation measurements. The traverses were usually taken without any filter at the output of the gamma preamplifier, in order to study how the voids varied due to boiling noise at different heights along the channel. Fairly regular signal variations, with frequencies in the order of 20 to 30 cycles per second, were always seen near the exit. At an average void amplitude of 50%, for instance, the variations could correspond to void changes as large as $\pm$ 20%.

It was later found (see Chapter VII) that traverses obtained in this manner were inaccurate. New traverses were therefore taken with a 1/32" wide gamma beam using a two stage RC filter at the gamma detector output. The test section was now traversed horizontally at each of the 16 measuring stations given in Table 1. This resulted in a family of curves as shown in Figure 29. It is seen near the inlet how bubbles created at the walls collapse in the cold water in the middle of the channel. Higher up, the steam bubbles tend to assemble in the middle of the channel, and slug flow is certainly developing in this area. This is borne out by the variations in the unfiltered gamma detector signal mentioned above. It should be noted that the curves shown in Figure 29 have been extrapolated out to the walls.

TABLE 1

MEASURING POINTS USED FOR VOID TRAVERSES

Point No.	Height Above Inlet in cm
1	6.3
2	13.9
3	21.5
4	29.5
5	36.8
6	44.4
7	52.0
8	59.6
9	67.3
10	74.9
11	82.5
12	90.1
13	97.7
14	105.4
15	113.0
16	120.6

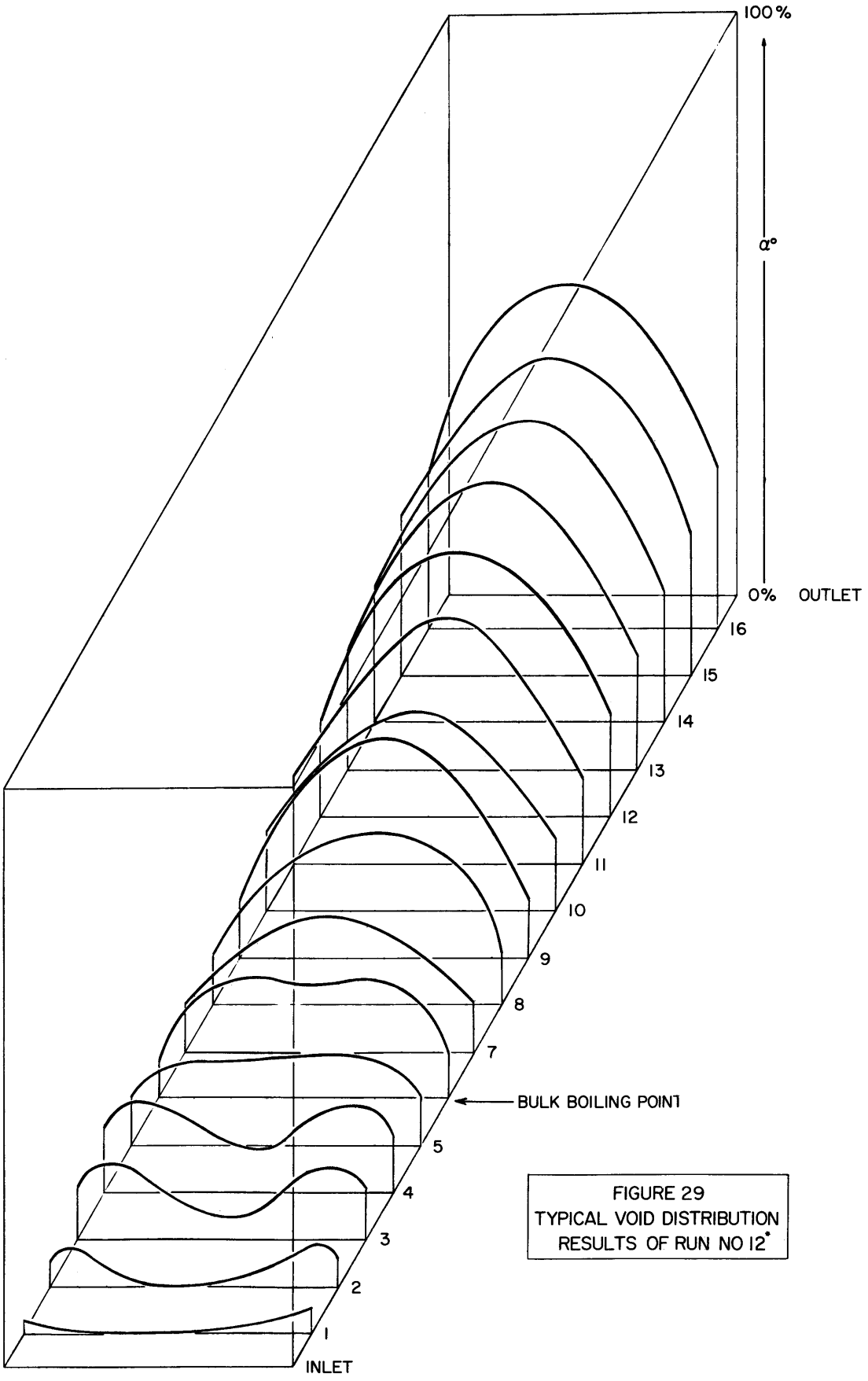

FIGURE 29
TYPICAL VOID DISTRIBUTION
RESULTS OF RUN NO 12*

Accurate measurements extremely near the wall are difficult due to the limited resolution of the gamma detector.

A set of curves like the one given in Figure 29 were now taken for each of the conditions (given in Table 2) at which oscillation runs had been taken. The area under the curves were integrated to give the average void fraction at each height. The results of these runs are given in Table 3. The run numbers correspond to the oscillation run numbers and the asterisk is a reminder that conditions are not exactly the same, as the subcooling was difficult to reproduce accurately.

Before the two last conditions could be reproduced, an unrepairable leak developed in the test section. For runs 15 and 16, therefore, the previous "one-shot" traverses were used, but corrected for errors as estimated by the other check measurements.

The probable error in the measurements of α° is estimated to be $\pm$ 2.5% for runs 9 through 13, and twice that for runs 15 and 16.

B. Calculation of Flow Velocities

Using the formulas presented in Section A of Chapter XI, the steam and water velocities for each oscillation run were calculated. The results have been presented in Table 3, and plotted in Figures 30 through 37.

As explained in Chapter XI, the steam velocity, C_g, does not go to zero at the bulk boiling point. The real value is expected to be indicated by the dashed lines shown in the figures. It is reasonable to assume that the steam velocity approaches the water velocity near the inlet. The value of C_g used in the next chapter has been taken off the curve (including the extrapolation), rather than using the individual points measured.

The water velocity can be well represented by a straight-line approximation in most cases. This approach has been used for convenience in the

Table 2

EXPERIMENTAL CONDITIONS OF THE VOID OSCILLATION RUNS

	PRESSURE		POWER		FLOW		SUBC. TEMP.	
	ATA	PSIA	KW	KW/l	cm/sec	GPM	^{o}C	^{o}F
Run 9	27.2	400	30	47.9	77	6	2.9	5.2
Run 10	27.2	400	30	47.9	77	6	8.7	15.6
Run 11	40.8	600	50	79.8	115	9	14.4	25.9
Run 12	40.8	600	50	79.8	115	9	7.2	13.0
Run 13	40.8	600	50	79.8	115	9	3.3	6.0
Run 15	54.4	800	70	111.7	115	9	12.5	22.5
Run 16	68.0	1000	70	111.7	115	9	12.1	21.8

calculation of water flow time from the inlet to a given point.

The uncertainty in α° is the dominating factor in the probable errors in the flow velocities as stated in Section B of Chapter XI. The outlet void fraction is in the order of 0.50 in most cases, and then the uncertainty in steam velocity at this point becomes:

Runs 9 through 13:

$$\frac{\Delta C_g}{C_g} = \frac{2.5}{0.5} = \underline{5\%}$$

Runs 15 and 16:

$$\frac{\Delta C_g}{C_g} = \frac{5}{0.5} = \underline{10\%}$$

C. Measurement of h_i. Wall Temperatures

In order to evaluate the function G(s) - the transfer function between heat production and heat flow into coolant in the simple case of Chapter XII - it is necessary to know the incremental heat transfer coefficient h_i (see equations 12.19 and 12.20).

Attention is now drawn to equations 12.15 and 12.16. These give the transfer functions between heat production Q, and inside and outside wall temperature, respectively. Both equations contain h_i. Other constants included are given by geometry, materials and saturation pressure, and all can be determined quite accurately. It is, therefore, conceivable to use either of these equations to determine h_i, through a measurement of power amplitude and of the amplitude in either of the temperatures. A measurement of phase will not be necessary.

As would be expected, the inside wall temperature is the strongest function of h_i. In the present case, there was no way it could be measured

easily, and an attempt was, therefore, made of measuring the swing in the outside wall temperature.

A voltage proportional to the difference between the inlet water temperature and the wall temperature near the inlet was formed by proper connection of two thermocouples. The variations in this voltage due to power variations were tried and measured three different ways: by the Sanborn recorder, by the wave analyzer, and by the potentiometer normally used for temperature measurements. All attempts failed for different reasons. The signal voltage was extremely low, and there was a large 60 cps noise signal superimposed. Ground loops through the wall thermocouple gave difficulties with the wave analyzer.

It is believed that this method of finding h_i is potentially useful, although it did not give positive results in the present case.

The outside wall temperatures were measured continuously at 12 points along the height of the test section. The thermocouple positions have been given in Figure 38, which also shows a typical temperature traverse. A slight increase in temperatures is indicated in the lower part of the channel, followed by a decreasing trend higher up. The temperature variations are small compared to ΔT_{sat}.

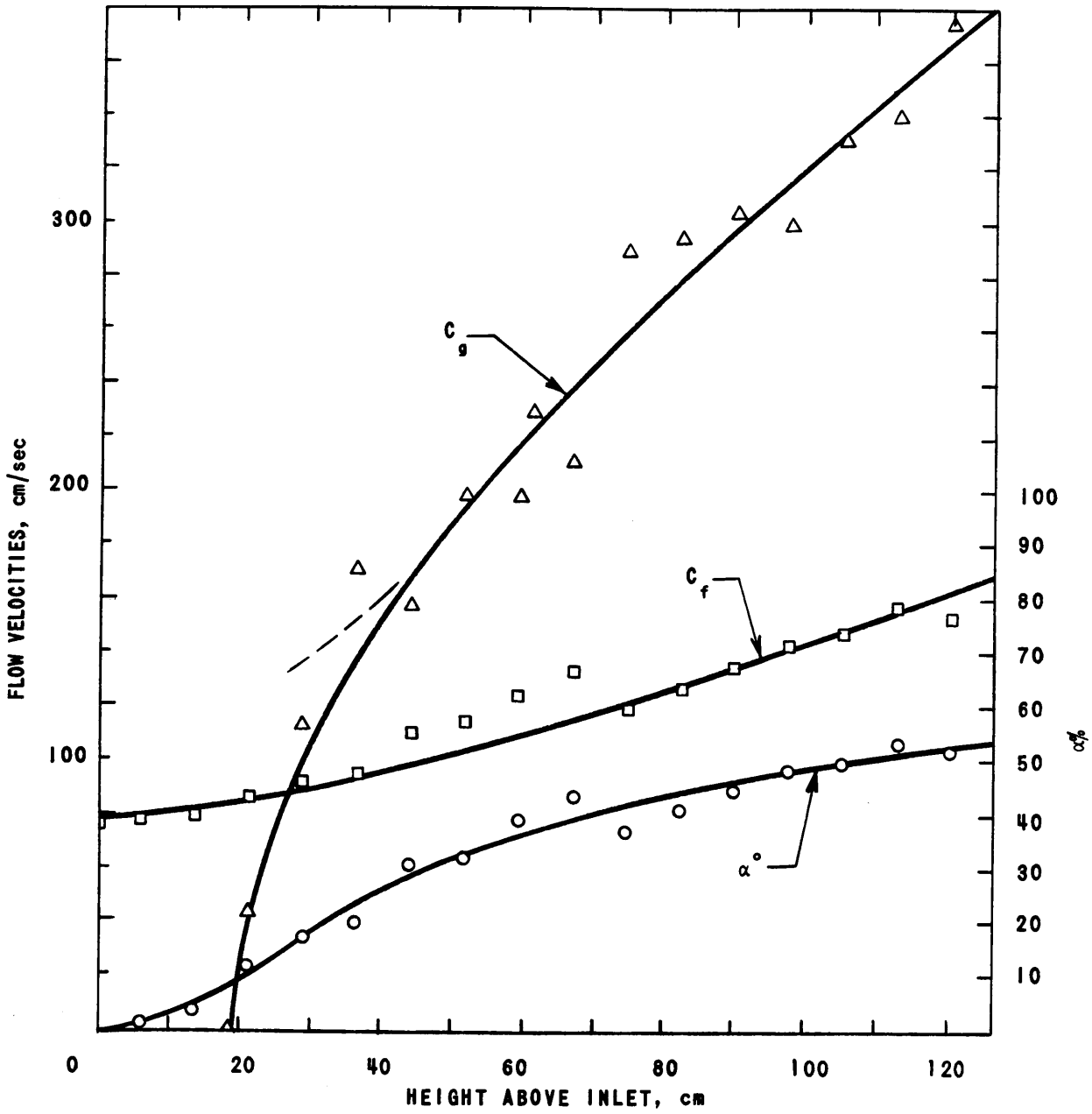

FIG. 30
RUN NO.9*, 27.2 Ata, 47.9 kw/l
ΔT_{sub} = 2.9°C

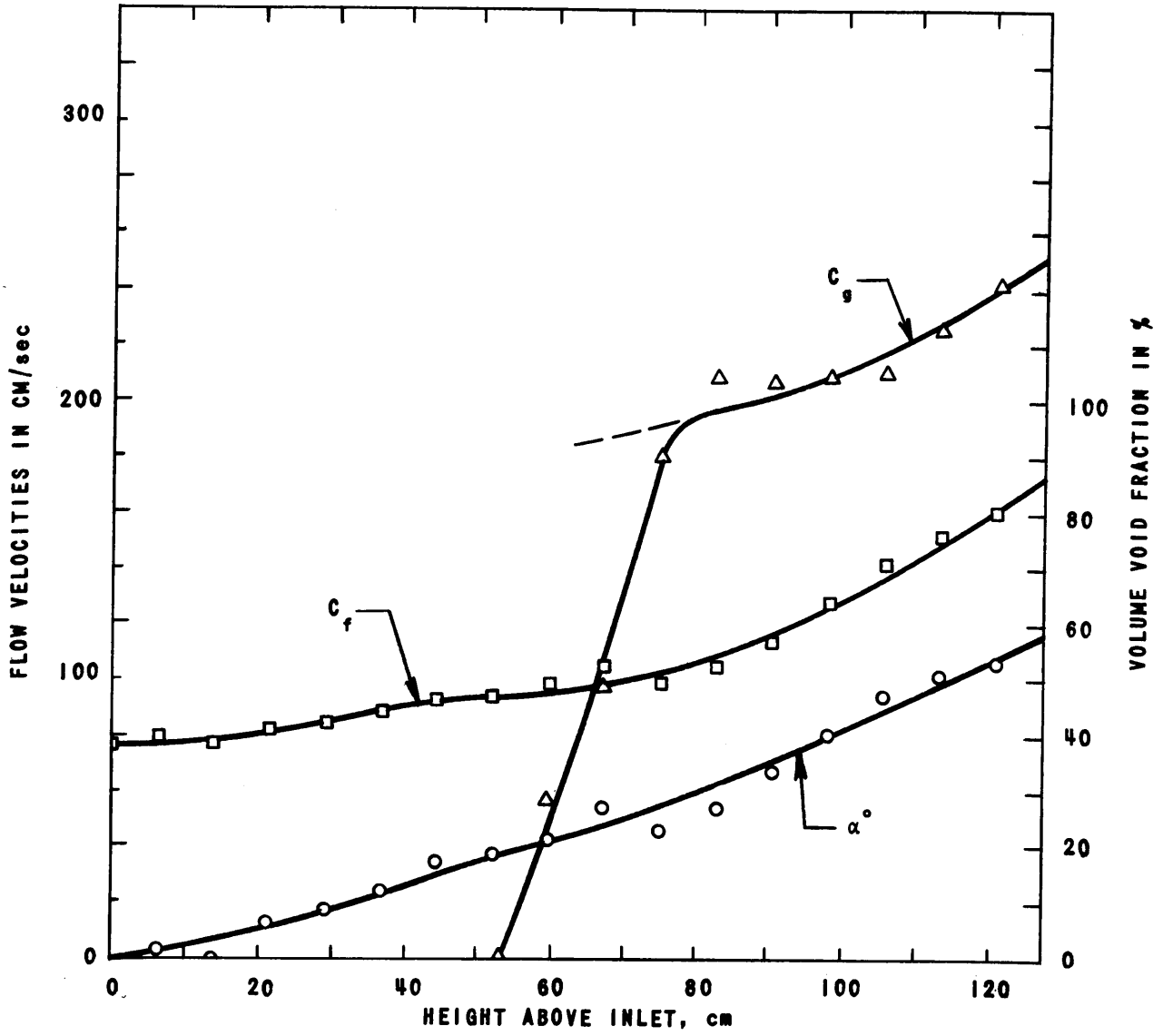

FIG. 31
RUN NO. 10*, 27.2 Ata, 47.9 kw/l
$\Delta T_{sub} = 8.7°C$

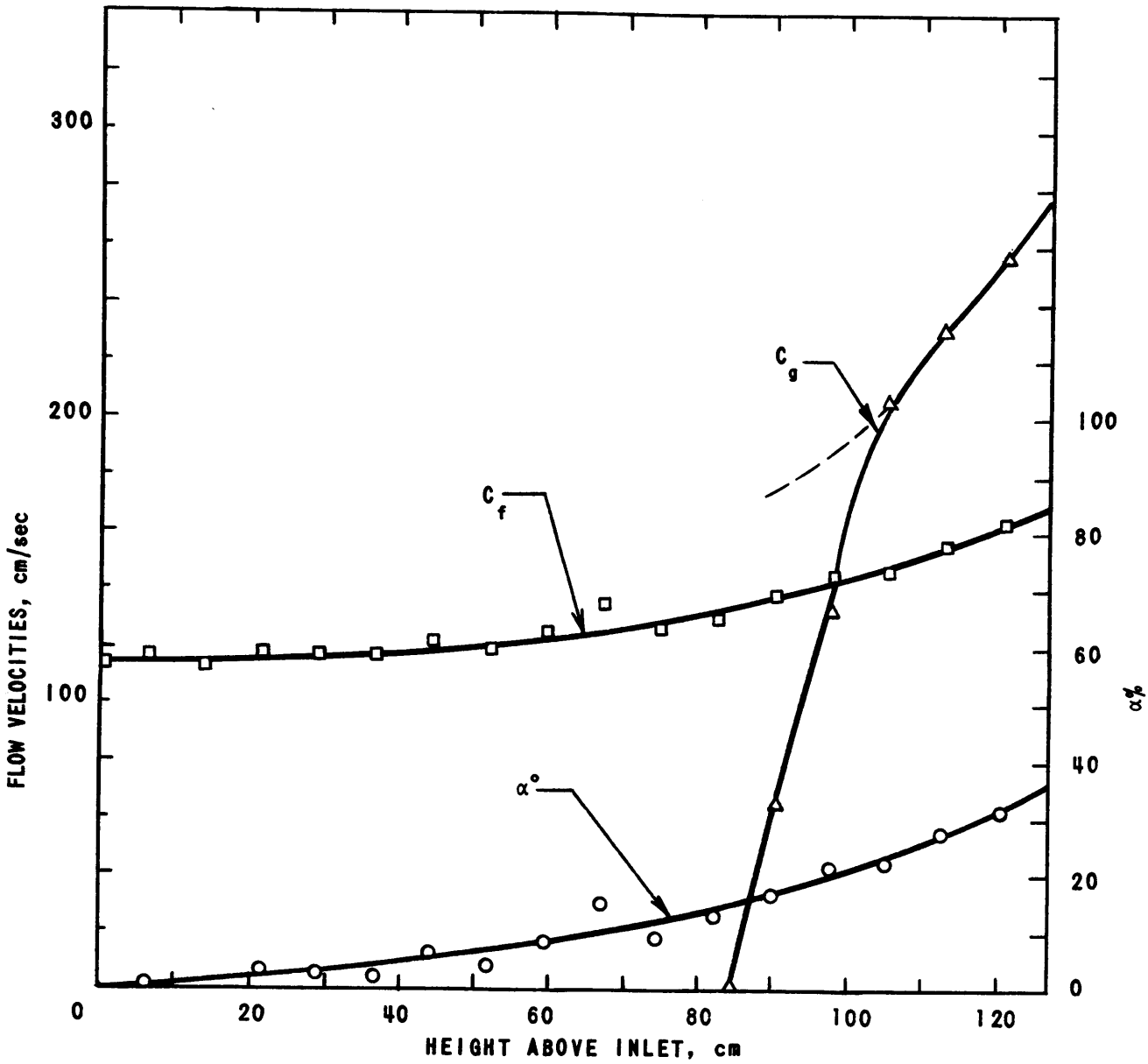

FIG. 32
RUN NO. 11*, 40.8 Ata 79.8 kw/l
ΔT_{sub} = 15.2°C

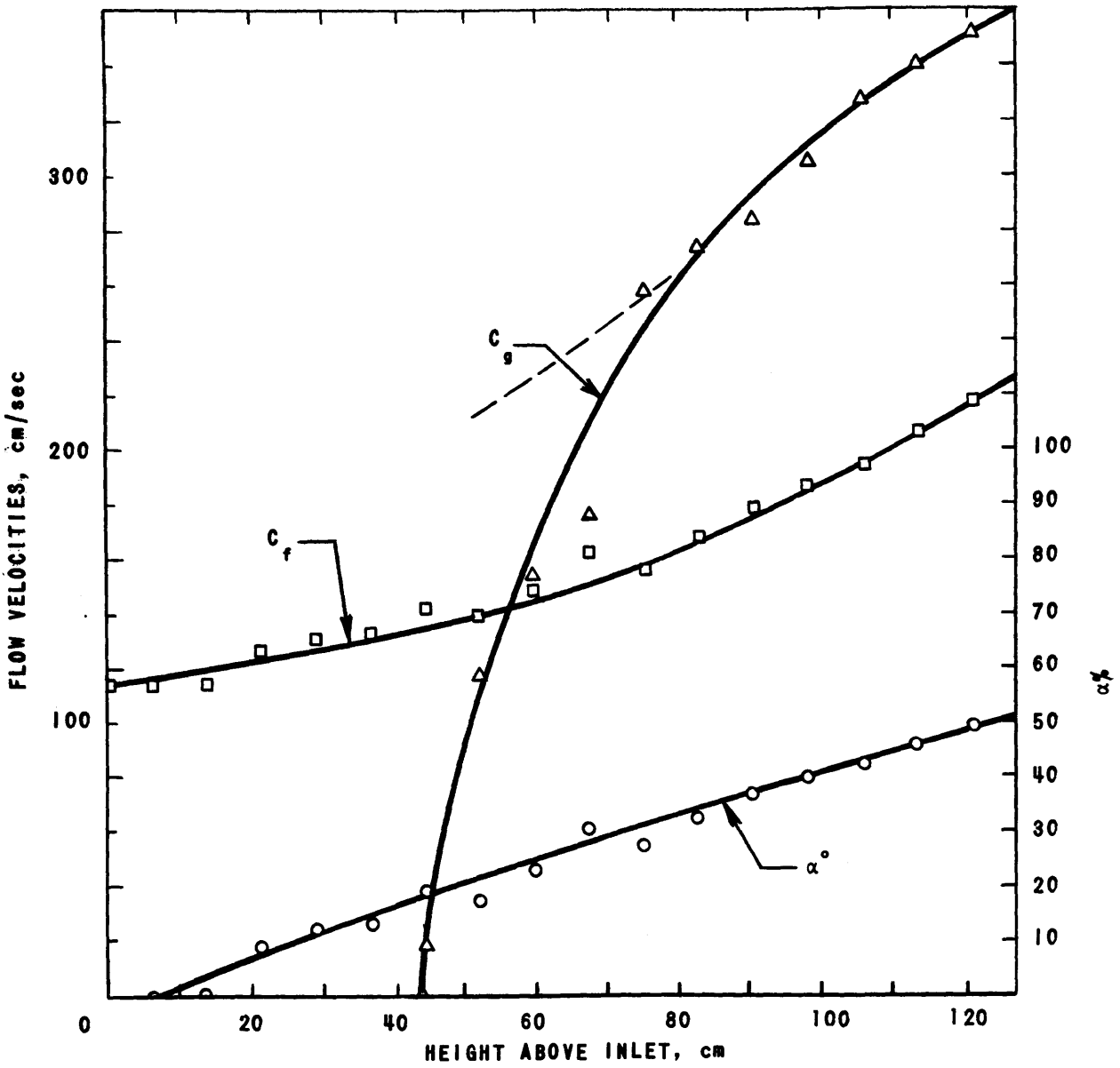

FIG. 33
RUN NO. 12*, 40.8 Ata, 79.8 kw/l
ΔT_{sub} = 7.9 °C

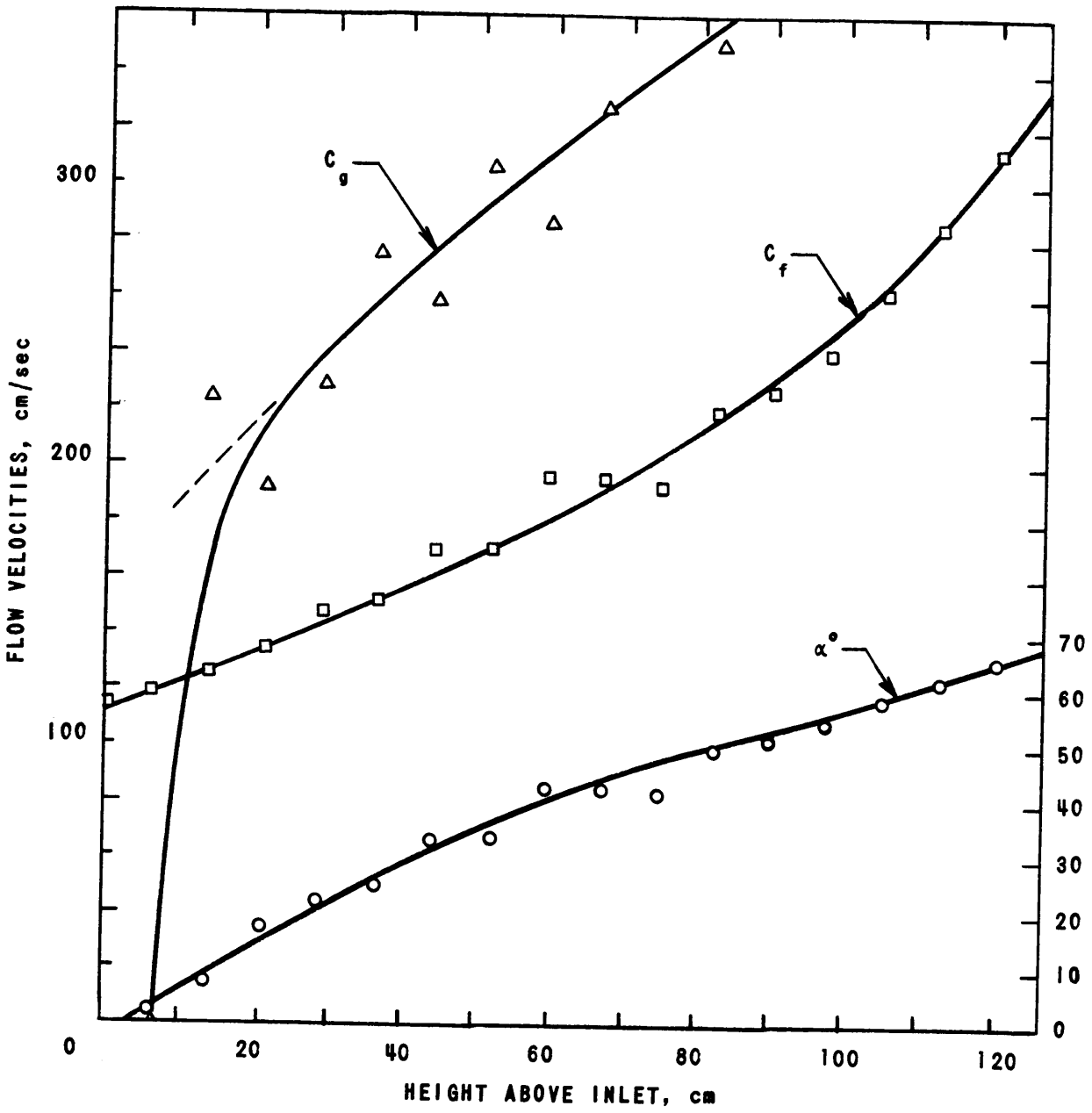

FIG. 34
RUN NO. 13*, 40.8 Ata 79.8 kw/l
ΔT_{sub} = 1.2 °C

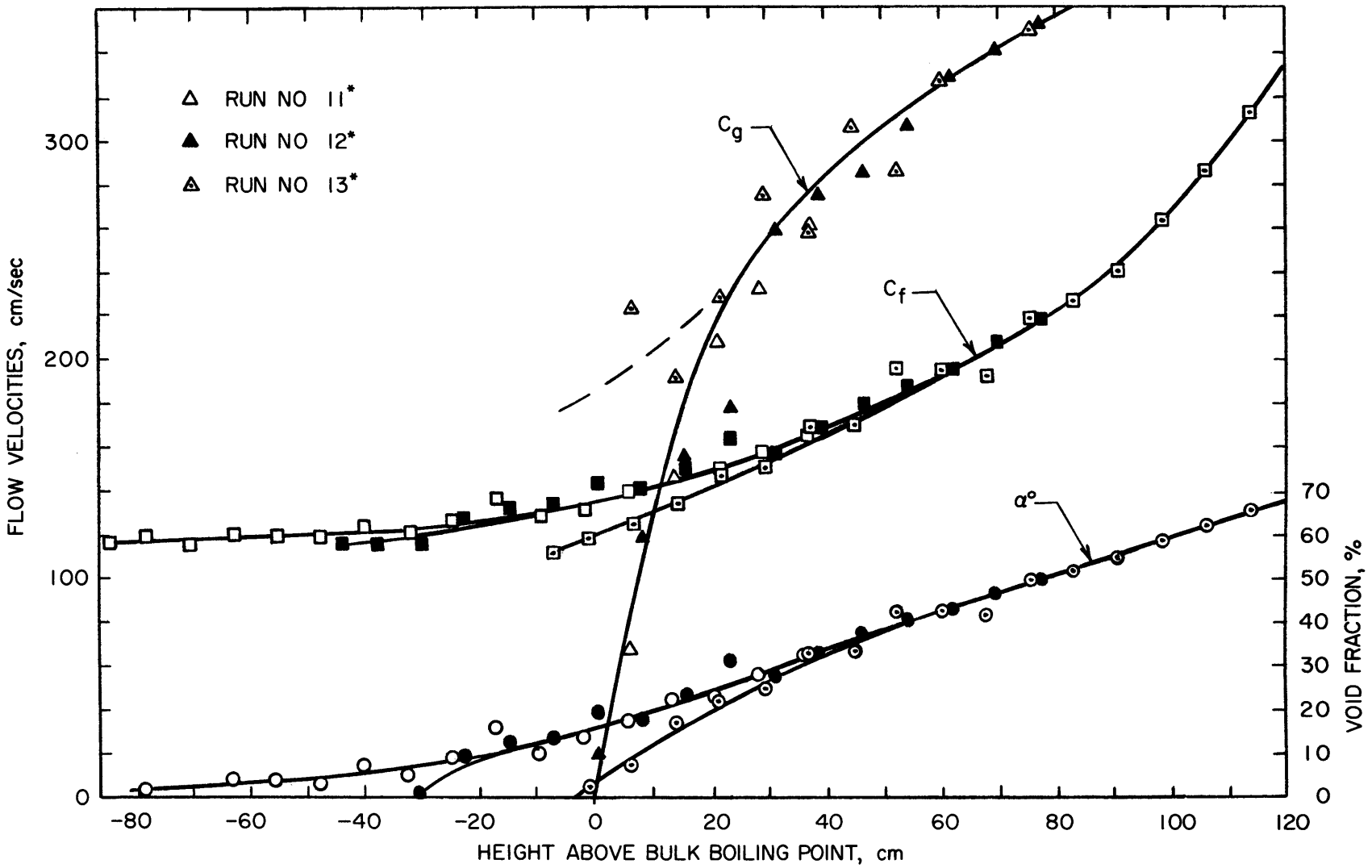

FIGURE 35

COMPOSITE TRAVERSE FOR RUNS 11*, 12*, AND 13*
THE FLOW HAS NO "MEMORY" OF INLET CONDITIONS

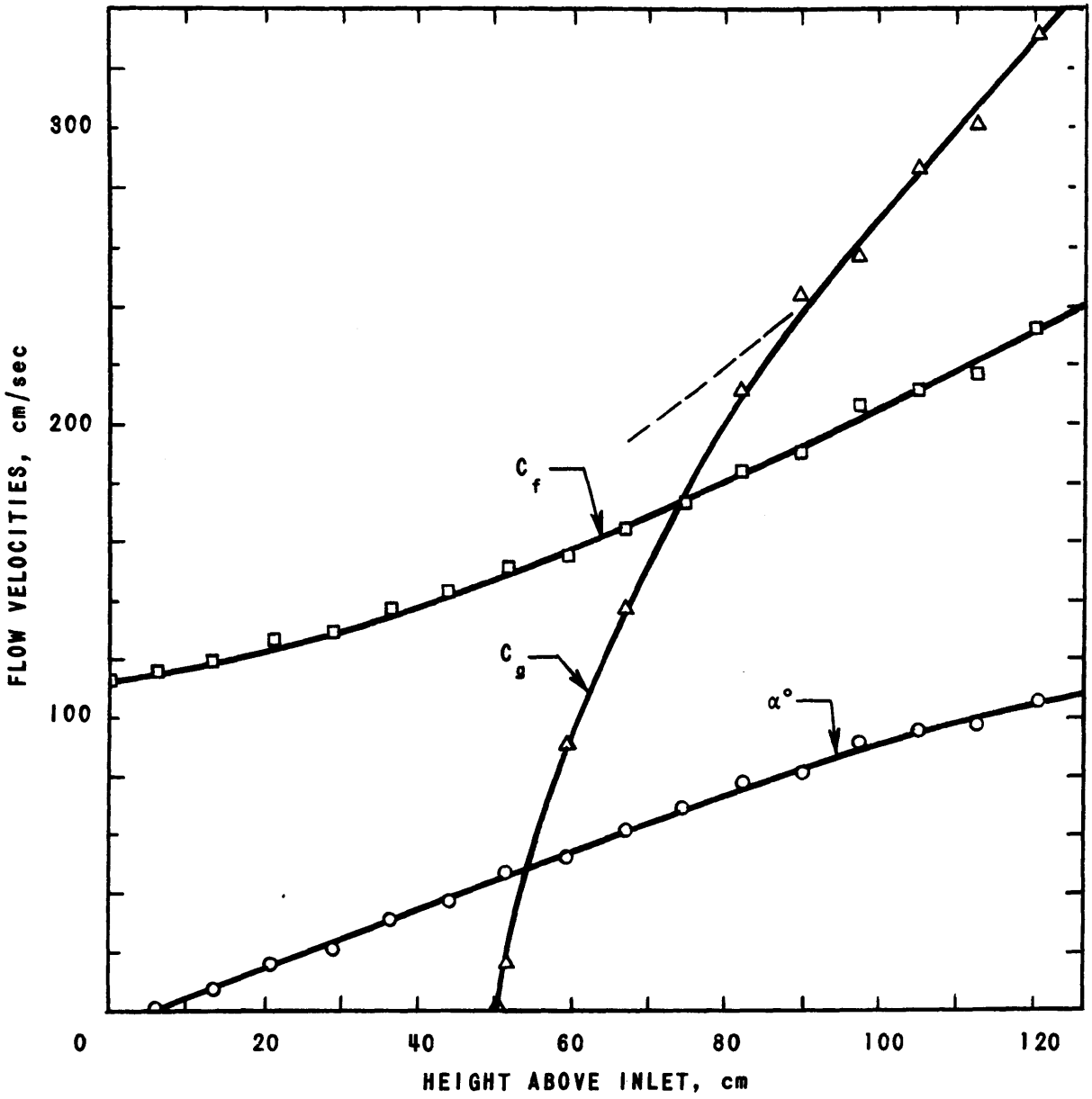

FIG. 36
RUN NO. 15, 54.4 Ata, 111.5 kw/l
ΔT_{sub} = 12.5°C

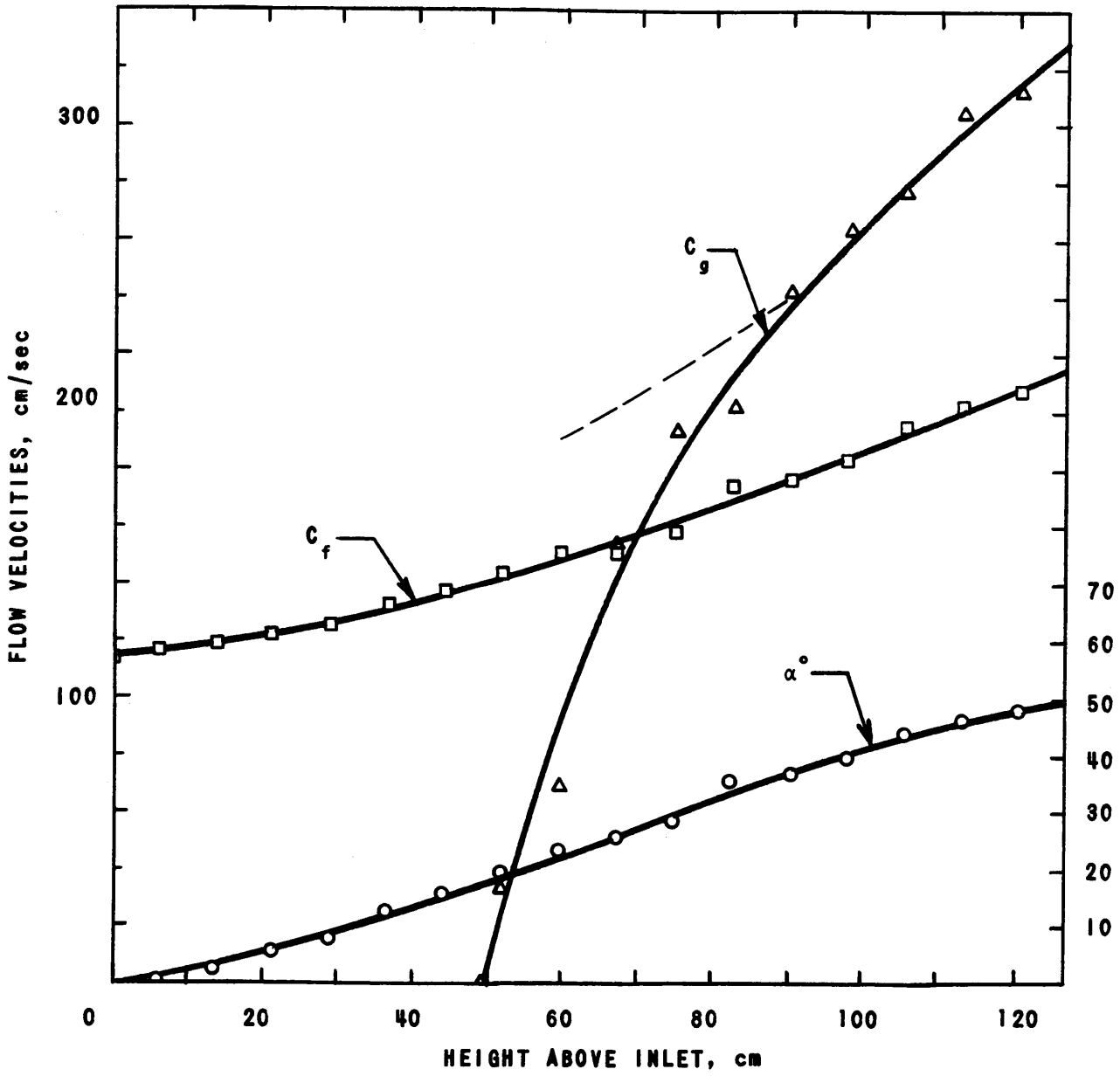

FIG. 37
RUN NO.16, 68 Ata. 111.5 kw/l
ΔT_{sub} = 12.1°C

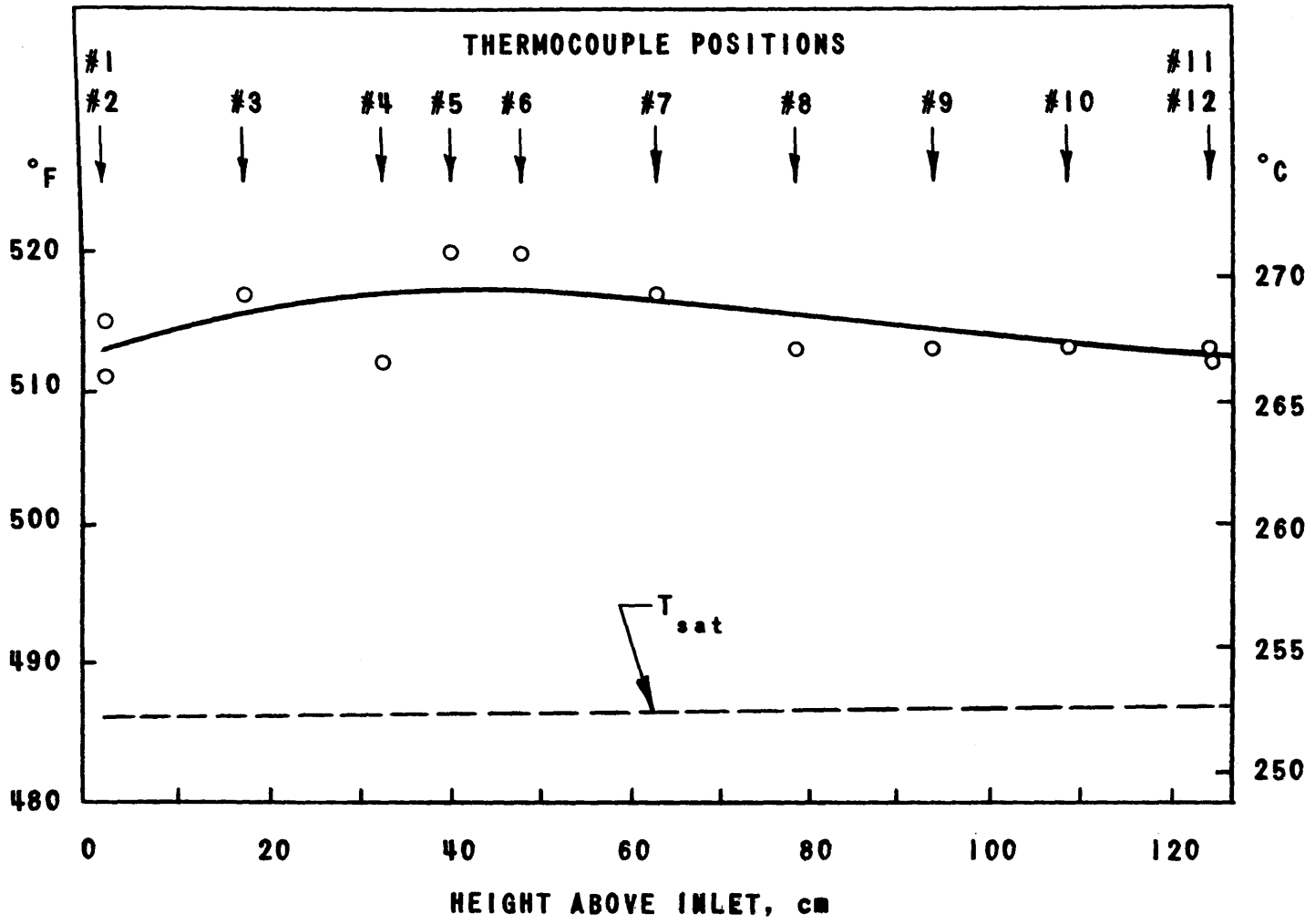

FIG. 38
TYPICAL OUTSIDE WALL TEMPERATURES
RUN NO. 8. 40.8 Ata, 63.8 kw/l

CHAPTER XVI

VOID OSCILLATIONS

A. Results of Transfer Function Measurements

Void amplitude and void phase have been plotted as functions of frequency in Figure 39 through 45. The measurements are given by the points, and the full lines represent the theoretical curves to be described in the next section.

A few general comments about the measurements and the presentation of the data will now be given. A discussion of the main features of the data will follow next.

Each of the Figures 39 through 45 represents a different set of conditions as listed in Table 2 and also in the figure headings.

Note that the void amplitude is given in percent of the channel cross section, and not in percent of the actual void fraction at the point in question.

It will be noticed that results have been obtained at four different pressures. At 27.2 Ata, there are two runs at different values of subcooling. At 40.8 Ata, three different subcoolings have been studied. There is one run each at the pressures 54.4 Ata and 68.0 Ata.

At most of the conditions, measurements were taken throughout the frequency range at three different heights. For each point, a pair of diagrams have been given, and the value of x and of average void fraction α^{o} have been given underneath each pair. Three measuring positions were all that could normally be covered during a 12 hour run.

All points at the same condition have been taken the same day, except in the case of run No. 9, Figure 39, which contains data taken on two consecutive days. The repeatability is seen to be quite good, and within the

normal spread of points.

A note about the data included in this report:

> Data runs 1 through 8 were short shakedown runs to test the procedures and the instrumentation. These runs have not been included because the phase measurements were incorrect. No oscillation data were taken during run No. 14; only traverses not utilized in this report.

Because of the characteristics of the power oscillator (see Chapter VI), the power amplitude was different for different oscillation frequencies. The data taken have been presented in Appendix 5, and the actual power and void amplitudes have been given there. In order to plot the data in a form suitable for correlation, the void amplitudes were normalized to correspond to a 10% power swing, using the fact that the response is linear. In the several cases where oscillations were performed at the same conditions, but at different power amplitudes, the results fall well within the general uncertainty of the measurement. There is no evidence of any non-linearity in the response.

In the results of run No. 13, Figure 43, the uncertainties in the measurement have been shown for all points.

The most prominent feature of the data is the node point, which is quite sharply defined, and found in all the runs taken. The amplitude measurements show minima which are quite sharp, and which are found at lower frequencies as the value of x is increased.

The phase measurements also show a dip at the node frequency. The dip is fairly small near the exit, but becomes more and more pronounced at lower positions. At some x value, it is no longer possible to tell with certainty whether the phase breaks through the 180° level, or whether it turns back up

towards zero phase lag. This uncertainty is due to the fact that the node in the amplitude curve is very sharp at the lower x values. As the phase is measured by the ratio of the amplitudes of the in-phase and out-of-phase signal components, it will be appreciated that definition is lost as both amplitudes tend towards zero. To bring out this ambiguity, the measured points where appropriate, have been plotted in two positions, 360 degrees apart.

It will be seen that the void oscillation leads the power at low values of the oscillation frequency. This effect, which is due to pressure feedback from the steam separator, will be discussed further in Section C of this chapter.

B. Comparison with Theory

When the experimental data were compared with the models of Zivi and Wright[16], and of Akcazu[15], it was found that these predicted node frequencies roughly twice as large as the values measured. This led to the development in Chapter 14 where pressure variations in the channel were taken into account. The final result of that chapter, equation 14.44, has been programmed for an IBM-650 computer (see Appendix 4), and fitted to the data by taking the constant δ' as an adjustable parameter. The calculated curves have been shown for all measuring positions in Figures 39 through 45.

Some of the important points brought out by the comparison between theory and experiment will now be discussed.

The zero frequency amplitude response is given by:

$$\left|\bar{a}(x,j0)\right| = \frac{\left|\bar{Q}(j0)\right|}{Q^o} \frac{Q^o x}{V \rho_g h_{fg} C'_g(x)} = B \frac{x}{C'_g(x)} \qquad (16.1)$$

The term $\frac{\left|\bar{Q}(j0)\right|}{Q^o}$ has always been taken equal to 0.1, corresponding to a

10% power swing. The calculated value of the steam velocity was used for C'_g in all cases. As the zero frequency response given by equation 16.1 fits the data very well, the assumption $c_g(x,t) \tilde{=} 0$ made in Chapter 14, is seen to be a good one.

It appears that the zero frequency response differs less at different points along the channel than predicted by the model. It is believed that this should be explained by the influence of the upper part of the channel on the conditions in the lower part. Such an effect was not considered in the theoretical derivations in Part III of this work. The assumption was always made that the conditions at a given point would be given exclusively by previous events in the up-stream part of the channel.

The node frequency is given approximately by the relation

$$\omega_c \cong \frac{2\pi}{(1 + \delta')t_x} \tag{16.2}$$

The value of δ' needed to bring the node frequency in line with the measured values has been given underneath the curves in each case. When these values are to be discussed, it should be kept in mind that t_x has been computed by the equation:

$$t_x = \frac{1}{a} \ln \frac{C_o + ax}{C_o} \tag{16.3}$$

where a (see equations 14.8 and 14.11 also) have been found by linearizing the water velocity calculated as described in the previous chapter. If the calculation of t_x had been based in the steam velocity instead, this would have led to larger values of δ'. Except for a very small change in the sharpness of the node, the theoretical curves would otherwise remain the same. The actual propagation velocity of disturbances, therefore, is lower than either the steam or the water velocity.

Values for δ' as defined by equation 14.40 has been calculated for different values of α° and β° (see the assumptions of Section C of Chapter 14), and the results are plotted in Figure 46. The calculations have been performed using steam table values for a saturation pressure of 40.8 Ata, and the methods presented in Appendix III. It is seen that quite small β° values are needed in order to arrive at the large values of δ' used in Figures 39 through 45. It becomes clear that β° must be redefined slightly to allow for values that small. Instead of letting β° be the total fraction of saturated water in the channel, it is necessary to assume that only part of this water remains at all times in temperature equilibrium with the steam.

It should be pointed out that δ' varies with conditions and with height in a manner that is consistent with the assumptions made in Chapter 14.

The sharpness of the node is determined by the time constant τ when the value of δ' is given. Smaller values of τ give more pronounced dips at the node frequencies. τ is defined by equation 13.13 as a first order approximation to the transfer function G(s). This function has been plotted in Figure 25 for various values of the incremental heat transfer coefficient h_i. If this constant is calculated from equations 10.8 and 10.5, and if G(s) is approximated as indicated in Figure 25, then τ values in the order of 0.1 second results for the conditions of the data runs. It will become clear from a study of Figures 39 through 45 that somewhat smaller numbers give better fit to the experimental data. No conclusions will be drawn from this fact, but it should be noted that direct measurements of h_i would be of great interest in the evaluation of the merits of equation 14.44.

There is one respect in which this relation does not follow the trend of the data. The experiments show an increasing sharpness in the node -

especially in the phase angle - as the x value decreases, while the opposite is the case for the calculated curves. A possible approach to a better formula is indicated through the discussion of assumptions a and b in Section B of Chapter XIV.

C. Steam Dome Pressure Variations

It was pointed out in Chapter IV that the volume of the steam separator was too small to accommodate the variations in the steam production rate at the lowest frequencies without small variations in pressure.

These pressure variations have a feedback effect on the voids in the channel as shown in Figure 49. If the pressure-to-void transfer function is written: $\bar{\alpha}_p(x,s)$, the total void effect is given by:

$$\bar{\alpha}(x,s) - \frac{k_1}{s} \bar{\alpha}_p(x,s) \tag{16.4}$$

At high oscillation frequencies, this will approach $\bar{\alpha}(x,j\omega)$. At very low frequencies, the expression approaches:

$$|\bar{\alpha}(x,j0)| + j \frac{k_1}{\omega} |\bar{\alpha}_p(x,j0)| \tag{16.5}$$

where the zero frequency response of the power-to-void and the pressure-to-void transfer functions have been introduced.

It will be appreciated that this expression has a positive phase angle that approaches + 90° as ω goes to zero. For frequencies of about 0.05 to 0.1 cps, the numerical value of the pressure term will be small, and it adds vectorially to the much greater power term at right angles approximately. The pressure feedback effect will, therefore, mainly be felt in the void phase, and the change in void amplitude will be small in the frequency range studied.

No attempt has been made to correct for this effect in the experimental results.

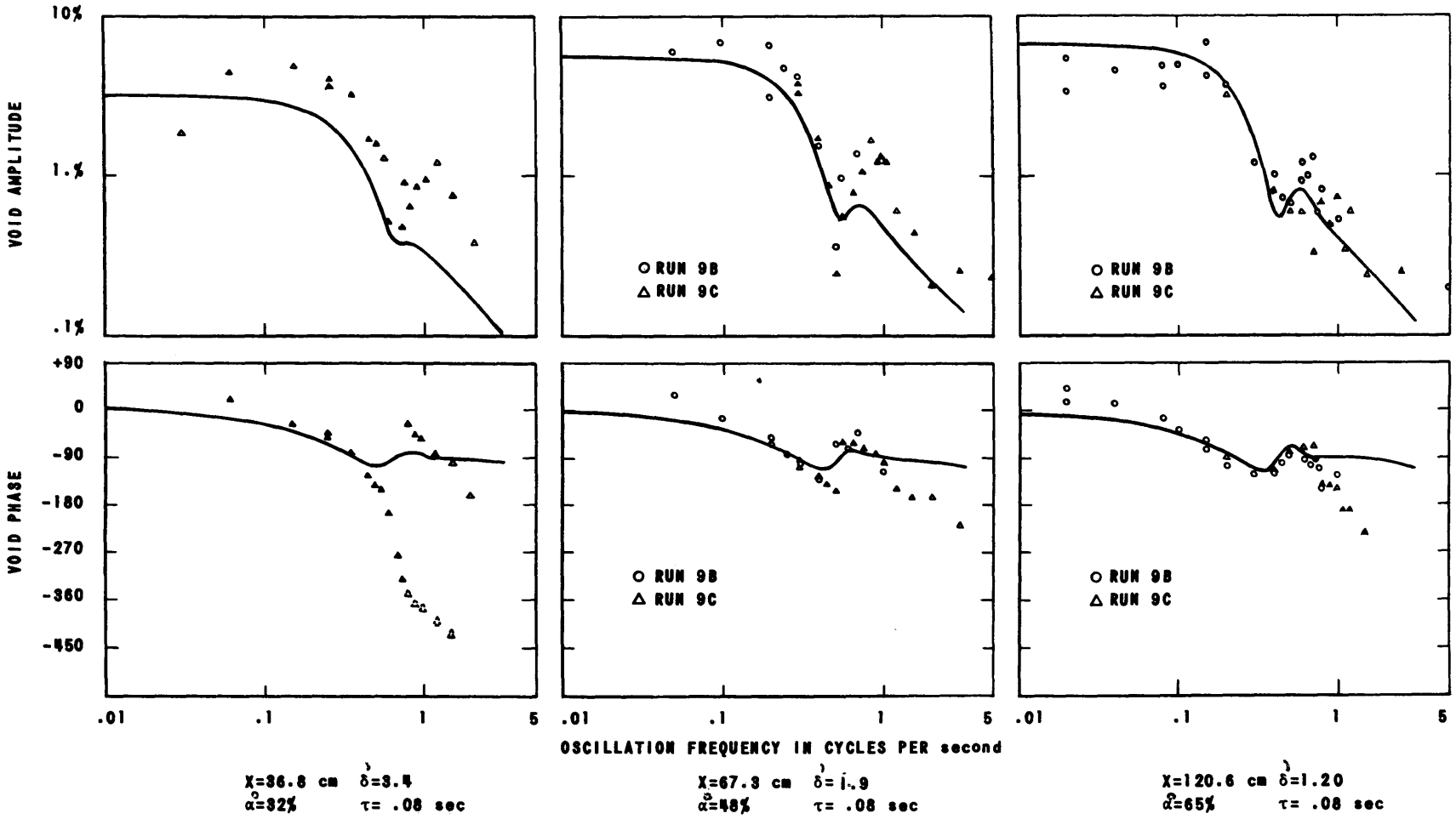

FIG. 39
OSCILLATION RESULTS - RUN NO. 9. 27 Ata, 47.9 kw/l, ΔT_{sub}=2.9°C, C_o=77 cm/sec

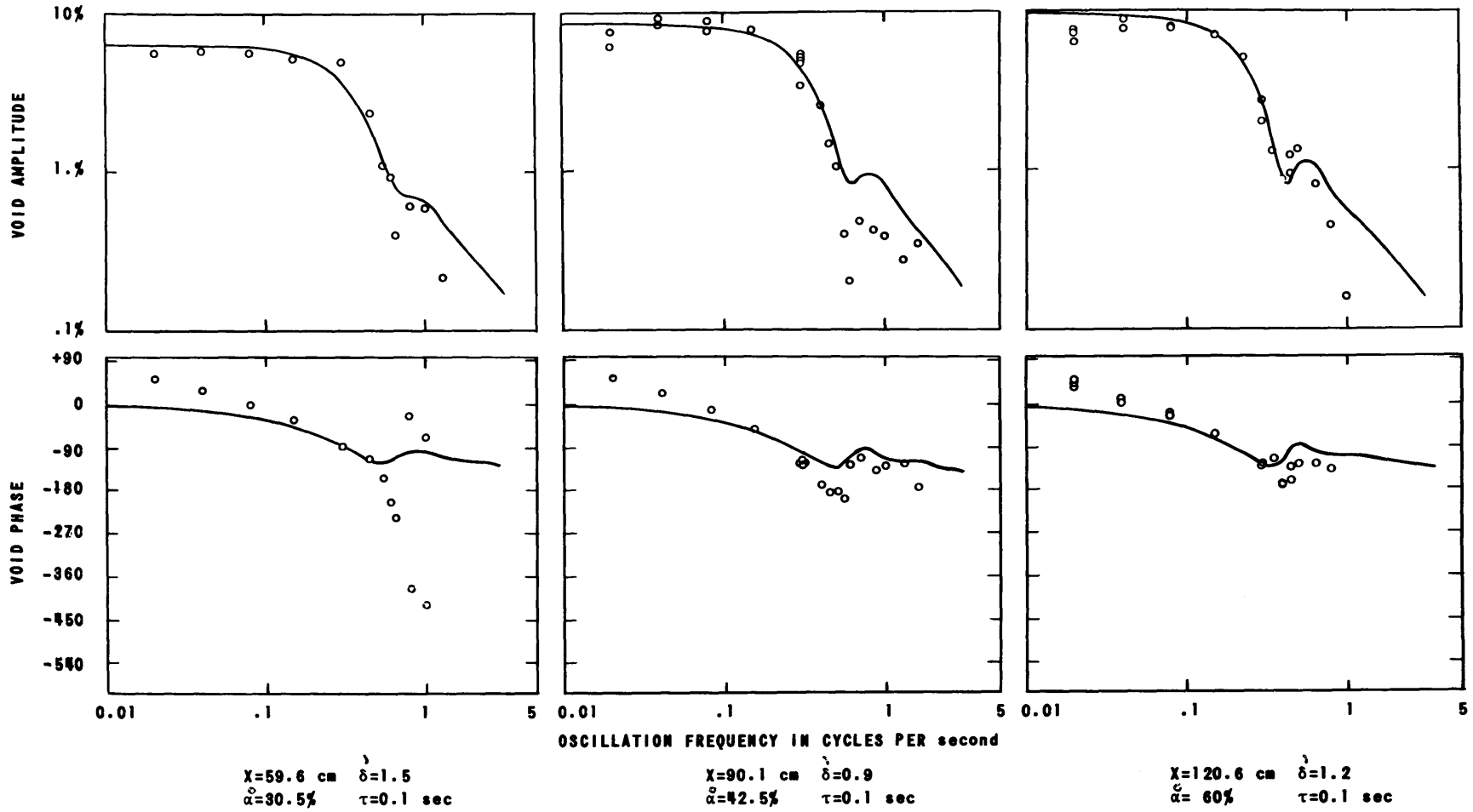

FIG. 40
OSCILLATION RESULTS - RUN NO. 10. 27 Ata, 47.9 kw/l, ΔT_{sub}=8.7°C, C_o=77 cm/sec

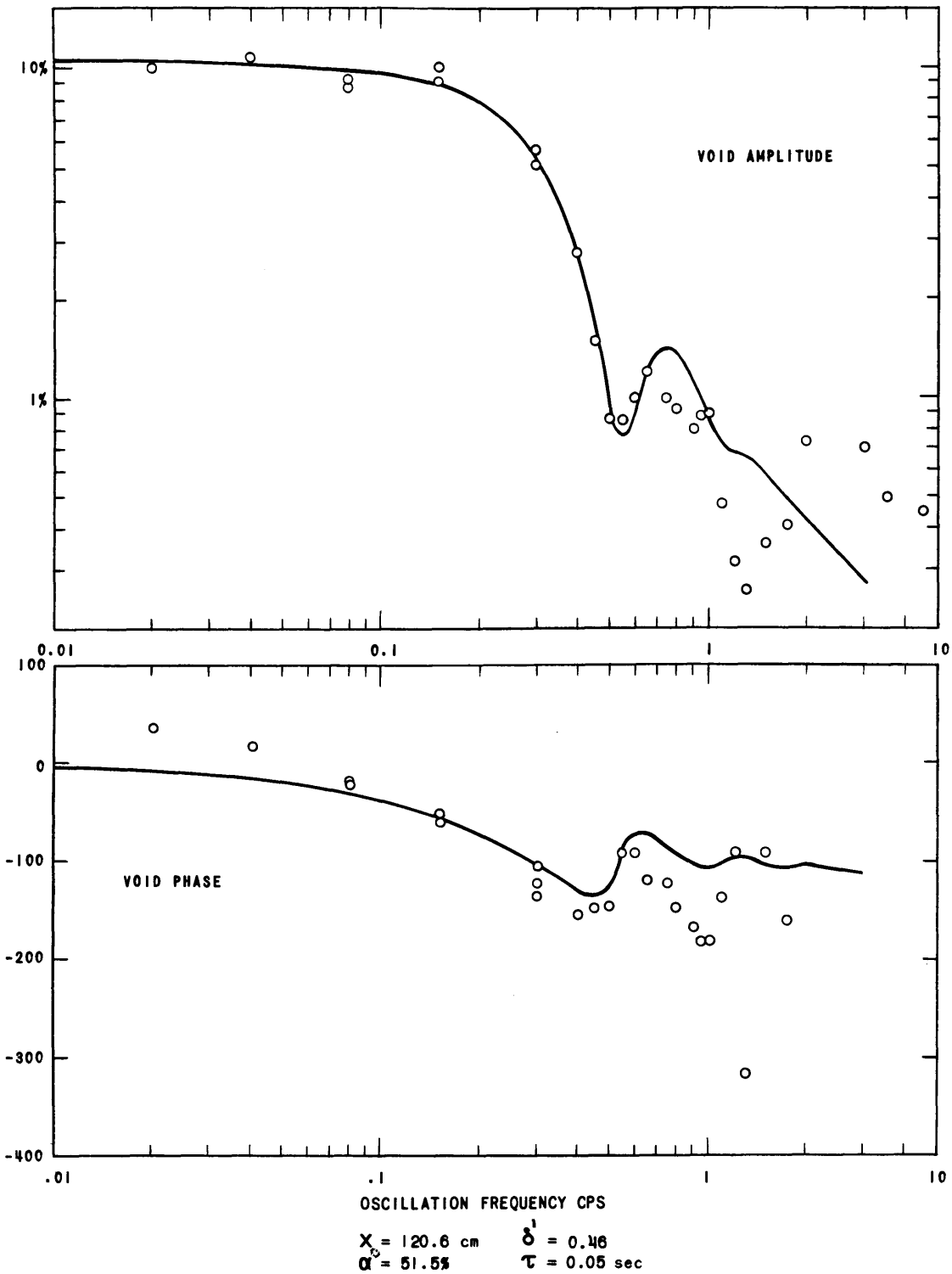

FIG. 41
OSCILLATION RESULTS - RUN NO. 11
40.8 Ata, 79.8 kw/l,
ΔT_{sub} = 14.4°C, C_o = 115 cm/sec

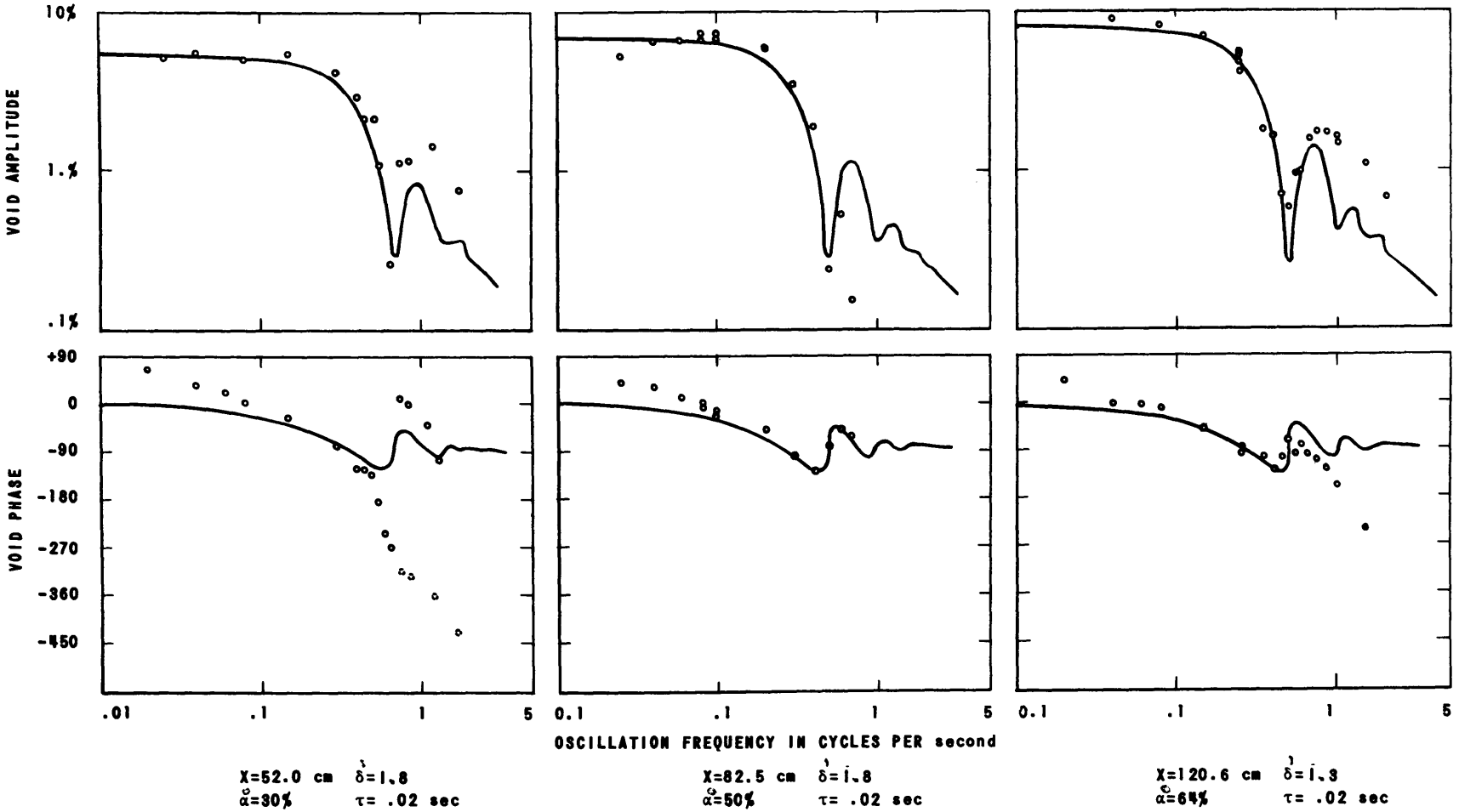

FIG. 42
OSCILLATION RESULTS - RUN NO. 12. 40.8 Ata, 79.8 kw/l, ΔT_{sub}=7.2°C, C_o=115 cm/sec

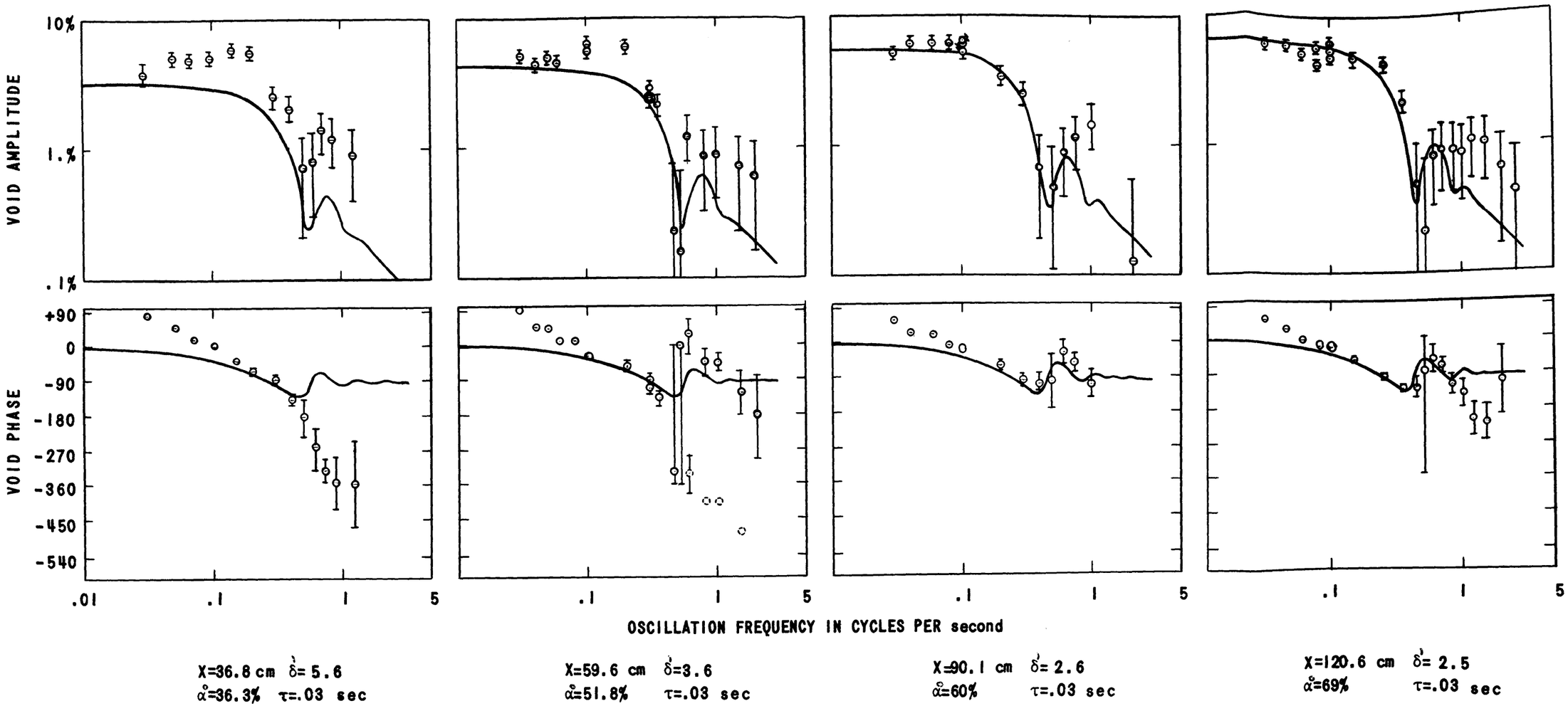

X=36.8 cm δ= 5.6
α=36.3% τ=.03 sec

X=59.6 cm δ=3.6
α=51.8% τ=.03 sec

X=90.1 cm δ= 2.6
α=60% τ=.03 sec

X=120.6 cm δ= 2.5
α=69% τ=.03 sec

FIG. 43

OSCILLATION RESULTS RUN NO. 13 . 40.8 Ata, 79.8 kw/l, ΔT_{sub}=3.3 °C, C_o=115 cm/sec

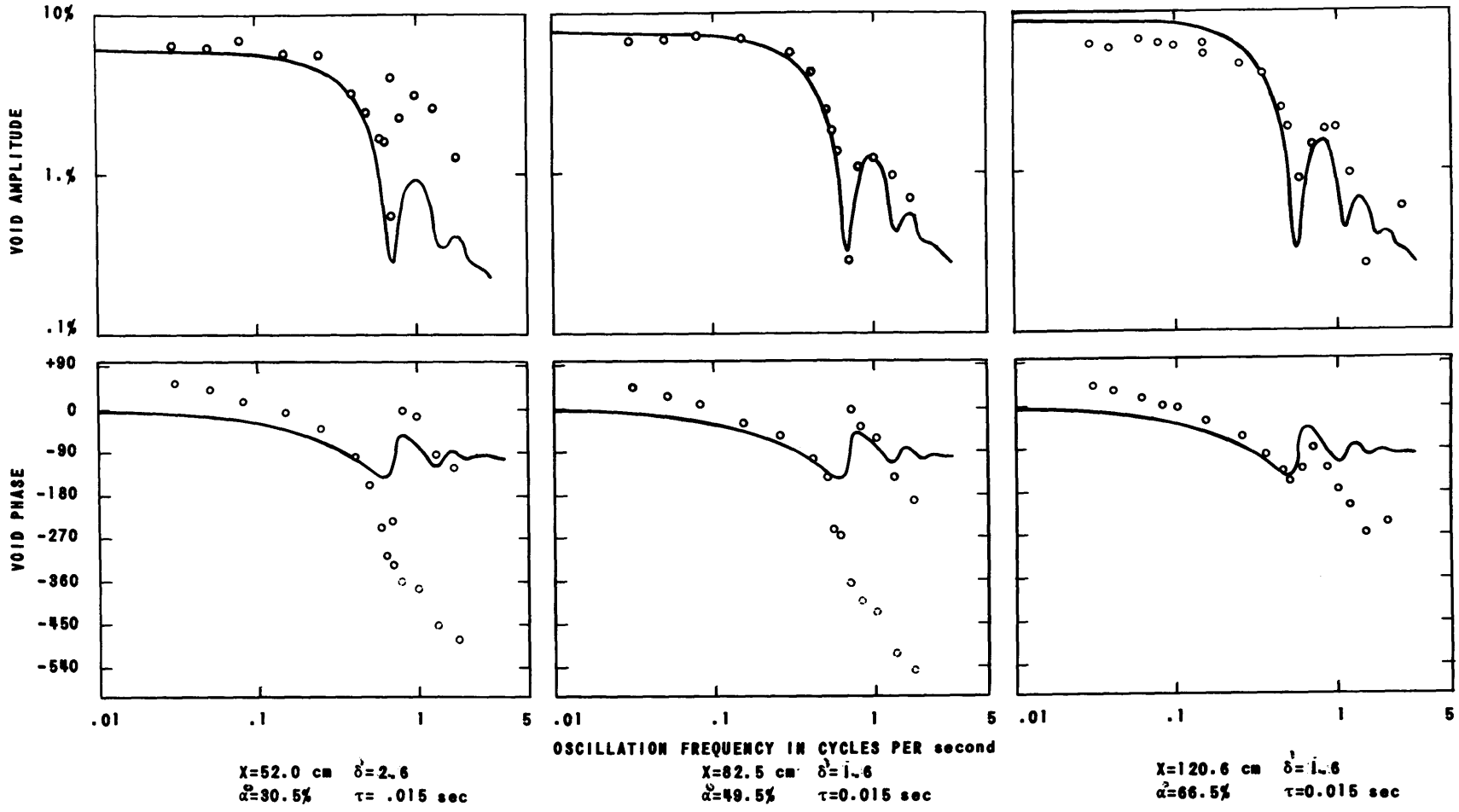

FIG. 44
OSCILLATION RESULTS - RUN NO. 15. 54.4 Ata, 79.8 kw/l, ΔT_{sub}=12.5%, C_o=115 cm/sec

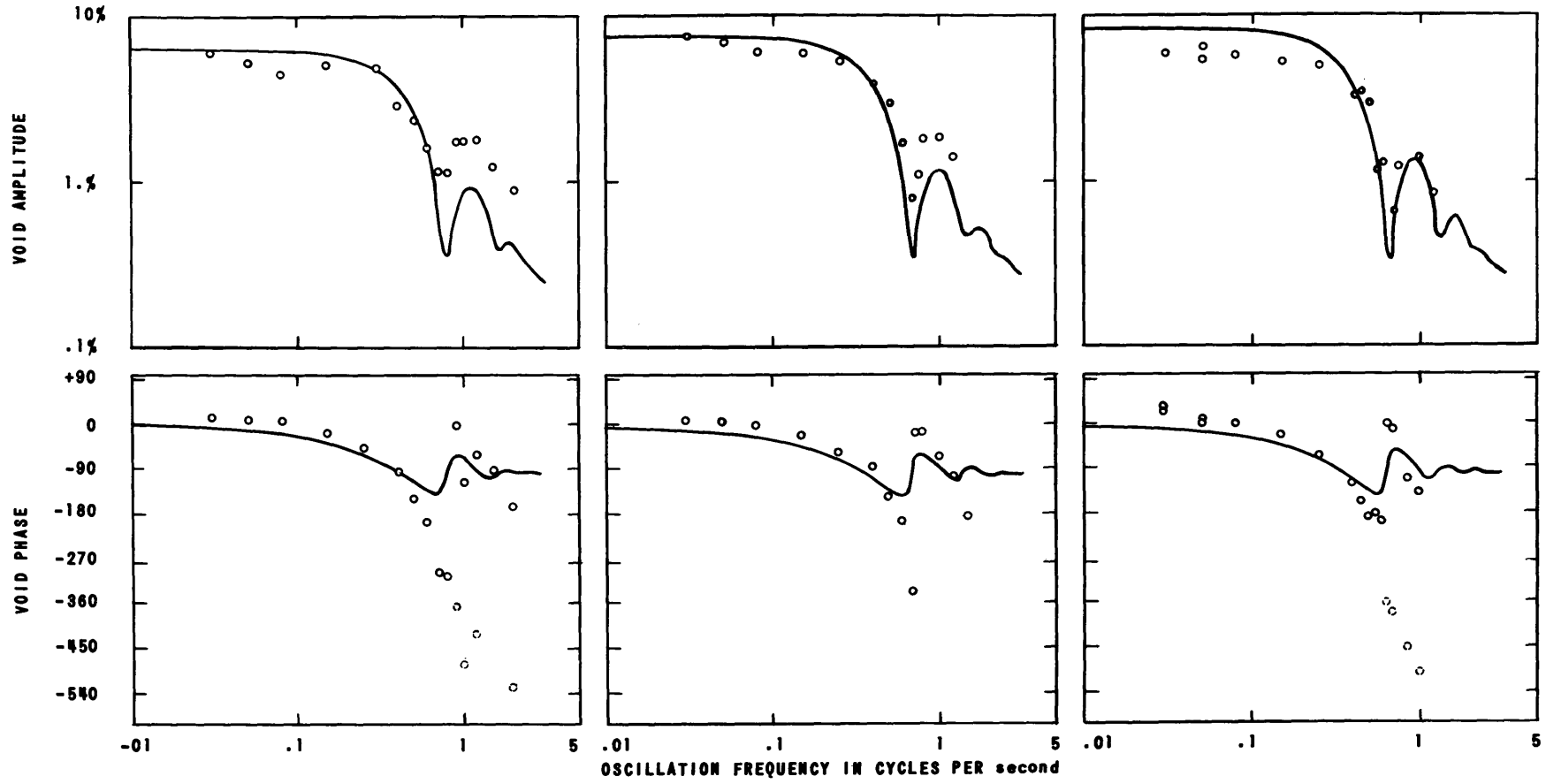

FIG. 45
OSCILLATION RESULTS - RUN NO. 16. 68 Ata, 111.5 kw/l, ΔT_{sub}=12.1°C, C_o= 115 cm/sec

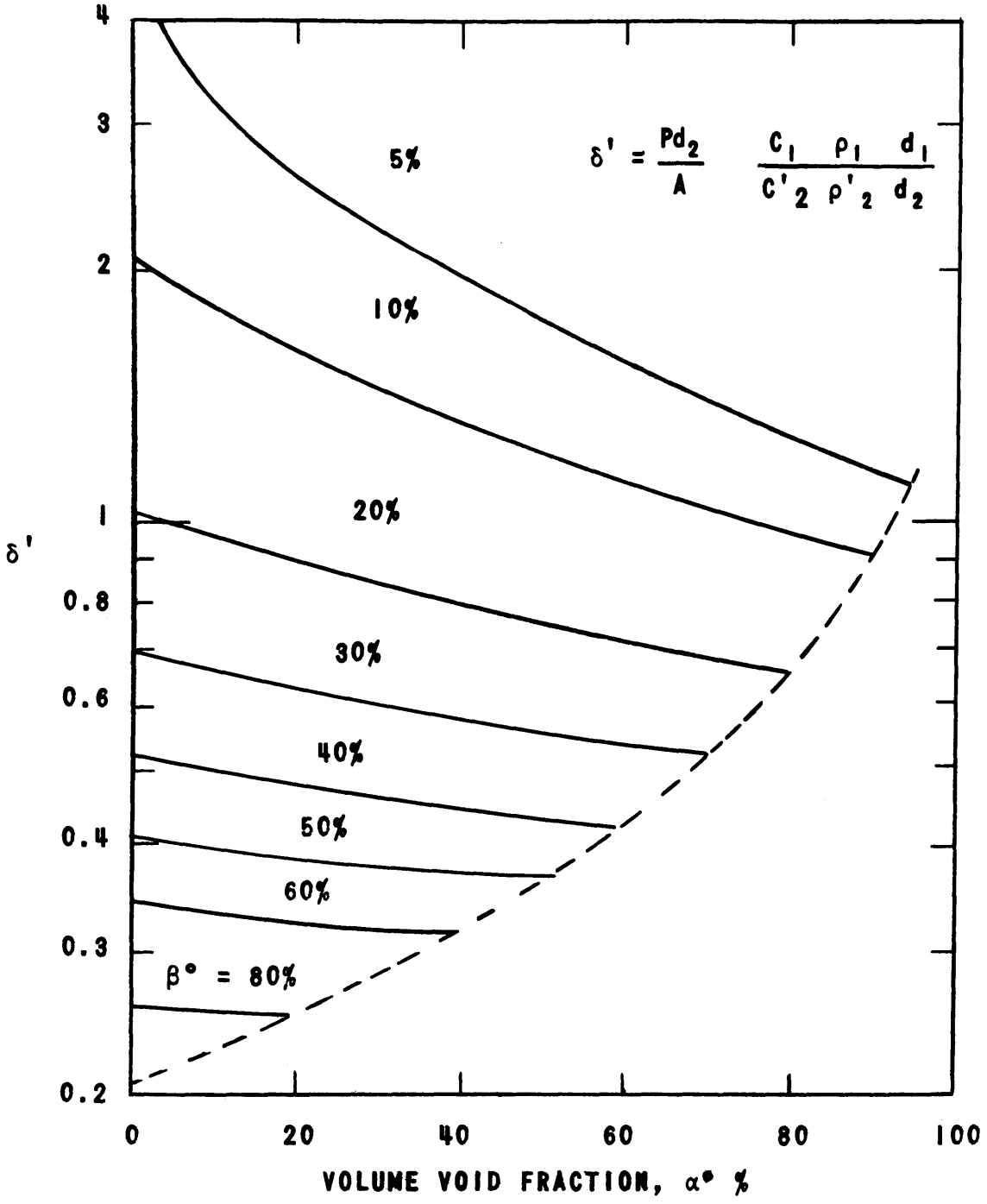

FIG. 46
THE VARIATION OF δ' AS A FUNCTION OF α° WITH β° AS A PARAMETER

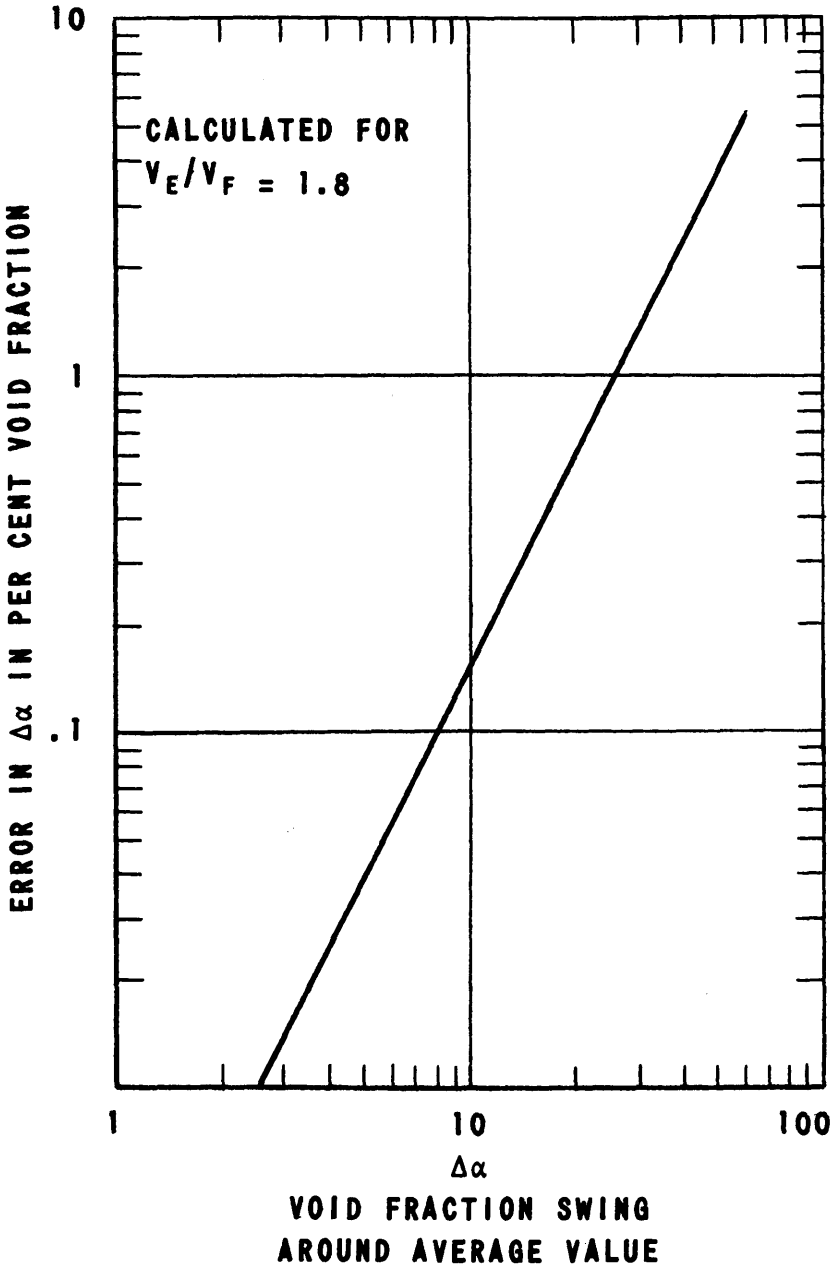

FIG. 47
ERROR IN MEAN VOID FRACTION AS MEASURED BY AVERAGING THE OUTPUT FROM THE VOID DETECTOR

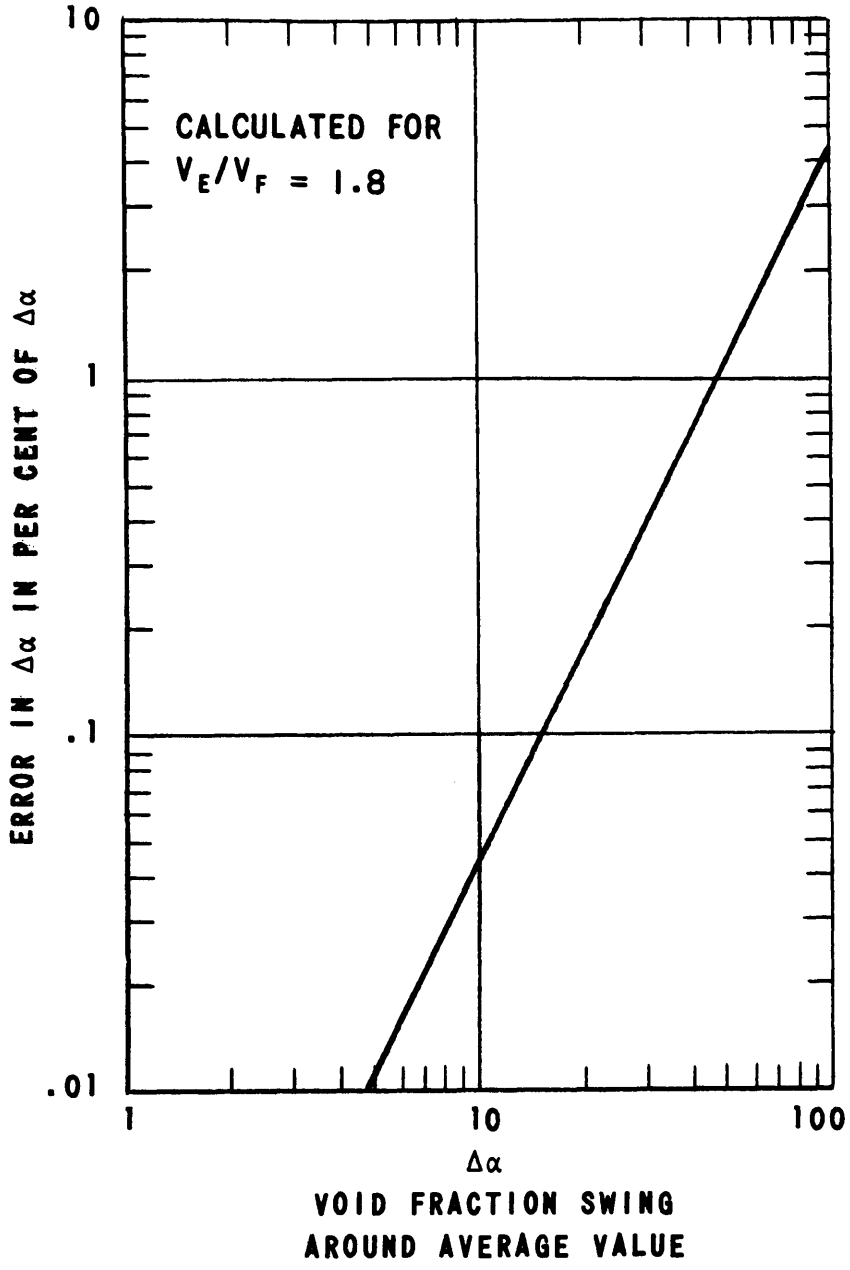

FIG. 48
ERROR IN COHERENT VOID AMPLITUDE DUE TO THE NON-LINEARITY OF THE VOID DETECTOR

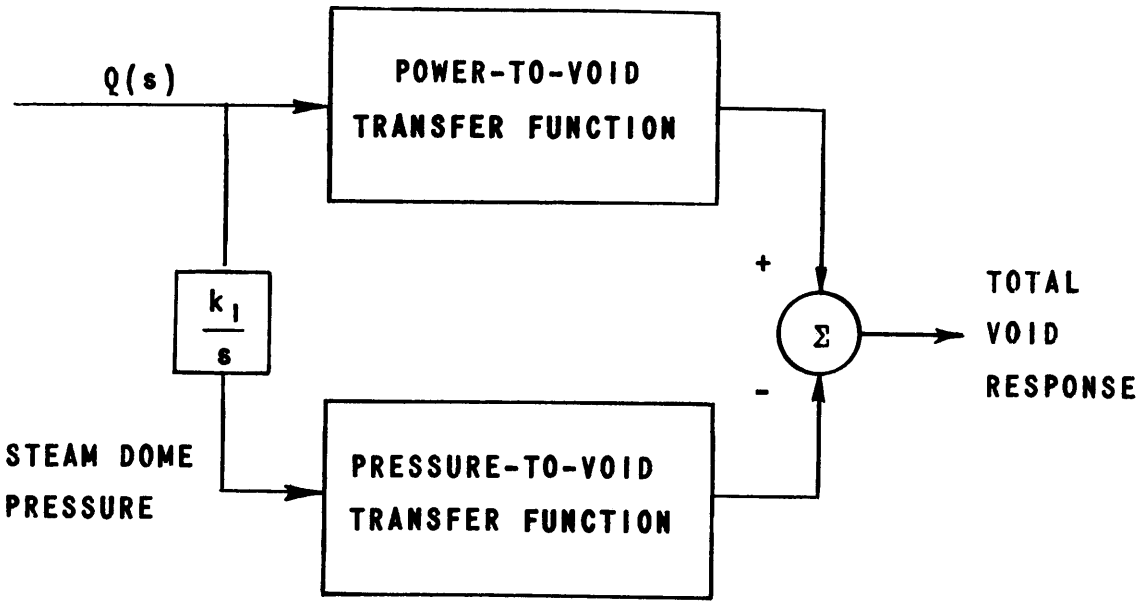

FIG. 49
BLOCK DIAGRAM SHOWING THE EFFECT
OF STEAM DOME PRESSURE VARIATIONS

CHAPTER XVII

CONCLUSIONS

A. Conclusions

The frequency response of the steam void fraction to sinusoidal power variations was measured for a pressurized boiling test section at a series of conditions. The results are believed to be the only existing direct measurements of the power-to-void transfer function taken at high pressures.

It was found that the cut-off frequency of the void amplitude response is much lower than that predicted by the theoretical power-to-void transfer functions previously used in reactor calculations.

The power-to-void transfer function for the test channel studied was derived through a new approach, and the result correlates the experimental data very well. The respects in which the basic assumptions used deviate from previous practice, will now be briefly mentioned.

It was found unnecessary to divide the channel into two sections separated by the bulk boiling point. Instead, the distributed parameter equations were solved for a single region. This simplifies the mathematics, and has the further advantage of predicting variations in void fraction below the bulk boiling point also. This is in accordance with reality in pressurized boiling channels where the power density is high.

The assumption of complete mixing at a given height had to be abandoned not only to justify the single region approach just mentioned, but also to explain the low cut-off frequencies measured.

For the latter purpose it was necessary to take into account pressure changes in the channel caused by variations in the power. In order to fit the cut-off frequency exactly, it was necessary to adjust a parameter δ' associated with the completeness of the mixing in the channel. Although it

has been shown that the values of δ' thus arrived at are in reasonable agreement with the assumptions, no method of accurately predicting these values for a given channel is as yet in sight.

The measured zero frequency amplitude response indicates that it is a valid approximation in the present case to assume that the steam velocity is time invariant at a given height during power oscillations.

An important result of the present work is to show that the power-to-void transfer function at high pressures cannot be derived without considering the details of such processes as nuclear boiling, mixing between the steam/water components, relative phase velocities, etc. These mechanisms are not fully understood today. Until they are, completely satisfactory power-to-void transfer functions cannot be arrived at through theoretical considerations alone.

B. Recommendations for Future Work

It can be stated that in general all theoretical and experimental work regarding boiling and two-phase flow have taken one of two very different approaches: Either 1) the microsopical approach where single bubbles are studied in growth, detachment, etc., or 2) the macroscopic approach where the conditions in boiling channels are described by empirical relations in terms of average values of the variables involved. Very few attempts have been made to bridge the gap between these two approaches.

Of the numerous experiments carried out in natural or forced circulation loops[56], all but an extremely small fraction have been devoted to the study of steady state conditions. A large amount of data have been compiled that is very useful for the designer who wants to predict the steady state performance of a given boiling channel. But this research has been less successful in advancing the fundamental understanding of the processes taking place in such a channel. This is borne out by the inadequacy of the present theory in describing situations like those studied in this work.

This author believes that more effort ought to be put into the study of transient phenomena, and that this is the best way to study the basic processes of boiling and two-phase flow. Transient experiments may well uncover mechanisms that would otherwise be difficult to bring out, and more information can be obtained from a single test.

While studies of transient states offer greater opportunities, the challenges are greater also. More elaborate experiments are needed and the complexity of the instrumentation will increase. The analysis of the results will also be more difficult.

Boiling is in nature a statistical phenomenon, and so is turbulent two-phase flow. Satisfactory description of the conditions in a boiling channel cannot be expected unless random noise theory is employed.

A few concrete suggestions for first steps along the road outlined above will now be given. Some possible improvements in the instrumentation used for the present experiment will be mentioned first.

As stated in Chapter VIII, the accuracy in the measurement of void variations is limited by the noise developed in the sine/cos potentiometer. This unit is subject to wear, and it has to be kept running continuously during the taking of data. A considerable noise reduction could be obtained by performing the sine and cosine multiplication in synchro resolvers instead. This requires a carrier wave system, preferably 400 cps, which would add to the cost and complexity of the instrumentation.

Larger power amplitudes could be obtained by increasing the capacity of the power oscillator, as mentioned in Chapter VI. Larger power amplitudes would result in larger void amplitudes, which could be detected more easily.

Attempts should be made to improve the void detector system further.

More theoretical and experimental work should be spent on a study of the "δ-effect" introduced in Chapters XIII and XIV. It should be determined how the number δ changes with conditions, and especially how it varies with the channel width. This might give important information about the effectiveness of the mixing in such channels.

Attempts should be made to measure the pressure variations in the channel at various positions, and if possible, correlate the pressure signal with the power signal. By measuring the pressure difference between neighboring points, and correlating this signal with the power variations, it should be possible to calculate the propagation velocity of pressure variations, as well as void variations, along the channel. Special pressure transducers would have to be developed in order to do this.

The possibility of measuring the incremental heat transfer coefficient was discussed in the previous chapter. Such an experiment would be of interest in the study of the nucleation process in boiling, and could be performed in a relatively small sized setup.

The present work has been concerned with the power-to-void transfer function only. As pointed out in Chapter I, the effects of changes in steam dome pressure, inlet flow, and inlet temperature on the steam bubble distribution is described by separate transfer functions: the pressure-to-void transfer function, etc. These are all very important to boiling water reactor stability analysis, and should be given careful study along lines similar to those adopted in the present work. The inlet flow rate could be oscillated sinusoidally (step response measurements are less difficult to perform, and could give very useful information also), and the effect on the steam voids detected. It should be stressed again that the importance of such measurements would be not only to give information useful for boiling water reactor design, but also to shed light upon the basic processes involved in the flow of two-phase mixtures in vertical channels.

APPENDIX I

Errors Due to the Non-Linearity of the Void Detector

The voltage output from the gamma preamplifier is related to the volume void fraction, as follows:

$$V_\alpha = V_F \left[\frac{V_E}{V_F}\right]^{\alpha^o(t)} \tag{I.1}$$

where: V_F = signal voltage for the full section,

V_E = signal voltage for the empty section.

If α^o varies, for instance sinusoidally given by

$$\alpha^o(t) = \alpha^o + \alpha \sin \omega t \tag{I.2}$$

the response in signal voltage can be found by expanding V_α in a Taylor series around the point:

$$V_{\alpha o} = V_F \left[\frac{V_E}{V_F}\right]^{\alpha^o} \tag{I.3}$$

Differentiating:

$$\frac{d\,V_\alpha}{d\,\alpha} = V_\alpha \ln \frac{V_E}{V_F}$$

$$\frac{d^2 V_\alpha}{d\alpha^2} = V_\alpha \left[\ln \frac{V_E}{V_F}\right]^2 \tag{I.4}$$

Taylors formula:

$$V_\alpha = V_{\alpha o} + \frac{1}{1!}\left[\frac{dV_\alpha}{d\alpha}\right]_o \Delta\alpha + \frac{1}{2!}\left[\frac{d^2V_\alpha}{d\alpha^2}\right]_o \Delta\alpha^2 + \frac{1}{3!}\left[\frac{d^3V_\alpha}{d\alpha^3}\right]_o \Delta\alpha^3 + \text{---} \tag{I.5}$$

where:

$$\Delta\alpha = \alpha \sin \omega t$$

$$\Delta\alpha^2 = \alpha^2 \left[\frac{1}{2} - \frac{1}{2}\cos 2\omega t\right]$$

$$\Delta\alpha^3 = \alpha^3 \left[\frac{3}{4} \sin \omega t - \frac{1}{4} \sin 3\,\omega t\right]$$

$$\Delta\alpha^4 = \alpha^4 \left[\frac{3}{8} - \frac{1}{2} \cos 2\omega t + \frac{1}{8} \cos 4\omega t\right] \qquad \text{(I.6)}$$

Inserting (I.4) and (I.6) into (I.5), there results:

$$\frac{V_\alpha}{V_{\alpha o}} = \left[1 + \frac{1}{4} P_o^2 + \frac{1}{64} P_o^4 + \text{---}\right] + \left[1 + \frac{1}{8} P_o^2 + \frac{1}{192} P_o^4 + \text{---}\right] P_o \sin \omega t \qquad \text{(I.7)}$$

+ terms of higher frequency

where:

$$P_o = \ln \frac{V_E}{V_F} \qquad \text{(I.8)}$$

Errors in Average Void Fraction

When this signal is filtered for the measurement of the average void value, there results:

$$V_\alpha = V_{\alpha o} \left[1 + \frac{1}{4} P_o^2 + \frac{1}{64} P_o^4 + \text{---}\right] \qquad \text{(I.9)}$$

as $V_{\alpha o}$ is the signal value corresponding to the average void fraction, it will be appreciated that the measured value is too large. By equation (I.4), the error in α^o becomes:

$$d\alpha^o = \frac{dV}{V_\alpha} \frac{1}{\ln \frac{V_E}{V_F}} = \frac{\frac{1}{4} P_o^2 + \frac{1}{64} P_o^4 + \text{---}}{\ln \frac{V_E}{V_F}} \qquad \text{(I.10)}$$

This equation has been plotted in Figure 47 for an empty-to-full ratio of 1.8. For the test section studied, variations of as much as $\pm$ 20% around the average void fraction was quite normal at "steady state" boiling. From Figure 47 it will be seen that the error in the measured void fraction will be less than 1%, even in this case.

Errors in Wave Analyzer Output Signal

It will be seen from equation I.7 that the coherent signal oscillation seen by the wave analyzer will be:

$$V_{\alpha o}\left[1 + \frac{1}{8}P_o^2 + \frac{1}{192}P_o^4 + \text{---}\right] P_o \sin \omega t \qquad \text{(I.11)}$$

while the "linearized" response should have been (equations I.2 and I.4):

$$\Delta V_\alpha = V_\alpha \ln \frac{V_E}{V_F} \Delta\alpha = V_{\alpha o} P_o \sin \omega t \qquad \text{(I.12)}$$

The fractional error in amplitude becomes:

$$\frac{d(\Delta\alpha)}{\Delta\alpha} = \frac{d(\Delta V_\alpha)}{\Delta V_\alpha} = \left[\frac{1}{8}P_o^2 + \frac{1}{192}P_o^4 + \text{---}\right] \qquad \text{(I.13)}$$

This equation has been plotted in Figure 48. It will be seen that the errors are insignificant.

APPENDIX II

The Rejection of Source Noise in the Void Detector

Assume that all gammas have equal energy, and that each on arrival at the scintillation crystal produces an impulse of charge q at the output of the photo-multiplier tube. It is further assumed that the cable and the first preamplifier stage can be represented by a time constant T_i, formed by the cable capacity C_i and the amplifier input resistance R_i. If the amplifier itself has a response in the order of microseconds, the addition to the output voltage from one single gamma, will be:

$$v(t) = k \frac{q}{C_i} e^{-\frac{t}{T_i}} \tag{II.1}$$

where k is the amplifier gain.

When n is the average gamma arrival rate, the autocorrelation function for the output voltage can be found by Campbell's Theorem[67]:

$$\phi(\tau) = n \int_{-\infty}^{\infty} v(t)\, v(t+\tau)\, dt + v_o^2 \tag{II.2}$$

$$= \frac{v_o^2}{2nT_i} e^{-\frac{|\tau|}{T_i}} + v_o^2 \tag{II.3}$$

where $v_o = kqnR$

The power spectrum of the output voltage is given by the Fourier transform:

$$\Phi(\omega) = \mathcal{F}\left\{ \frac{v_o^2}{2nT_i} e^{-\frac{\tau}{T_i}} \right\} = \frac{v_o^2}{n\left[T_i^2\omega^2 + 1\right]} \tag{II.5}$$

The standard deviation of this signal:

$$\sigma_1^2 = \int_0^\infty \Phi(\omega)d\omega = \frac{\pi v_o^2}{2nT_i} \qquad (II.6)$$

or:

$$\frac{\sigma_1}{v_o} = \left[\frac{\pi}{2nT_i}\right]^{1/2} \qquad (II.7)$$

As would be expected, the noise ratio can be reduced either by increasing the source strength, or by increasing the time constant for the preamplifier input circuit.

Conditions can be further improved by filtering the output from the preamplifier. For an RC-filter with time constant T_o, the power spectrum at the output becomes:

$$\Phi_2(\omega) = \frac{v_o^2}{n\left[T_i^2\omega^2 + 1\right]\left[T_o\omega^2 + 1\right]} \qquad (II.8)$$

By the above procedure:

$$\frac{\sigma_2}{v_o} = \left[\frac{\pi}{2n(T_i+T_o)}\right]^{1/2} \qquad (II.9)$$

It is convenient to keep T_i low, and adjust T_o for the purpose at hand: For the measurement of average void fractions, a large T_o should be chosen. If boiling noise or void oscillations are to be studied, T_o must be chosen to give a filter cut-off frequency:

$$f_2 = \frac{1}{2\pi T_o} \qquad (II.10)$$

well above the frequency spectrum of interest.

APPENDIX III

Specific Heat of Steam/Water Mixture at Constant Volume

Consider a volume element $\Delta V = A\Delta x$ containing:

1. Volume fraction α^o saturated steam.
2. Volume fraction β^o saturated water.
3. Volume fraction $\gamma^o = 1-(\alpha^o + \beta^o)$ subcooled water.

γ^o must approach zero near the outlet, but may be of appreciable magnitude near the inlet.

The specific heat for the volume element ΔV will now be calculated under the assumption (see Chapter XIV, Section C) that the volume fraction $\alpha^o + \beta^o$ only is taking part in the exchange of heat.

The difference ΔU in internal energy between an initial state 1 and a final state 2 is to be found.

Initial conditions:

$$m_{g1} = \Delta V \alpha^o \rho_{g1} \tag{III.1}$$

$$m_{f1} = \Delta V \beta^o \rho_{f1} \tag{III.2}$$

Conservation of mass:

$$m_{g1} + m_{f1} = m_{g2} + m_{f2} \tag{III.3}$$

Constant volume process:

$$m_{g1} v_{g1} + m_{f1} v_{f1} = m_{g2} v_{g2} + m_{f2} v_{f2} \tag{III.4}$$

Solving equations III.3 and III.4:

$$m_{g2} = m_{g1} \frac{v_{g1}-v_{f2}}{v_{g2}-v_{f2}} + m_{f1} \frac{v_{f1}-v_{f2}}{v_{g2}-v_{f2}} \qquad \text{(III.5)}$$

$$m_{f2} = m_{g1} \frac{v_{g2}-v_{g1}}{v_{g2}-v_{f2}} + m_{f1} \frac{v_{g2}-v_{f1}}{v_{g2}-v_{f2}} \qquad \text{(III.6)}$$

The change in internal energy:

$$\Delta U = (u_{g2}m_{g2} + u_{f2}m_{f2}) - (u_{g1}m_{g1} + u_{f1}m_{f1}) \qquad \text{(III.7)}$$

Elminating the m's in equation III.7 by means of equations III.1, III.2, III.5 and III.6:

$$\frac{\Delta U}{\Delta V} = \alpha^{o} \rho_{g1} \left\{ \frac{1}{v_{g2}-v_{f2}} \left[u_{g2}(v_{g1}-v_{f2}) + u_{f2}(v_{g2}-v_{g1}) \right] - u_{g1} \right\}$$
$$+ \beta^{o} \rho_{f1} \left\{ \frac{1}{v_{g2}-v_{f2}} \left[u_{g2}(v_{f1}-v_{f2}) + u_{f2}(v_{g2}-v_{f1}) \right] - u_{f1} \right\} \qquad \text{(III.8)}$$

The specific heat of the mixture considered is now given by:

$$\rho'_2 c'_2 = \frac{\Delta U/\Delta V}{T_{2_{sat}} - T_{1_{sat}}} \qquad \text{(III.9)}$$

The average density is given by:

$$\rho'_2 = \frac{\alpha^{o}}{\alpha^{o}+\beta^{o}} \rho_{g1} + \frac{\beta^{o}}{\alpha^{o}+\beta^{o}} \rho_{f1} \qquad \text{(III.10)}$$

ρ'_2 and c'_2 can be evaluated for given values of α^{o} and β^{o} by means of tables for saturated steam and saturated water[35].

APPENDIX IV

COMPUTER PROGRAM FOR THE EVALUATION OF EQUATION 14.44

The 650 FORTRAN system requires the following equipment:

Basic IBM 650

Index Registers

Alphabetic Device

Special Character Device, Group II

Floating Point Arithmetic Device

The 650 FORTRAN statements for the source program are the following:

Statement No.	FORTRAN Statement
	POWER-VOID FRACTION TRANSFER FUNCTION CALCULATION
	DIMENSION EX(20), FREQ(30)
1	READ, M, N, K
2	READ, EX
3	READ, FREQ
4	READ, DELTA, TAU, A, CO, B
5	PUNCH, DELTA, TAU, A, CO, B
6	DO 36 I = 1, M
7	X = EX(I)
8	CX = CO + A*X
9	TX = (LOGEF (CX/CO))/A
10	FX = B*X/CX
11	PUNCH, X
12	DO 36 J = 1, N

Statement No.	FORTRAN Statement
13	OMEGA = 6.28318 * FREQ (J)
47	PUNCH, OMEGA
14	V = TAU * OMEGA/(1.0 + DELTA)
15	R1 = SQRTF (1.0 + V**2)
16	PHI1 = 57.2958 * ARTNF(V)
160	GO TO (161, 17), K
161	PUNCH, R1, PHI1
17	R2 = TX * OMEGA * (1.0 + DELTA)
18	PHI2 = 90.0
180	GO TO (181, 19), K
181	PUNCH, R2, PHI2
19	R3 = R1 * R2
20	PHI3 = PHI1 + PHI2
200	GO TO (201, 21), K
201	PUNCH, R3, PHI3
21	V = TAU * OMEGA
22	R4 = SQRTF (1.0 + V**2)
23	PHI4 = 57.2958 * ARTNF (V)
230	GO TO (231, 24), K
231	PUNCH, R4, PHI4
24	R5 = R3/R4
25	PHI5 = PHI3 - PHI4
250	GO TO (251, 26), K
251	PUNCH, R5, PHI5
26	PHI5 = PHI5/57.2958

Statement No.	FORTRAN Statement
27	U5 = R5 * COSRF (PHI5)
28	V5 = R5 * SINRF (PHI5)
29	U6 = 1.0 - EXPEF (-U5) * COSRF(V5)
30	V6 = EXPEF (-U5) * SINRF (V5)
31	R6 = SQRTF (U6**2 + V6**2)
32	PHI6 = 57.2958 * ARTNF (V6/U6)
320	GO TO (321, 33), K
321	PUNCH, R6, PHI6
33	R7 = R6/R3
34	PHI7 = PHI6 - PHI3
35	AMPL = R7 * FX
36	PUNCH, AMPL, PHI7
37	CONTINUE
38	GO TO 4
39	END

Six subroutines are required in this program for calculating various functions. Two of the subroutines, LOGEF and EXPEF, are included in the 650 FORTRAN system. The remaining four subroutines : SQRTF, ARTNF, SINRF (radians) and COSRF (radians) must be supplied.

The input and output are in the standard 650 FORTRAN format. The input consists of the following:

1. A card with values of M, N and K;

   where M = number of axial positions (EXs) being studied.

   $1 \leq M \leq 20$

N = number of frequencies (FREQs) being studied for each EX. $1 \leq N \leq 30$

K = code number for conditional punch out of intermediate Rs and PHIs; for K = 1 - conditional output

K = 2 - no conditional output

2. Three data cards containing EXs. If less than twenty EXs are being studied, the cards must have zeros punched in the remaining 20-M words.

3. Five data cards containing FREQs. If less than thirty FREQs are being studied, the cards must have zeros punched in the remaining 30-N words.

4. Data cards containing DELTA, TAU, A, CO, B

The standard output format is the following:

1 DELTA, TAU, A, CO, B

2 EX (1)

3 OMEGA (1)

4 AMPL, PHI7 (PHI7 = phase angle in degrees)

5 OMEGA (2)

6 AMPL, PHI7

OMEGA (N)

AMPL, PHI7

EX (2)

EX (M)

DELTA, TAU .....

The conditional output format is the same as the standard output format with the exception that

R1, PHI1

R2, PHI2

R6, PHI6

are included between each OMEGA (J) and AMPL, PHI7.

TABLE 3a

STEADY STATE VALUES AT CONDITIONS OF DATA RUNS

MEAS. POINT		1	2	3	4	5	6	7	8	9	10	11	12	13	14	15	16
	α	.015	.04	.122	.18	.202	.31	.322	.395	.44	.372	.415	.45	.482	.50	.533	.522
RUN NO. 9*	C_f	78	80	88	94	95	110	116	125	134	120	128	136	144	149	159	154
ΔT_{sub}=3.0°C	C_g			44	114	172	159	199	199	212	290	295	304	300	332	340	374
	S			.50	1.21	1.8	1.54	1.73	1.59	1.58	2.42	2.3	2.24	2.09	2.24	2.14	2.43
	α	.015	.005	.06	.085	.12	.17	.18	.21	.27	.23	.27	.335	.405	.47	.505	.53
RUN NO. 10*	C_f	79	77	82	85	88	93	94	98	105	99	105	114	128	142	152	160
ΔT_{sub}=8.6°C	C_g								56	98	180	208	207	208	210	226	242
	S								.58	.93	1.82	1.98	1.82	1.63	1.48	1.49	1.51
	α	.015	.010	.035	.033	.028	.070	.045	.085	.155	.095	.13	.17	.220	.23	.275	.315
RUN NO. 11*	C_f	117	114	119	119	118	123	120	126	136	127	131	139	147	148	157	165
ΔT_{sub}=15.2°C	C_g												68	134	207	232	258
	S												.49	.91	1.40	1.48	1.56
	α	.005	.025	.095	.120	.138	.190	.175	.23	.30	.273	.32	.37	.40	.425	.46	.49
RUN NO. 12*	C_f			127	131	133	143	140	149	163	157	167	179	187	195	207	218
ΔT_{sub}=7.9°C	C_g						19	119	155	177	258	274	284	305	328	340	350
	S							.85	1.04	1.08	1.64	1.64	1.59	1.63	1.68	1.64	1.61

TABLE 3b

STEADY STATE VALUES AT CONDITIONS OF DATA RUNS

MEAS. POINT		1	2	3	4	5	6	7	8	9	10	11	12	13	14	15	16
	α	.025	.075	.175	.22	.25	.33	.335	.425	.425	.42	.49	.51	.54	.58	.62	.65
RUN NO. 13*	C_f	119	125	134	147	151	169	170	196	195	192	219	226	240	262	285	312
ΔT_{sub}=1.2°C	C_g		224	191	229	274	258	306	286	328	369	349	371	380	385	390	418
	S		1.79	1.43	1.56	1.81	1.53	1.80	1.46	1.68	1.92	1.59	1.64	1.57	1.47	1.37	1.34
	α	.01	.04	.085	.11	.16	.19	.24	.26	.31	.35	.39	.41	.46	.48	.49	.53
RUN NO. 15	C_f	117	120	127	130	138	143	152	155	165	175	185	190	206	212	216	232
corrected	C_g							18	92	138	177	212	244	258	288	321	332
	S							.12	.59	.84	1.01	1.15	1.29	1.25	1.36	1.49	1.43
RUN NO. 16	α	.01	.03	.06	.08	.13	.16	.20	.24	.26	.29	.36	.37	.40	.44	.46	.48
corrected	C_f	117	119	123	126	133	138	144	151	153	159	175	177	184	196	202	208
	C_g							36	70	154	195	202	242	264	278	305	313
	S							.25	.48	1.01	1.23	1.16	1.37	1.44	1.42	1.51	1.51

DATA RUN NO. 9B

INLET VEL.: 77.25 cm/sec			SUBCOOL.: 2.5°C		PRESSURE: 27.0 Atm			POWER: 47.85 kw/liter	
Meas. Point: x=120.6 cm, Av. Void Fraction: 53%					Meas. Point: x=67.3 cm, Av. Void Fraction: 40%				
FREQ.	POWER AMPL	VOID AMPL	NORM VOID AMPL	VOID PHASE	FREQ.	POWER AMPL	VOID AMPL	NORM VOID AMPL	VOID PHASE
.02	8.28	4.55	5.48	+ 43	.05	11.3	6.92	6.14	+ 31
.02	8.28	2.8	3.4	+ 20	.1	9.1	6.26	6.88	- 16
.04	8.12	3.76	4.64	+ 17	.2	7.30	6.70	6.70	- 57
.08	7.57	2.81	3.70	- 17	.2	7.1	2.20	3.12	- 70
.08	10.1	4.9	4.84	- 18	.25	9.9	4.76	4.80	- 88
.1	9.33	4.68	5.02	- 39	.3	9.6	3.92	4.08	-108
.15	8.0	5.48	6.84	- 82	.4	8.7	1.354	1.56	-141
.15	12.6	5.38	4.28	- 61	.5	8.3	.306	.368	- 67
.2	5	1.874	3.74	-116	.6	8.2	.814	.992	- 78
.3	5.96	.91	1.528	-136	.7	8.0	1.106	1.38	- 45
.4	5.68	.572	1.06	-135	1.0	7.6	.94	1.24	-127
.45	9.15	.693	.758	-109					
.5	8.7	.61	.70	- 95					
.6	5.02	.618	1.23	- 99					
.6	8.36	.814	.976	-100					
.65	8.5	.88	1.03	-102					
.7	8.0	1.08	1.354	-101					
.75	8.13	.498	.612	-120					
.8	4.95	.418	.844	-166					
1.0	7.85	.432	.557	-137					
2.0	7.95	.0506	.091	-					
3.0	7.32	~0	~0	-					
5.0	7.33	.152	.207	-					

Table 4

DATA RUN NO. 9C

INLET VEL.: 77.25 cm/sec			SUBCOOL.: 2.9°C		PRESSURE: 27.2 Ata			POWER: 47.9 kw/liter	
Meas. Point: x=36.8 cm, Av. Void Fraction: 23%					Meas. Point: x=67.3 cm, Av. Void Fraction: 40%				
FREQ.	POWER AMPL	VOID AMPL	NORM VOID AMPL	VOID PHASE	FREQ.	POWER AMPL	VOID AMPL	NORM VOID AMPL	VOID PHASE
.03	13.8	2.80	1.89	+ 90	.3	7.15	2.38	3.33	-112
.06	12.5	6.12	4.62	+ 24	.3	13.1	5.00	3.82	-102
.15	9.15	4.62	5.10	- 28	.4	12.1	2.14	1.77	-135
.25	7.6	3.20	4.20	- 54	.45	11.5	1.07	.932	-151
.25	12.9	4.88	3.78	- 51	.5	11.4	2.92	.256	-165
.35	11.75	3.95	3.36	- 87	.55	11.3	.644	.570	- 62
.45	11.2	1.91	1.706	-135	.65	11.1	.883	.796	- 65
.5	11.02	1.84	1.670	-153	.75	10.8	1.18	1.10	- 76
.55	10.8	1.424	1.32	-162	.85	10.53	1.79	1.7	- 92
.6	10.6	.562	.530	-212	1.0	10.33	1.28	1.237	-108
.7	10.4	.516	.496	-309	1.2	10.1	.446	.442	-180
.75	10.2	.956	.934	-355	1.5	9.95	.212	.212	-180
.8	10.0	.660	.660	-25	2.0	10.0	.262	.262	-240
.9	9.9	.852	.862	- 50	3.0	10.2	.648	.635	-161
1.0	9.7	.924	.952	- 57	5.0	10.3	.235	.228	-
1.2	9.45	1.15	1.276	- 90					
1.5	9.6	.730	.760	-106					
2.0	9.1	.350	.384	-180					
3.0	9.15	.10	.109	-					

Table 5a

DATA RUN NO. 9C

PRESSURE: 27.2 Ata			POWER: 47.9 kw/liter	
INLET VEL.: 77.25 cm/sec			SUBCOOL.: 2.9°C	
Meas. Point: x=120.6 cm, Av. Void Fraction: 53%				
FREQ.	POWER AMPL	VOID AMPL	NORM VOID AMPL	VOID PHASE
.2	6.7	2.18	3.24	- 87
.4	9.0	.742	.824	-132
.5	8.3	.500	.602	- 90
.6	8.0	.490	.612	- 75
.7	7.6	.262	.344	- 73
.8	7.6	.550	.724	-156
.9	7.6	.360	.502	-158
1.0	7.3	.554	.760	-162
1.1	7.3	.270	.368	-208
1.2	10.35	.650	.628	-208
1.3	10.0	~0	~0	-
1.5	9.9	.250	.252	.258
2.5	9.7	.250	.258	-

Table 5b

DATA RUN NO. 10

INLET VEL.: 76.7 cm/sec			SUBCOOL.: 8.7°C		PRESSURE: 27.2 Ata			POWER: 47.9 kw/liter	
Meas. Point: x 59.6 cm, Av. Void Fraction: 21%					Meas. Point: x 90.1 cm, Av. Void Fraction: 35%				
FREQ.	POWER AMPL	VOID AMPL	NORM VOID AMPL	VOID PHASE	FREQ.	POWER AMPL	VOID AMPL	NORM VOID AMPL	VOID PHASE
.02	9.84	5.60	5.69	+ 54	.02	10.05	7.61	7.57	+ 56
.04	9.33	5.45	5,84	+ 29	.02	10.05	6.24	6.20	+ 56
.08	7.58	4.37	5.76	0	.04	9.98	8.54	8.55	+ 22
.15	5.97	3.15	5.27	- 31	.04	9.98	9.08	9.09	+ 21
.30	6.78	3.41	5.02	- 85	.08	7.63	6.77	8.87	- 10.5
.45	10.98	2.68	2.44	-112	.08	7.63	5.89	7.71	- 10
.55	10.92	1.22	1.12	-156	.15	6.3	4.91	7.79	- 48
.60	10.74	1.01	0.940	-207	.3	4.95	2.50	5.05	-120
.65	10.75	0.435	0.405	-238	.3	4.95	1.71	3.45	-117
.7	10.49	0	0	-	.3	6.73	3.17	4.71	-112
.8	10.17	0.630	0.619	- 22	.3	12.75	6.65	5.21	-117
1.0	9.77	0.583	0.596	- 70	.3	12.75	6.64	5.20	-119
1.3	9.72	0.212	0.218	-	.3	12.75	6.50	5.09	-121
					.3	12.75	6.50	5.09	-121
					.4	11.5	3.10	2.69	-165
					.45	11.05	1.62	1.47	-180
					.50	10.7	1.13	1.06	-180
					.55	10.77	0.435	0.403	-196
					.6	10.45	0.211	0.201	-121
					.7	10.45	0.513	0.490	-107
					.85	10.0	0.434	0.434	-137
					1.0	10.15	0.404	0.398	-124
					1.3	10.15	0.286	0.281	-121
					1.6	9.67	0.348	0.359	-170

Table 6a

DATA RUN NO. 10

PRESSURE: 27.2 Ata			POWER: 47.9 kw/liter	
INLET VEL.: 76.7 cm/sec			SUBCOOL.: 8.7°C	
Meas. Point: x=120.6 cm, Av. Void Fraction: 53%				
FREQ.	POWER AMPL	VOID AMPL	NORM VOID AMPL	VOID PHASE
.02	14.72	11.14	7.56	+ 41
.02	14.72	9.57	6.5	+ 45
.02	14.72	10.60	7.2	+ 53
.04	13.95	12.85	9.21	+ 5
.04	13.95	11.04	7.92	+ 10
.08	11.95	9.98	8.35	- 24
.08	11.95	9.82	8.22	- 22
.15	9.53	6.81	7.15	- 62
.22	12.1	6.28	5.18	-102
.3	6.98	1.438	2.05	-129
.3	12.1	3.45	2.85	-124
.35	11.62	1.535	1.32	-112
.4	6.63	.597	.90	-164.5
.45	6.58	.846	1.285	-158
.45	11.34	1.104	.974	-130
.50	6.48	.892	1.375	-127
.65	9.97	.842	.844	-122
.80	9.68	.446	.461	-135
1.0	9.86	.163	.1655	

Table 6b

DATA RUN NO. 11

INLET VEL.: 115 cm/sec			SUBCOOL.: 14.4°C		PRESSURE: 40.8 Ata			POWER: 79.75 kw/liter	
Meas. Point: x=120.6 cm, Av. Void Fraction: 31%					Meas. Point: x=120.6 cm, Av. Void Fraction: 31%				
FREQ.	POWER AMPL	VOID AMPL	NORM VOID AMPL	VOID PHASE	FREQ.	POWER AMPL	VOID AMPL	NORM VOID AMPL	VOID PHASE
1.2	4.95	.157	.317	- 90	.02	7.42	7.36	9.92	+ 37
1.3	4.9	.127	.259	-315	.04	6.62	7.0	10.57	+ 19
1.5	4.8	0.56	.116	-	.08	6.00	5.21	8.68	- 21
1.5	4.8	.180	.375	-	.08		5.48	9.13	- 17
1.75	4.75	.192	.404	159	.15	6.6	6.62	10.0	
2	4.7	.346	.736	-	.15	5.97	5.39	9.03	- 52
2.5	4.7	~0	~0	-	.3	4.75	2.63	5.54	-104
3	4.6	.322	.70	-	.3	7.26	4.11	5.65	-153
3.5	4.6	.229	.497	-	.3	7.26	3.64	5.01	-120
4.5	4.5	.201	.446	-	.4	6.65	1.80	2.71	-153
					.45	6.4	.942	1.47	-172
					.5	6.2	.525	.846	-144
					.55	6.05	.516	.852	- 90
					.6	5.9	.584	.989	- 90
					.65	5.8	.685	1.18	-119
					.75	5.4	.525	.972	-121
					.80	5.35	.486	.908	-146
					.90	5.2	.414	.796	-167
					.95	5.1	.471	.872	-180
					1.0	5.1	.449	.88	-180
					1.1	5.0	.235	.470	-135

Table 7

DATA RUN NO. 12

INLET VEL.: 115 cm/sec			SUBCOOL.: 7.2°C		PRESSURE: 40.8 Atm			POWER: 79.8 kw/liter	
Meas. Point: x=52.0 cm, Av. Void Fraction: 20%					Meas. Point: x=82.5 cm, Av. Void Fraction: 34%				
FREQ.	POWER AMPL	VOID AMPL	NORM VOID AMPL	VOID PHASE	FREQ.	POWER AMPL	VOID AMPL	NORM VOID AMPL	VOID PHASE
.025	7.21	3.65	5.07	+ 72	.025	7.04	3.72	5.38	+ 42
.04	7.0	3.88	5.55	+ 39	.040	6.87	4.52	6.57	+ 35
.06	6.42	3.91	6.1	+ 24	.060	6.18	4.18	6.77	+135
.08	6.23	3.17	5.08	+ 4	.08	6.03	4.05	6.72	+7.5
.15	4.67	2.58	5.53	- 27	.08	8.06	5.85	7.25	0
.3	6.96	2.89	4.16	- 87	.1	7.78	5.16	6.63	- 14
.4	6.35	1.85	2.91	-133	.1	11.75	8.53	7.26	- 23
.45	5.97	1.31	2.19	-133	.2	8.94	5.40	6.28	- 55
.5	6.02	1.29	2.14	-147	.3	7.04	2.53	3.59	-111
.55	5.80	.632	1.09	-203	.4	6.34	1.22	1.925	-139
.6	5.58	.5	.975	-270	.5	5.97	.149	.2495	- 90
.65	5.40	.141	.261	-300	.6	5.74	.318	.553	- 51
.75	5.21	.582	1.115	+ 11	.7	5,53	.884	.1597	- 69
.85	5.18	.61	1.18	0					
1.2	4.97	.71	1.43	- 42					
1.75	4.78	.372	.777	-117					

Table 8a

DATA RUN NO. 12

PRESSURE: 40.8 Atm			POWER: 79.8 kw/liter	
INLET VEL.: 115 cm/sec			SUBCOOL.: 7.2°C	
Meas. Point: x=120.6 cm, Av. Void Fraction: 49%				
FREQ.	POWER AMPL	VOID AMPL	NORM VOID AMPL	VOID PHASE
.02	7.38	2.96	4.02	+ 48
.04	6.72	5.97	8.89	- 0
.06	6.56	6.40	9.77	- 1
.08	5.97	4.97	8.33	- 9
.15	4.55	3.25	7.15	- 52
.25	3.56	1.86	5.22	- 102
.25	4.98	2.82	5.66	- 90
.25	8.0	3.3	4.12	- 102
.25	7.82	3.78	4.83	- 108
.25	7.82	3.32	4.29	- 102
.35	7.23	1.33	1.84	- 111
.40	6.96	1.15	1.65	- 137
.45	6.44	.90	.715	- 115
.50	6.58	.39	.592	- 79
.55	6.18	.588	.951	- 103
.6	6.18	.617	1.0	- 88
.65	5.97	.917	1.54	- 105
.75	5.82	1.04	1.75	- 119
.85	5.47	.948	1.73	- 139
1.0	5.43	.815	1.5	- 172
1.5	4.80	.53	1.1	- 265
2.0	4.38	.30	.683	- 260

Table 8b

DATA RUN NO. 13

INLET VEL.: 115.2 cm/sec			SUBCOOL.: 3.3°C		PRESSURE: 40.8 Atm			POWER: 79.8 kw/liter	
Meas. Point: x=36.8 cm, Av. Void Fraction: 25%					Meas. Point: x=59.6 cm, Av. Void Fraction: 39%				
FREQ.	POWER AMPL	VOID AMPL	NORM VOID AMPL	VOID PHASE	FREQ.	POWER AMPL	VOID AMPL	NORM VOID AMPL	VOID PHASE
.03	7.02	2.73	3.89	+ 84	.03	6.9	3.58	5.2	+ 94
.05	6.64	3.52	5.30	+ 52	.04	6.7	3.03	4.50	+ 48
.07	6.06	3.11	5.13	+ 28	.05	6.58	3.38	5.14	+ 46
.1	5.44	2.90	5.33	+ 2	.06	6.21	2.96	4.77	+ 15
.15	4.83	2.92	6.05	- 34	.08	6.01	3.32	5.53	+ 14
.2	5.03	2.87	5.70	- 60	.1	5.39	3.06	5.68	- 29
.3	4.46	1.16	2.60	- 81	.1	6.88	4.4	6.38	- 11
.4	6.17	1.28	2.08	-137	.2	5.26	3.14	5.97	- 54
.5	5.95	.44	.739	-183	.3	4.44	1.14	2.56	- 60
.6	5.53	.452	.817	-257	.3	6.93	2.02	2.92	- 88
.7	5.38	.793	1.47	-322	.3	6.97	1.78	2.56	-108
.85	5.18	.642	1.24	-351	.35	6.40	1.41	2.20	-137
1.2	4.82	.441	.915	-360	.45	5.90	.137	.232	-329
					.52	5.80	.094	.159	0
					.6	5.62	.705	1.25	-329
					.8	4.97	.432	.870	- 41
					1.0	5.19	.47	.906	- 45
					1.5	4.98	.359	.75	-122
					2.0	4.57	.282	.618	-180

Table 9a

DATA RUN NO. 13

INLET VEL.: 115.2 cm/sec		SUBCOOL.: 3.3°C		PRESSURE: 40.8 Atm		POWER: 79.8 kw/liter		
Meas. Point: x=90.12 cm, Av. Void Fraction: 52%				Meas. Point: x=120.6 cm, Av. Void Fraction: 65%				
FREQ.	POWER AMPL	VOID AMPL	NORM VOID AMPL	VOID PHASE	FREQ.	POWER AMPL	VOID AMPL	NORM VOID AMPL	VOID PHASE
.03	6.8	3.54	5.21	+ 57	.03	6.73	3.99	5.93	+ 52
.04	6.79	4.2	6.19	+ 28	.045	6.58	3.93	6.06	+ 28
.06	6.4	4.0	6.26	+ 23	.06	6.0	3.17	5.29	+ 4
.08	5.78	3.59	6.21	- 4	.08	5.83	2.59	4.44	- 18
.1	5.58	3.42	6.11	- 11	.1	7.42	4.69	6.32	- 26
.1	7.43	4.77	6.42	- 18	.1	11.47	5.67	4.95	- 21
.1	7.43	3.91	5.3	- 9	.15	9.67	4.66	4.82	- 55
.2	5.78	1.99	3.44	- 60	.25	7.75	3.20	4.13	- 99
.3	6.97	1.79	2.57	- 99	.35	6.93	1.51	2.17	-126
.4	6.18	.428	.692	-108	.45	6.44	.317	.493	-124
.5	5.98	.298	.498	- 99	.5	6.22	.132	.212	- 90
.6	5.67	.518	.912	- 29	.6	6.00	.502	.836	- 52
.75	5.22	.617	1.18	- 54	.7	5.82	.545	.937	- 76
1.0	5.0	.713	1.43	-107	.85	5.44	.502	.923	-113
					1.0	5.05	.435	.862	-135
					1.2	4.77	.51	1.07	-205
					1.5	4.8	.488	1.02	-216
					2.0	4.55	.299	.658	-106
					2.5	4.59	.197	.429	-

Table 9b

DATA RUN NO. 15

INLET VEL.: 115 cm/sec			SUBCOOL.: 12.5°C		PRESSURE: 54.4 Ata			POWER: 111.7 kw/liter	
Meas. Point: x=52.02 cm, Av. Void Fraction: 23%					Meas. Point: x=82.50 cm, Av. Void Fraction 39%				
FREQ.	POWER AMPL	VOID AMPL	NORM VOID AMPL	VOID PHASE	FREQ.	POWER AMPL	VOID AMPL	NORM VOID AMPL	VOID PHASE
.03	7.14	4.72	6.60	+ 58	.03	7.14	4.76	6.74	+ 50
.05	6.57	4.00	6.10	+ 42	.05	7.14	4.98	6.96	+ 31
.08	6.28	4.40	7.00	+ 19	.08	6.87	5.04	7.32	+ 13
.15	5.72	3.30	5.77	- 6	.15	6.02	4.20	6.98	-245
.25	5.00	2.86	5.72	- 38	.25	5.30	3.04	5.72	- 51
.4	4.43	1.48	3.34	- 99	.40	4.57	1.98	4.32	-102
.5	4.00	.984	2.46	-156	.50	4.00	1.00	2.50	-139
.6	3.71	.630	1.70	-243	.55	4.02	.748	1.86	-249
.65	3.64	.600	1.65	-304	.60	3.85	.614	1.396	-262
.7	3.57	1.454	4.08	-324	.70	3.87	.112	.290	0
.7	3.57	.204	.57	-236	.80	3.59	.400	1.116	- 36
.8	3.50	.818	2.34	0	.10	3.43	.424	1.238	- 58
1.0	3.35	1.040	3.10	- 12	.13	3.30	.320	.970	-141
1.3	3.23	.846	2.62	- 90	.17	3.15	.224	.714	-180
1.8	3.07	.396	1.29	-120					

Table 10a

DATA RUN NO. 15

PRESSURE: 54.4 Ata			POWER: 111.7 kw/liter	
INLET VEL.: 115 cm/sec			SUBCOOL.: 12.5°C	
Meas. Point: x=120.6 cm, Av. Void Fraction: 52%				
FREQ.	POWER AMPL	VOID AMPL	NORM VOID AMPL	VOID PHASE
.03	5.30	3.36	6.34	+ 45
.04	5.18	3.06	5.90	+ 33
.06	4.88	3.32	6.80	+ 20
.08	4.71	3.04	6.46	+ 4
.1	4.55	2.79	6.14	0
.15	4.29	2.40	5.60	- 29.6
.15	5.85	3.24	5.54	- 28.4
.15	5.85	3.80	6.50	- 28.8
.25	4.97	2.38	4.79	- 61
.35	4.46	1.83	4.11	- 99
.45	3.99	1.00	2.5	-137
.50	4.42	8.37	1.89	-155
.55	4.27	~0	~0	-
.6	4.13	.378	.915	-130
.7	3.87	.578	1.49	- 84
.85	3.59	.672	1.87	-128
1.0	3.40	.640	1.88	-173
1.2	3.29	.326	.992	-209
1.5	3.13	.082	.262	-270
2.5	3.08	.183	.594	-243

Table 10b

DATA RUN NO. 16

INLET VEL.: 115 cm/sec				SUBCOOL.: 12.1°C	PRESSURE: 68.0 Ata				POWER: 111.65 kw/liter
Meas. Point: x=52.02 cm, Av. Void Fraction : 19%					Meas. Point: x=82.5 cm, Av. Void Fraction: 34%				
FREQ.	POWER AMPL	VOID AMPL	NORM VOID AMPL	VOID PHASE	FREQ.	POWER AMPL	VOID AMPL	NORM VOID AMPL	VOID PHASE
.03	6.60	4.05	6.13	+ 15	.03	6.28	4.68	7.50	+ 13
.05	6.42	3.40	5.30	+ 10	.05	6.12	4.24	6.96	+ 9
.08	6.25	2.78	4.48	+ 10	.08	5.93	3.56	6.04	+ 4
.15	5.67	2.89	5.10	- 15	.15	5.43	3.20	5.96	- 16
.25	4.77	2.32	4.86	- 45	.25	4.91	2.60	5.36	- 51
.40	4.27	1.236	2.94	- 90	.40	4.29	1.72	4.00	- 82
.50	3.99	.932	2.34	-145	.5	3.87	1.176	3.04	-142
.60	3.71	.566	1.54	-194	.6	3.73	.648	1.74	-193
.70	3.56	.416	1.172	-297	.7	3.58	.292	.818	-333
.80	3.56	.418	1.176	-302	.75	3.52	.392	1.116	- 7
.90	3.42	.614	1.796	+ 1	.8	3.42	6.36	1.860	- 7
1.0	3.30	.586	1.774	-113	1.0	3.30	.624	1.894	- 59
1.2	3.28	.672	1.82	- 59	1.2	3.13	.448	1.464	-102
1.5	3.16	.3836	1.23	- 90	1.5	3.14	.1	.062	-180
2.0	3.13	.284	.910	-163	2.0				
3.0	3.13	.143	.046						

Table 11a

DATA RUN NO. 16

PRESSURE: 68.0 Ata			POWER: 111.65 kw/liter	
INLET VEL.: 115 cm/sec			SUBCOOL.: 12.1°C	
Meas. Point: x= 115.9 cm, Av. Void Fraction: .48%				
FREQ.	POWER AMPL	VOID AMPL	NORM VOID AMPL	VOID PHASE
.03	7.03	4.13	5.87	+ 28
.03	7.03	4.14	5.88	+ 37
.05	6.83	4.45	6.52	+ 7
.05	6.83	3.74	5.48	+ 9
.08	6.83	3.91	5.73	+ 1
.15	6.03	3.14	5.22	- 22
.25	5.33	2.66	5.0	- 64
.40	4.60	1.53	3.33	-119
.45	4.42	1.52	3.44	-154
.50	4.44	1.32	2.97	-185
.55	3.93	.467	1.185	-180
.60	3.72	.485	1.303	-195
.65	3.58	.170	.0475	- 10
.70	3.58	.239	.668	-110
.77	3.57	.478	1.34	-139
.85	3.42	1.5	1.245	
1.0	3.28	1.065	1.38	
1.2	3.14	.633	.852	
1.5	2.98	.35	.05	
2.0	3.00			

Table 11b

NOMENCLATURE

Note that barred symbols indicate Laplace transformed variables.

A	Test channel cross section
A_1	Amplitude of first harmonic of v_s
A_n	Amplitude of nth harmonic of v_s
A_w	Total wall heating surface
a	Acceleration constant, equation 14.8
B	Amplitude constant for IBM-650 code
C	Integrator amplifier shunt capacity
C_o	Inlet velocity
C_d	Propagation velocity of steam voids
C_f	Water velocity
ΔC_f	Uncertainty in C_f
C_g	Steam velocity
C'_g	Modified steam velocity, equation 14.22
ΔC_g	Uncertainty in C_g
C_i	Gamma detector cable capacitance
c_1	Specific heat capacity of wall material
c_2	Specific heat capacity of water
c_2'	Specific heat capacity of $(\alpha^o + \beta^o)$-mixture
c_g	Perturbation in steam velocity
D_{max}	Maximum bubble growth radius
d_1	Wall thickness (half thickness of fuel plate)

d_2 Half width of the test channel

d_s Thickness of superheated water film

E_B Wave analyzer Cosine channel output signal

E_R Wave analyzer Sine channel output signal

$f(x)$ Function defined by equation 14.21

f_2 Filter cut-off frequency, equation II.9

$G(s) = \bar{Q}_1/\bar{Q}$ Wall transfer function, equation 12.20

$H(s) = \bar{Q}_2/\bar{Q}$ Transfer function for heat flow past point x, equation 13.14

$H'(s)$ As above for simplified case, equation 13.15

h "Average" heat transfer coefficient

h_{fg} Latent heat of evaporation

h_i Incremental heat transfer coefficient

J_a Jacob Number, defined by equation 10.2

K Wave analyzer scale factor

K_1 Constant defined by equation 10.4

K_2 Constant defined by equation 10.4

K_3 Dimensionless constant, equation 14.30

k Gamma preamplifier gain factor

L Heated height of test channel

m_f Mass of water in control volume $\beta^o \Delta V$

m_g Mass of steam in control volume ΔV

n Average gamma arrival rate, Appendix II

P Perturbation in test channel pressure

ΔP Overpressure inside steam bubble

P^o Total test channel pressure

P_o Amplitude constant used in Appendix I, equation I.8

p Perimeter of test channel

Q Perturbation in total heating power to the test channel

ΔQ Uncertainty in Q^o

Q^o Total heating power to the test channel

Q_1 Perturbation in heat flow into coolant

Q^o_1 Total heat flow into coolant

Q_2 Perturbation in heat flow past point x

q Charge per gamma quantum in input to preamplifier

R Integration amplifier input resistance

R_i Input resistance to gamma preamplifier

r Steam bubble radius

S Steam slip ratio

s Complex frequency

T Integration time of wave analyzer

T_o^o Inlet temperature

T_1 Perturbation in wall temperature

T_2 Perturbation in water temperature

T_f Water temperature

T_i Gamma preamplifier input time constant

T_o Gamma preamplifier output filter time constant

T_{sat} Perturbations in the saturation temperature

T^o_{sat} Saturation temperature of coolant mixture

ΔT^o_{sat} Surface temperature above saturation

$T_{1_{sat}}$ Temperature in initial state, equation 14.38

$T_{2_{sat}}$ Temperature in final state, equation 14.38

T_w Wall surface temperature

t Time

t' Time, integration variable

t_L Water flow time through the test channel

t_x Perturbation propagation time, equations 12.26 or 14.11

$t_{x'x}$ Perturbation flow time from x' to x, equation 14.2

ΔU Change in internal energy for control volume of Appendix III

u_f Specific internal energy of water

u_g Specific internal energy of steam

V Total coolant volume of test channel

ΔV Control volume in Appendix III

V_E Gamma preamplifier output signal with empty channel

V_F Gamma preamplifier output signal with full channel

V_α Gamma preamplifier output signal with void fraction α°

ΔV_α Error in V_α

v Perturbation in gamma preamplifier output

v_o DC-component of v

v_b Random noise component of v

v_f Specific volume of water

v_{fg} Change in specific volume of evaporation

v_g Specific volume of steam

v_s Void response component of v

W_o Inlet mass flow rate

W_f Mass flow rate of water

W_g Mass flow rate of steam

ΔW_g Uncertainty in W_g

w_g Perturbation in steam mass flow rate

x Height above test channel inlet

x' Height above inlet, integration variable

x_s Bulk boiling point

Δx_s Uncertainty in x_s

y Distance from outside wall of test tube (see Figure 24)

α Perturbation in steam volume fraction

$\Delta\alpha$ Equivalent void fraction value of calibration disk
Also uncertainty in a in equation 11.7

α° Average steam volume fraction

α_p Perturbation in void fraction due to pressure changes

β^{o} Volume fraction of water in temperature equilibrium with steam

γ^{o} $= 1 - (\alpha^{o} + \beta^{o})$

δ Heat capacity ratio, equation 13.10

δ' Heat capacity ratio, equation 14.40

κ_1 Thermal conductivity of wall

κ_2 Thermal conductivity of water

λ Removal fraction of steam by condensation

ρ_1 Density of section wall

ρ_2 Coolant density

ρ'_2 Coolant density for $(\alpha^{o} + \beta^{o})$-mixture

ρ_f Water density

ρ_g Steam density

σ Surface tension of water

σ_1 Standard deviation of gamma preamplifier output signal, equation II.5

σ_2 Standard deviation of gamma preamplifier output signal, equation II.8

τ Approximate wall time constant, equation 13.13

$\tau_{1/2}$ Steam bubble half life

τ_1 Wall time constant, equation 12.18

τ_i Heat transfer time constant, equation 12.19

$\bar{\Phi}$ Power spectrum of gamma preamplifier output signal

ϕ Phase delay in void oscillation (first harmonic of v_s)

$\phi(\tau)$ Autocorrelation function for gamma preamplifier output signal

ϕ_n Phase delay of nth harmonic of v_s

ω Frequency in radians per second

ω_c Node frequency, equation 13.18

ω_c' Node frequency for simplified case, equation 13.17

REFERENCES

1. A. W. Kramer: Boiling Water Reactors, Addison-Wesley 1958.
2. S. G. Forbes, F. Schroeder, W. E. Nyer: "Instability in the SPERT-I Reactor. Preliminary Report". IDO - 16309, Oct. 1956.
3. A. S. Jameson and P. A. Lottes: "Natural Circulation Boiling of Water Flowing Upward Through an Annulus". ANL-5208, 1953.
4. W. H. Cook and J. F. Marchaterre: "Single and Multi Channel Natural Circulation Boiling at 600 psig". ANL-5561, 1955.
5. R. P. Andersen and P. A. Lottes: "Boiling Stability". To be published in Vol. IV, Series IV of Pergamon Press Progress in Nuclear Energy.
6. Technical Staff, Ramo-Wooldridge Div. of Thompson Ramo Wooldridge Inc.: "Kinetic Studies of Heterogeneous Water Reactors". RWD-RL-167, Feb. 1960.
7. W. A. Horning and H. C. Corben: "Theory of Power Transients in the SPERT-I Reactor. Final Report". IDO-16446, Aug. 1957.
8. M. Iriarte: "Dynamic Behaviour of Boiling Water Reactors". PhD Thesis 1958, University of Michigan.
9. E. S. Beckjord: "Dynamic Analysis of Natural Circulation Boiling Water Power Reactors". ANL-5799, March 1958.
10. J. A. Thie: "Boiling Water Reactor Instability". Nucleonics, Vol 16, 3, 1958.
11. J. A. Thie: "Theoretical Reactor Statics and Kinetics of Boiling Water Reactors". P/638 Vol. 11, Second UN International Conference on the Peaceful Uses of Atomic Energy. Sept. 1958.
12. J. A. Thie: "Dynamic Behaviour of Boiling Reactors". ANL-5849, May, 1959.
13. J. A. Fleck and J. Huseby: "A Mathematical Model for Calculating Boiling Reactor Transients". P/581 Vol 11, Second UN International Conference on the Peaceful Uses of Atomic Energy.

14. J. A. Fleck: "The Dynamic Behaviour of Boiling Water Reactors". J. of Nuclear Energy, Vol 11, 114, 1960.

15. A. Z. Akcazu: "Theoretical Feedback Analysis in Boiling Water Reactors". ANL-6221, Oct. 1960.

16. S. Zivi and R. W. Wright: "Power-Void Transfer Function Measurements in a Simulated SPERT-IA Moderator Coolant Channel". Proc. of Conf. on Transfer Function Measurement and Reactor Stability Analysis, May 1960. ANL-6205.

17. E. P. Gyftopoulos: "Transfer Function Representation of Nuclear Power Plants", Proc. of the Conf. on Transfer Function Measurement and Reactor Stability Analysis, ANL-6205, May 1960.

18. D. Daavettila: "Dynamic Steam Void Experiment in ZPR-VII": M. S. Thesis 1958, Michigan College of Mining and Technology.

19. V. O. Eriksen: "Void Effects in Boiling Heavy Water Reactors". P/572 Vol 11, Second UN International Conference on the Peaceful Uses of Atomic Energy. Sept. 1958.

20. J. A. DeShong and W. C. Lipinski: "Analysis of Experimental Power-Reactivity Feedback Transfer Functions for a Natural Circulation Boiling Water Reactor". ANL-5850, July 1958.

21. W. Chestnut and R. Mayer: Servomechanisms and Regulating System Design, J. Wiley and Sons, N.Y., 1951.

22. G. B. Wallis and J. H. Heasley: "Oscillations in Two-Phase Flow Systems". Paper No. 60-WA-209. Annual Winter Meeting the Am. Soc. of Mech. Eng., Nov/Dec. 1960.

23. E. S. Beckjord: "The Stability of Two-Phase Flow Loops and Response to Ship's Motion". GEAP 3493, Revision I, Sept. 1960.

24. S. Zivi: "Analytical Model Describing Transfer Functions". STL/TN-60-000-AE192. Nov. 1960

25. Space Technology Laboratories Inc.: "Quarterly Report March 1961, Kinetic Studies of Heterogeneous Water Reactors". 8977-0004-SU-000.

26. C. E. Dengler and I.N. Addoms: "Heat Transfer Mechanism for Vaporization of Water in a Vertical Tube", C.E.P. Symposium Series: 52, No 18, 95, 1956.

27. P. G. Poletavkin and N. A. Shapkin: "Water and Steam Contents in Surface Boiling of Water". Teploenergetica, Vol. 5, No 4, 54-558, 1958.

28. W. P. Ball, D. B. Langmuir and R. W. Wright: "X-ray Measurement of Time Varying Steam Void Fraction in a Thin Water Channel". RW-RL-137, Dec. 1958.

29. H. H. Hooker and G. F. Popper: "A Gamma-Ray Attenuation Method for Void Fraction Determinations in Experimental Boiling Heat Transfer Test Facilities". ANL-5766, Nov. 1958.

30. M. Petrick and B. S. Swanson: "Radiation Attenuation Method of Measuring Density of a Two-Phase Fluid", Rev. of Sci. Inst. 29 No 12, Dec. 1958.

31. S. S. Sidhu, F. P. Campos and D. D. Zauberis: "Radiography with Thulium Sources", Special Techn. Publ., No 223, Am. Soc. for Testing Materials, 1958.

32. Grouthamel: "Applied Gamma Ray Spectrometry", Pergamon Press 1960.

33. B. L. Richardson: "Some Problems in Horizontal Two-Phase Two-Component Flow", ANL-5949, 1958.

34. M. Petrick: "Investigation of Two-Phase Air-Water Flow Phenomena". ANL-5787, 1958.

35. J. H. Keenan and F. G. Keyes: Thermodynamic Properties of Steam, J. Wiley & Sons, 1936.

36. J. A. DeShong: "Power Transfer Functions of the EBWR obtained using a Sinusoidal Reactivity Driving Function". ANL-5798, Jan. 1958.

37. A. A. Wasserman: "High and Low Power SPERT I Transfer Function Measurements". ANL-6205, Proceedings of the Conference on Transfer Function Measurements and Reactor Stability Analysis, May 1960.

38. R. M. Kiehn and E. O. Swickard: "Progress in Frequency Response Measurements at Los Alamos. ANL-6205, as above.

39. A. R. Baker: "Oscillator Tests in British Fast Reactors". ANL-6205, as above.

40. P. Schmid : "High Precision Detector for Periodic Power Modulations in JEEP, Jener. Report No 42, 1956.

41. Z. Akcazu and J. A. Thie: "Methods of Investigating Noisy Power Reactors". ANL-6205.

42. Novak Zuber: "Hydrodynamic Aspects of Boiling Heat Transfer". AECU-4439, June 1959.

43. Jacob: Heat Transfer, Vol I, John Wiley and Sons, 1956.

44. F. C. Gunther and F. Kreith: "Photographic Study of Bubble Formation in Heat Transfer to Subcooled Water". Report 4-120, Jet. Prop. Lab., Calif. Inst. of Technology, March 1950.

45. K. Engelberg-Forster and R. Greif: "Heat Transfer to a Boiling Liquid-Mechanism and Correlations. I. of Heat Transfer, Feb. 1959.

46. P. A. Lottes, M. Petrick and J. F. Marchaterre: "Lecture Notes for the Advanced Summer Institute at Kjeller, Norway". ANL-6063

47. W. H. Jens and P. A. Lottes: "Analysis of Heat Transfer, Burnout, Pressure Drop and Density Data for High Pressure Water". ANL-4627, May 1951.

48. P. Griffith: "Bubble Growth Rates in Boiling". Technical Report No. 8, NSFG-1706, June 1956.

49. J. B. Heineman: "EBWR Core II Hydrodynamics". ANL Reactor Eng. Div. Memo March 1961.

50. General Nucl. Eng. Corp. Staff: "A Study of the Variation of Steam Velocity in Vertical Boiling Channels". ANL-6251, Nov. 1960.

51. J. F. Marchaterre and M. Petrick: "The Prediction of Steam Volume Fractions in Boiling Systems". Nucl. Sci. and Eng. Vol. 7, No. 6, June 1960.

52. G. W. Maurer: "A Method of Predicting Boiling Vapour Fractions in Reactor Coolant Channels". WAPD - AD - TH 556, Nov. 1959.

53. P. A. Lottes, Reactor Eng., Argonne Natl. Lab. Private Communication, Nov. 1960.

54. Proceedings of the Power Reactor In-Core Instrumentation Meeting, Wash. D.C. April 28-29, 1960, pg. 39-43. USAEC, TID - 7598, March 1961.

55. J. H. Vohr: "Flow Patterns of Two-Phase Flow - A Survey of Literature", TID-1151, December 1960.

56. Maung Maung-Myint: "A Literature Survey on Two Phase Flow of Gas and Liquid". B.S. Thesis, June 1959, Mass. Inst. of Technology.

57. P. Griffith and G. B. Wallis: "Slug Flow". Technical Report No. 15, The Office of Naval Research, NONR-1841 (39), May 1959.

58. R. Moissis and P. Griffith: "Entrance Effects in a Developing Slug Flow". Technical Report No. 18, The Office of Naval Research, NONR-1841 (39), June 1960.

59. H. S. Isbin, J. E. Moy, and A.J.R. Da Cruz: "Two-Phase Steam-Water Critical Flow". A.I.Ch.E. Journal 3 No. 3, Sept. 1957.

60. H. B. Karplus: "The Velocity of Sound in a Liquid Containing Gas Bubbles". Armour Research Foundation Report COO-248, June 1958.

61. G. Heinrich: "Uber Stromungen von Schaumen". Z. fur Angewandte Mathematic und Mechanik, Vol 22, No. 2, 1942.

62. H. B. Karplus: "Velocity of Sound in Water-Steam Mixture as a Function of Quantities of the Two Components". Armour Research Foundation, Monthly Progress Report, June 1958.

63. Jacobs: "Thermal Transfer Functions for Two-Region Fuel Pins". Reactor Engineering Memo, Argonne Natl. Lab., May 1958.

64. F. Narin and D. Langford: "Analytical Solution for Transient Temperature Distributions in Two-Region Nuclear Reactor Fuel Elements". Nucl. Sci. and Eng., 6, 386 (1959).

65. E. P. Gyftopoulos and H. B. Smets: "Transfer Functions of Distributed Parameter Nuclear Reactor Systems". Nucl. Sci. and Eng., 5, 405 (1959)

66. F. Storrer: "Temperature Response to Power, Inlet Coolant Temperature and Flow Transients in Solid Fuel Reactors". APDA-132, June 1959.

67. Newton, Gould, Kaiser: Analytical Design of Linear Feedback Controls. John Wiley and Sons, 1957.

BIOGRAPHICAL NOTE

Helge Christensen was born in Bergen, Norway on March 20, 1929. After graduating from high school in Bergen in 1947, he attended the Bergen Seamen's School for a year, and graduated as Radio Operator, First Class.

He entered The Royal Danish Technical University, Copenhagen, in the Fall of 1948. He graduated with honors in January, 1954, receiving a Master's Degree in Engineering Physics. The thesis work was done on the development of an electrolytic tank for field measurements.

From March, 1954, he worked under the direction of Dr. Odd Dahl at the Chr. Michelsen Institute, Dept. of Applied Physics in Bergen, Norway.

Helge Christensen designed and supervised the building of a fast neutron chopper (now at the MIT Reactor), and also the control rods with drives and control equipment for the Halden Boiling Water Reactor.

In 1957 he entered Massachusetts Institute of Technology as a graduate student in Nuclear Engineering. He worked half time for a period of two years as Research Assistant on the MIT Nuclear Reactor Staff, headed by Professor Theos. J. Thompson. The present work was carried out at Argonne National Laboratory, from March, 1960.

Publications

Helge Christensen and Bjarne Aarseth: "Development and Design of the Cadmium Control Stations for a Boiling Heavy Water Reactor." Chr. Michelsen Institute, Beretninger XXI, 3, Bergen, 1958.

Helge Christensen and Robert B. Stanfield: "The Log Count-Rate Period Meter Used with Safety Circuits." To be published in the July, 1961 issue of PGNS Transactions, Institute of Radio Engineers.